

SMALL-MOLECULE ENZYME INHIBITORS UTILIZING ACTIVE-SITE METAL
CHELATION: PROLYL 4-HYDROXYLASE AND MICROBIAL RIBONUCLEASES

by

Joshua James Higgin

A dissertation submitted in partial fulfillment
of the requirements for the degree of

Doctor of Philosophy

(Chemistry)

at the

UNIVERSITY OF WISCONSIN-MADISON

2004

A dissertation entitled

SMALL-MOLECULE ENZYME INHIBITORS UTILIZING ACTIVE-SITE METAL CHELATION: PROLYL 4-HYDROXYLASE AND MICROBIAL RIBONUCLEASES

submitted to the Graduate School of the
University of Wisconsin-Madison
in partial fulfillment of the requirements for the
degree of Doctor of Philosophy

by

Joshua James Higgin

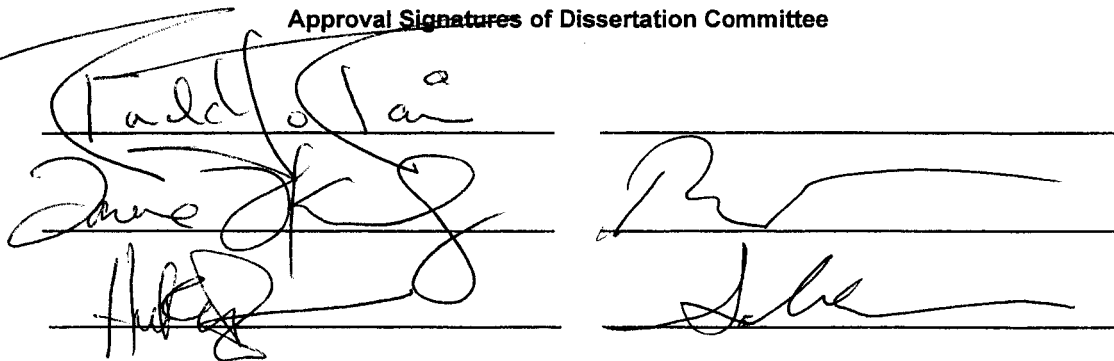
Date of Final Oral Examination: May 12, 2004

Month & Year Degree to be awarded: **December**

May 2004

August

Approval Signatures of Dissertation Committee

The block contains five handwritten signatures of the Dissertation Committee members, arranged in two columns. Each signature is written over a horizontal line.

Signature, Dean of Graduate School

The block contains the handwritten signature of Martin Cadwallader, written over a horizontal line.

SMALL-MOLECULE ENZYME INHIBITORS UTILIZING ACTIVE-SITE METAL CHELATION: PROLYL 4-HYDROXYLASE AND MICROBIAL RIBONUCLEASES

Joshua James Higgin

Under the supervision of Professor Ronald T. Raines

At the University of Wisconsin-Madison

Metal cofactors play a variety of structural and reactive roles in enzymes. Their versatility makes them both a viable target for binding small-molecule inhibitors, and an excellent vehicle for specific inhibition in the active sites of both metalloenzymes and non-metalloenzymes. This dissertation describes the development of novel inhibitors by exploiting the diverse roles that metals play in enzymic systems.

The iron-dependent enzyme prolyl 4-hydroxylase (P4H) catalyzes the post-translational modification of proline residues to form 4-hydroxyproline, an essential residue for collagen stability. Chapter Two describes the development of a screen for bioavailable inhibitors of P4H using the nematode, *Caenorhabditis elegans*. Using this assay, an epoxy ketone was discovered that specifically inhibits the P4H enzyme *in vivo*. To characterize this interaction, a simple *in vitro* assay for P4H was used to demonstrate that the epoxy ketone binds in the enzymic active site, presumably with the oxygens of the ketone and epoxy groups as ligands of the endogenous cationic iron. There, the epoxy group undergoes nucleophilic attack by an enzymic residue to inactivate the enzyme irreversibly. The mass of trypsin-generated peptides indicates that the side chain of Lys253 reacts with the epoxide functionality of the inhibitor. The ketone of the inhibitor

provides a functional group of unique reactivity that can be utilized in proteomics applications.

Chapter Three describes the inhibition of a ribonuclease by a small-molecule in a complex with an exogenous metal. The inhibition of ribonuclease Bi by 3'-*N*-hydroxyurea-3'-deoxythymidine 5'-phosphate is enhanced by 30-fold in the presence of Zn^{2+} . Thus, an *N*-hydroxyurea nucleotide can recruit Zn^{2+} to inhibit the enzymatic activity of a ribonuclease. This result engenders a general strategy for the inhibition of non-metalloenzymes by metal complexes.

Chapter Four describes the basis for the competitive inhibition of ribonuclease Sa (RNase Sa) by 3'-*N*-hydroxyurea-3'-deoxythymidine 5'-phosphate. Inhibition is enhanced by nearly 10-fold in the presence of Zn^{2+} , which could coordinate to the *N*-hydroxyurea group along with enzymic residues. The data indicate that an *N*-hydroxyurea nucleotide can recruit Zn^{2+} to inhibit the enzymatic activity of RNase Sa, and suggest that the carboxylate of Glu54 is a ligand for that Zn^{2+} . These results extend the generality of zinc(II) complexes with an *N*-hydroxyurea nucleotide as inhibitors of ribonucleases.

Acknowledgements

First I'd like to thank my advisor Ron Raines for giving me the chance to do interdisciplinary research beyond chemistry into biology. My career as a scientist has been influenced greatly by his guidance and knowledge of these diverse fields.

I need to thank all of the present and past members of the Raines Lab for helping me with all aspects of my project both technique and overall direction in research. The lab is a great place scientifically and socially for a grad student to be. I'll always remember the fun times. I'd like to specifically thank Betsy Kersteen for working with me on the prolyl hydroxylase project. I could never have finished without you. I'd like to thank Brian Smith for working with me on the folate project. I'd like to thank Dr. Lisa Freidman for teaching me all about worms. Thanks to the great post-docs and senior students in the Raines Lab for giving me a lot of advice on my projects, Dr. Brian Miller, Dr. Jonathan Hodges, Dr. Sunil Chandran, Dr. Frank Kotch, Dr. Byung-Moon Kim, Dr. Ken Woycechowsky, Dr. Marcia Haigis, Dr. Brad Kelemen, Dr. Chiwook Park, Dr. Brad Nilsson, Cara Jenkins, Matt Soelner, Kim Dickson and all of the rest of the lab who helped me with my work.

My family has been so supportive of me during grad school. I wish I would have gone home more while I was this close to Minnesota. My mom and dad have always given me all their love even though they didn't understand all of what I was doing here in Madison. Finally, my wife Michelle, who encouraged me and pushed me to finish this thesis. You have worked just as hard on my thesis as your own. I am so grateful to you for your love and support.

Table of Contents

Abstract.....	<i>i</i>
Acknowledgements.....	<i>iii</i>
Table of Contents	<i>iv</i>
Table of Figures.....	<i>vi</i>
Table of Schemes	<i>vii</i>
Table of Tables	<i>viii</i>
List of Abbreviations.....	<i>ix</i>
Chapter One-Introduction.....	<i>1</i>
1.1 Inhibition of a Metalloenzyme Involved in Collagen Biosynthesis	<i>2</i>
1.1.1 Collagen.....	<i>2</i>
1.1.2 Collagen Related Diseases.....	<i>4</i>
1.1.3 Prolyl 4-Hydroxylase.....	<i>5</i>
1.1.4 Inhibitors of Prolyl 4-Hydroxylase.....	<i>7</i>
1.1.4.1 Prolyl 4-Hydroxylaseinhibitors Targeting the Cationic Iron Cofactor	<i>8</i>
1.1.4.2 Ascorbate Analogs.....	<i>9</i>
1.1.4.3 α -Ketoglutarate Mimics	<i>10</i>
1.1.4.4 Peptide Mimics	<i>12</i>
1.1.5 The Role of Prolyl 4-Hydroxylase in the Hypoxia Signaling Cascade.....	<i>12</i>
1.2 Metal-Mediated Inhibition of Microbial Ribonucleases.....	<i>14</i>
1.2.1 Ribonucleases	<i>14</i>
1.2.2 Microbial Ribonucleases	<i>15</i>
1.2.3 Small-Molecule Ribonuclease Inhibitors	<i>16</i>
Chapter Two-Bioavailable Inhibitors of Prolyl 4-Hydroxylase.....	<i>27</i>
2.1 Abstract.....	<i>28</i>
2.2 Introduction	<i>29</i>
2.3 Results and Discussion	<i>33</i>
2.3.1 Development of an Assay for Bioavailable Inhibitors of P4H Using <i>C. elegans</i>	<i>33</i>
2.3.2 Development and Screening of Novel α -Ketoglutarate Mimics in <i>C. elegans</i>	<i>35</i>
2.3.2.1 Library of <i>N</i> -Branched Oxalylglycine Compounds.....	<i>35</i>
2.3.2.2 Dimethyl-6-hydroxy-2,4-pyridine dicarboxylate	<i>37</i>
2.3.2.3 Hydroxamic Acid Analog of α -Ketoglutarate	<i>38</i>
2.3.2.4 Electrophilic α -Ketoglutarate Analogs	<i>38</i>
2.3.2.5 Epoxy Ketone Analog of α -Ketoglutarate.....	<i>39</i>
2.3.3 <i>In Vitro</i> Characterization of the Epoxy Ketone as an Irreversible Inhibitor.....	<i>40</i>
2.3.3.1 Development of a Simple <i>in vitro</i> Assay for Prolyl 4-Hydroxylase	<i>40</i>
2.3.3.2 Assessment of <i>in vitro</i> Inactivation of P4H by Epoxy Ketone Inhibitor.....	<i>43</i>
2.3.3.3 Determination of Chiral Preference for Inactivation of P4H by Epoxy Ketones.....	<i>44</i>
2.3.4 Identification of Enzyme Residue Targeted by Epoxy Ketone Inhibitor.....	<i>45</i>
2.3.5 Immobilization of Prolyl 4-Hydroxylase by Epoxy Ketone Inhibitor	<i>46</i>
2.4 Conclusion.....	<i>47</i>
2.5 Future Directions.....	<i>48</i>

2.6 Materials and Methods	48
<i>Chapter Three-Zinc(II)-Mediated Inhibition of a Ribonuclease</i>	
<i>by an N-Hydroxyurea Nucleotide</i>	<i>115</i>
3.1 Abstract.....	116
3.2 Introduction	117
3.3 Results and Discussion	119
3.4 Conclusion.....	122
3.5 Materials and Methods	122
<i>Chapter Four-Zinc(II)-Mediated Inhibition of Ribonuclease Sa</i>	
<i>by an N-Hydroxyurea Nucleotide and its Basis</i>	<i>131</i>
4.1 Abstract.....	132
4.1 Abstract.....	132
4.3 Results and discussion.....	134
4.4 Conclusion.....	137
4.5 Materials and methods.....	138
<i>Appendix I</i>	<i>149</i>
A.1 Abstract.....	150
A.2 Introduction	151
A.3 Materials and Methods	152
<i>References.....</i>	<i>158</i>

Table of Figures

Figure 1.1 Collagen triple helices _____	20
Figure 1.2 Reaction catalyzed by of P4H _____	21
Figure 1.3 Proposed chemical mechanism of P4H _____	22
Figure 1.4 Examples of known P4H inhibitors _____	23
Figure 1.5 Structure of bis(5-amidino-2-benzimidazolyl)methane (BABIM) _____	24
Figure 1.6 Proposed catalytic mechanism of ribonucleases _____	25
Figure 1.7 Examples of small molecule ribonuclease inhibitors _____	26
Figure 2.1 Example of prodrugs of P4H with <i>in vivo</i> activity _____	64
Figure 2.2 The <i>dpy-18</i> and <i>phy-2</i> <i>C. elegans</i> phenotypes _____	65
Figure 2.3 Nomarski differential interference image of dead embryos _____	66
Figure 2.4 <i>C. elegans</i> P4H <i>in vivo</i> assay _____	67
Figure 2.5 Dose response of <i>C. elegans</i> to compounds 2.1 and 2.2 _____	68
Figure 2.6 Library of <i>N</i> -branched oxalylglycine compounds _____	70
Figure 2.7 Rationally designed inhibitors of P4H based on α -KG _____	71
Figure 2.8 Comparison of bioavailable inhibitors in the <i>C. elegans</i> assay _____	74
Figure 2.9 Representative HPLC trace for P4H <i>in vitro</i> assay _____	76
Figure 2.10 Comparison of catalysis by P4H enzymes from different systems _____	77
Figure 2.11 Time and concentration dependent inactivation of P4H _____	79
Figure 2.12 Kitz and Wilson plot of half times for inactivation of P4H _____	80
Figure 2.13 Protection from P4H inactivation by α -KG _____	81

Figure 2.14 Comparison of enantiomers 2.13 in the <i>C. elegans</i> assay	82
Figure 2.15 P4H immobilization assay	84
Figure 3.1 Lineweaver–Burk plot for the inhibition of binase by 3.1	126
Figure 4.1 Strategy for zinc(II)-mediated inhibition by <i>N</i> -hydroxyurea 4.1	143
Figure 4.2 Active site of RNase Sa	144
Figure 4.3 Dixon plot for the inhibition of wild-type RNase Sa and its E54Q variant by <i>N</i> -hydroxyurea 4.1	145
Figure 4.4 Lineweaver-Burk plot for the inhibition of wild-type RNase Sa and its E54Q variant by <i>N</i> -hydroxyurea 4.1	146
Figure 4.5 Dependence of the relative ribonucleolytic activity of RNase T1 on 4.1 and zinc(II)	147
Figure 4.6 Scheme for the zinc(II)-mediated inhibition of RNase Sa by 4.1	148

Table of Schemes

Scheme 2.1 Synthetic scheme for <i>N</i> -branched oxalyl glycine compounds	69
Scheme 2.2 Synthetic scheme for C3-C4 electrophilic α -KG analogs	72
Scheme 2.3 Synthetic scheme for bioavailable epoxy ketone 2.13	73
Scheme 2.4 Synthetic scheme for dansylated peptide substrates	75
Scheme 2.5 Synthetic scheme for the epoxy ketone 2.19	78
Scheme 2.6 Proposed mechanism for biotin conjugation	83
Scheme 3.1 Basis for zinc(II)-mediated inhibition by <i>N</i> -hydroxyurea 3.1	124
Scheme 3.2 Route for the synthesis of <i>N</i> -hydroxyurea 3.1	125

Scheme 3.3 Scheme for zinc(II)-mediated inhibition of enzymatic activity	127
---	-----

Scheme A.1 Synthetic scheme for BAm-folate synthesis	156
---	-----

Table of Tables

Table 3.1 Parameters for inhibition of ribonuclease Bi catalysis by <i>N</i> -hydroxyurea 3.1 and Zn^{2+}	128
---	-----

Table 4.1 Parameters for catalysis of poly(I) cleavage by RNase Sa and its E54Q variant, and for its inhibition by <i>N</i> -hydroxyurea 4.1	140
---	-----

Table 4.2 Parameters for inhibition of wild-type RNase Sa catalysis by <i>N</i> -hydroxyurea 4.1 and Zn^{2+}	141
--	-----

Table 4.3 Parameters for inhibition of E54Q RNase Sa catalysis by <i>N</i> -hydroxyurea 4.1 and Zn^{2+}	142
---	-----

List of Abbreviations

α -KG	α -ketoglutarate
aq	aqueous
Arg, R	arginine
Asn, N	asparagine
Asp, D	aspartic acid
BABIM	bis(5-amidino-2-benzimidazolyl)methane
Binase	ribonuclease Bi
Boc	<i>tert</i> -butoxycarbonyl
BSA	bovine serum albumin
cDNA	complimentary DNA
<i>C. elegans</i>	<i>Caenorhabditis elegans</i>
Cyc, C	cysteine
Dansyl	5-dimethylamino-1-naphthalenesulfonic acid
DCC	dicyclohexylcarbodiimide
DMAP	4- <i>N,N</i> -dimethylaminopyridine
DMF	<i>N,N</i> -dimethylformamide
DMSO	dimethyl sulfoxide
DNA	deoxyribonucleic acid
<i>dpy</i>	dummy
DTT	dithiothreitol
<i>E. coli</i>	<i>Escherichia coli</i>

EDC	1-ethyl-3-(3-dimethylaminopropyl)carbodiimide
EMM	exact mass measurement
ER	endoplasmic reticulum
ESI	electrospray ionization
Et	ethyl
EtOAc	ethyl acetate
Gln, Q	glutamine
Glu, E	glutamic acid
Gly, G	glycine
HATU	<i>N</i> -[(dimethylamino)(3 <i>H</i> -1,2,3-triazole(4,5- <i>b</i>)pyridine-3-yloxy)methylene]- <i>N</i> -methylmethanaminium hexafluorophosphate
Hepes	4-(2-hydroxyethyl)-1-piperazineethanesulfonic acid
HIF	hypoxia inducible factor
His, H	histidine
HMPA	hexamethylphosphoramide
HOBt	1-hydroxybenzotriazole
HOE 077	pyridine-2,4-dicarboxylic-di-(2-methoxyethyl)amide
HPLC	high pressure liquid chromatography
Hyp, O	4(<i>R</i>)-hydroxy-L-proline
Ile, I	isoleucine
Leu, L	leucine
Lys, K	lysine

MALDI-TOF	matrix-assisted laser desorption/ionization time of flight
Me	methyl
MES	4-morpholine ethane sulfonic acid
Met, M	methionine
NEM	<i>N</i> -ethylmorpholine
NMR	nuclear magnetic resonance
P4H	prolyl 4-hydroxylase
PBS	phosphate buffered saline
PDI	protein disulfide isomerase
pdUppAp	5'-phospho-2'-deoxyuridine 3'-pyrophosphate P'→5' ester with adenosine 3'-phosphate
pdT	2'-deoxythymidine 5'-monophosphate
Ph	phenyl
Phe, F	phenylalanine
Poly(I)	poly(inosinic acid)
Pro, P	proline
pyr	pyridine
RI	ribonuclease inhibitor
RNA	ribonucleic acid
RNase	ribonuclease
RT	room temperature
salen	bis(salicylidene)ethylenediaminato
Ser, S	serine

SDS-PAGE	sodium dodecyl sulphate-polyacrylamide gel electrophoresis
SPPS	solid phase peptide synthesis
$t_{1/2}$	half-time
TBAF	tetrabutylammonium fluoride
tBu	<i>tert</i> -butyl
TEA	triethylamine
TFA	trifluoroacetic acid
Thr, T	threonine
Tris-HCl	tris(hydroxymethyl)aminomethane hydrochloride
Tyr, Y	tyrosine
U>p	uridine 2',3'-cyclic phosphate
U>v	uridine 2',3'-cyclic vanadate
UpOC ₆ H ₄ - <i>p</i> -CH ₂ F	uridine 3'-[4-(fluoromethyl)phenyl] phosphate
UV	ultraviolet
v/v	volume per volume
Val, V	valine
VHL	von Hippel-Lindau

Chapter One

Introduction

One third of all enzymes are metalloenzymes (Thorp, 1998). The versatility of metal cofactors allows them to play a variety of roles in enzymes. They can act as Lewis acids or nucleophiles and, they can mediate various redox chemistries. In addition, metals can coordinate water molecules and amino acid side chains to tune their reactivity as acids, bases, or nucleophiles. Moreover, metal cofactors can serve a structural role in proteins such as the zinc finger proteins. This versatility makes metals both a viable target for binding small-molecule inhibitors and an excellent vehicle for specific inhibition in the active sites of both metalloenzyme and non-metalloenzymes.

In this thesis, I have attempted to develop novel inhibitors by exploiting the diverse roles metals play in several enzyme systems. Here, I describe (1) the development of a bioavailable and irreversible inhibitor for prolyl 4-hydroxylase (P4H), an α -ketoglutarate (α -KG) dependent non-heme iron oxygenase enzyme involved in collagen biosynthesis and (2) the development of a zinc(II)-mediated inhibitor for microbial ribonucleases (RNases).

1.1 Inhibition of a Metalloenzyme Involved in Collagen Biosynthesis

1.1.1 Collagen

Collagen is the most abundant protein in animals (Prockop & Kivirikko, 1995; Kivirikko & Pihlajaniemi, 1998; Myllyharju & Kivirikko, 2001; Jenkins & Raines, 2002). There are 27 different types of collagens found in vertebrates and more than 20 additional proteins containing collagen-like domains (Myllyharju & Kivirikko, 2004). Collagen plays an important role in maintaining the structural integrity of various

connective tissues, including basement membranes, cartilage, ligaments, tendons, bone, and skin. The structure of the highly abundant collagen proteins is primarily comprised of a triple helix of three left-handed polyproline II strands with a shallow right-handed superhelical pitch (Figure 1.1). The sequence of collagen-like domains contains repeating sequences of Xaa-Yaa-Gly. Every third residue must be a glycine, which is essential for the packing of the coiled-coil structure. In addition, L-proline (Pro) often occupies the Xaa position and 4(*R*)-hydroxy-L-proline (Hyp) often occupies the Yaa position.

The stability of collagen is due in large part to several important post-translational modifications. The most prevalent and important post-translational modification to collagen is hydroxylation of the proline residues in the Yaa position by prolyl 4-hydroxylase (P4H) (EC 1.14.11.2) (Kivirikko *et al.*, 1992). This hydroxylation enhances collagen stability at physiological temperatures. Non-hydroxylated collagen is 50% unfolded at 24 °C, while the addition of hydroxyl groups increases its melting temperature to 39 °C (Berg & Prockop, 1973b; Rosenbloom *et al.*, 1973). Additionally, hydroxylation of proline in the Xaa position by prolyl 3-hydroxylase (Clifton *et al.*, 2001) occurs to yield the sequence 3-Hyp-4-Hyp-Gly (Gryder *et al.*, 1975). This modification has recently been shown to impart destabilization to the collagen triple helix (Jenkins *et al.*, 2003; Mizuno *et al.*, 2004), and occurs with much less frequency than does proline 4-hydroxylation (less than 1% of collagen stands undergo proline 3-hydroxylation (Kivirikko *et al.*, 1992)). Finally, some collagen lysine residues are hydroxylated by the enzyme lysyl hydroxylase and are later converted to reactive aldehyde groups via the lysyl oxidase enzyme to facilitate interchain crosslinking (Passoja *et al.*, 1998; Valtavaara

et al., 1998; Ito *et al.*, 2001; Maki & Kivirikko, 2001). Aggregation of long, covalently crosslinked, tensile fibrils provides even further stability and structural integrity to collagen found in connective tissues.

The increased stability of a proline-hydroxylated collagen triple helix compared to that of an unhydroxylated triple helix is not due to a more stable water-bridged hydrogen bond network (Bella *et al.*, 1994), but rather to stereoelectronic effects (Holmgren *et al.*, 1998; Bretscher *et al.*, 2001; Hodges & Raines, 2003). Collagen mimics utilizing a 4(*R*)-fluoroproline analog in the Yaa position, which cannot form hydrogen bonds to the fluorine, hyperstabilize the triple helical structure. Therefore, the role of the hydroxyl group in Hyp at the Yaa position likely acts to stabilize the Hyp ring pucker in a conformation that preorganizes the collagen strands into the conformation they assume in a triple helix.

1.1.2 Collagen Related Diseases

The overproduction and overaccumulation of collagen is associated with fibrotic diseases such as scleroderma, organ fibrosis, cirrhosis, keloids, and scarring (Hanauske-Abel & Guenzler, 1982; Franklin *et al.*, 1991; Cunliffe *et al.*, 1992; Franklin, 1995; Bickel *et al.*, 1998; Kim *et al.*, 2000; Franklin *et al.*, 2001). Liver cirrhosis alone affects nearly 1 million people in the U.S. and hundreds of millions worldwide (Friedman, 2003). In addition, loss of P4H activity from diets lacking vitamin C results in the disease state of scurvy (Barnes, 1975). In the absence of vitamin C (ascorbic acid), P4H enzymes become trapped in a non-productive oxidation state and are unable to catalyze proline hydroxylation. Due to the chronic nature of many of these diseases, effective

therapeutics have been difficult to develop and the current treatments are largely unsatisfactory, as they come with significant side effects (Franklin, 1995). Therefore, there is ample opportunity for the development of effective new treatments. Inhibition of P4H provides an attractive target for protein-directed drug development as it is an essential enzyme for maintaining collagen stability.

1.1.3 Prolyl 4-Hydroxylase

The enzyme P4H is a $\alpha_2\beta_2$ tetramer located in the lumen of the endoplasmic reticulum (ER). P4H enzymes from humans, mice, chickens, and worms have been characterized in the most detail. (Guzman, 1998; Kivirikko & Pihlajaniemi, 1998; Myllyharju, 2003; Myllyharju & Kivirikko, 2004). The α subunit contains the hydroxylase active site. Animals contain at least three distinct types of α subunits. The functional differences between the various homologs are still being established. Protein disulfide isomerase (PDI) (EC 5.3.4.1) serves as the β subunit of the P4H $\alpha_2\beta_2$ tetramer. PDI serves multiple roles in collagen synthesis (Kivirikko & Pihlajaniemi, 1998; Kersten & Raines, 2003). It catalyzes the formation and isomerization of interchain and intrachain disulfide bonds. It also acts as a chaperone to bind nascent collagen chains and to prevent aggregation.

P4H catalyzes the processive, post-translational hydroxylation of proline to hydroxyproline coupled with the oxidative decarboxylation of α -ketoglutarate (α -KG) to succinate and CO_2 (Figure 1.2) (De Waal & De Jong, 1988). Like clavamate synthase (Zhang *et al.*, 2000), deacetoxycephalosporin C synthase (Valegard *et al.*, 2004), and taurine/ α -ketoglutarate dioxygenase (Ryle *et al.*, 2003), P4H is a member of the family of

Fe(II) α -ketoglutarate-dependent oxygenases. These non-heme iron enzymes require α -KG which is usually converted to succinate during the course of 2-electron substrate oxidation. In addition to α -KG and Fe(II), P4H also requires O_2 and ascorbate. Cosubstrates and cofactors are expected to bind P4H in succession. Fe(II) binds first into an iron-binding domain within the α -subunit ($K_m = 4 \mu M$). α -KG then binds ($K_m = 22 \mu M$) before a proline substrate (K_m varies based on substrate) can dock into the active site. Finally, oxygen ($K_m = 43 \mu M$) binds to the cationic iron cofactor before the enzymatic transformation occurs (Kivirikko & Pihlajaniemi, 1998). Although ascorbate is not required for catalytic turnover, it does serve to rescue a non-productive, reactive Fe(III)O⁻ species, which forms as a byproduct of the uncoupled decarboxylation of α -KG (Figure 1.2) (Gunzler *et al.*, 1988a). Without reduction by ascorbate, the enzyme rapidly undergoes inactivation by self-oxidation (Myllyla *et al.*, 1978).

Information regarding the catalytic mechanism of P4H suggests that proline hydroxylation proceeds via a radical mechanism (Wu *et al.*, 1999). Fe(II) contains six available coordination sites. Apparently, three ligands are derived from enzymic side chains and two from α -KG C1 carboxyl and C2 carbonyl oxygens. Based on experimental evidence from other α -KG dependent enzymes, it is proposed that molecular oxygen occupies the final available site, and there forms a reactive superoxide-like species, (Figure 1.3). The C2 carbonyl of α -KG then undergoes attack by the superoxide species forming a Fe(IV)-peroxo species (Costas *et al.*, 2004). A planar Fe(II)-peracid adduct intermediate has been proposed to result from decarboxylation of α -KG. Heterolytic cleavage of the peracid adduct produces a reactive Fe(IV)-oxo species.

In two steps, this species can then abstract a hydrogen atom from the C4 position of the proline substrate, followed by oxygen rebound to form the hydroxylated product (Groves & McClusky, 1976). At this point, the cationic iron cofactor returns to its Fe(II) resting state and can resume catalytic cycles.

Several key enzyme residues play major roles in substrate binding and catalysis by P4H. The iron-binding domain is believed to be located in a pocket of the α subunit, coordinated by three enzymic side chains. Using site-directed mutagenesis, Myllyharju and Kivirikko identified His412, Asp414, and His483 as residues likely involved in cationic iron chelation (Myllyharju & Kivirikko, 1997). They further characterized the α -KG binding site, which is proposed to consist of three parts. A positively charged Lys493 binds the C5 carboxyl of α -KG at one end of the binding site, and the enzyme-bound cationic iron coordinates the keto-acid functionality of α -KG in an *S-cis*-confirmation on the other end. Finally, His501 appears to be an important active site residue, and is probably involved in binding the C1 carboxyl of α -KG and assisting in decarboxylation (Myllyharju, 2003).

Little detailed information regarding the peptide binding site exists. Studies of the peptide-binding region of crystalline P4H by x-ray diffraction analysis indicate that substrate binding occurs at the N-terminus of the α -subunit consisting of about 100 amino acids, beginning near residue 140. Key contacts are proposed between Ile182 and Tyr233 and the substrate (Myllyharju & Kivirikko, 1999; Hieta *et al.*, 2003; Pekkala *et al.*, 2003).

1.1.4 Inhibitors of Prolyl 4-Hydroxylase

Gunzler and Weidmann have suggested that P4H inhibitors must overcome a few major barriers to become clinically effective (Gunzler & Weidmann, 1998). First, because P4H is located in the cisternae of the rough ER, bioavailable inhibitors must possess the ability to transverse both the cell membrane and the ER membrane. Second, inhibitors must target only the fibrotic organs, as collagen is present in almost all bodily organs. Finally, potential therapeutics must maintain sustained inhibition to overcome the eventual restoration of P4H activity (Franklin, 1995). It has been found that as a result of P4H inhibition, unhydroxylated procollagen does not undergo rapid proteolysis as was once thought. Instead it accumulates within the ER until drug clearance occurs within the tissue. This accumulation allows P4H activity to reactivate, and accrued procollagen promptly becomes hydroxylated and secreted (Franklin, 1995).

As the three-dimensional structure of the full-length P4H enzyme has not yet been determined, current strategies used for inhibitor development of P4H involve compounds designed to mimic the cofactors and cosubstrates (Figure 1.4).

1.1.4.1 Prolyl 4-Hydroxylase inhibitors Targeting the Cationic Iron Cofactor

The activity of P4H is dependent on its Fe(II) cofactor. Divalent metal ions such as Zn(II) have been used to inhibit P4H enzymes by competing with the cationic iron in the metal-binding site and providing potent inhibition due to their similarities in ionic radii (Tuderman *et al.*, 1977). As such, zinc(II) has been shown to successfully act as a fibrosuppressive agent in CCl₄-induced liver injury in rats (Anttinen *et al.*, 1984). In addition, cationic iron chelators such as 2,2'-dipyridyl (**1.1**) and 2,2'-dipyridyl-5,5'-dicarboxylate (**1.2**) inhibit P4H (Guenzler *et al.*, 1986). Although compound **1.1** is more

commonly used as a metal chelator, its derivative **1.2** provides greater inhibition ($IC_{50} = 0.185 \mu M$), due to its specificity for iron center in the enzyme active site. Compound **1.1**, on the other hand, binds all of the free cationic iron in solution (Hales & Beattie, 1993). This approach could result in significant toxicity as the chelators access the intracellular cationic iron pools and inhibit any Fe-containing enzyme or promote Fe-mediated free radical damage (Chaston & Richardson, 2003).

1.1.4.2 Ascorbate Analogs

Ascorbate plays an unusual but critical role in P4H catalysis. It is not formally a component of the catalytic cycle, but is required to maintain the active oxidation state of the cationic iron cofactor. Dihydroxybenzoic acid (**1.3**) mimics the ascorbate structure and displays inhibitory activity against P4H. Due to structural similarities, **1.3** competes with ascorbate and α -KG with a K_i value equal to $5 \mu M$ (Majamaa *et al.*, 1986). In addition, doxorubicin (**1.4**) and daunorubicin (**1.5**), redox-active anthracycline compounds, display competitive inhibition with ascorbate at low concentrations while displaying irreversible inhibition of P4H at higher concentrations (Gunzler *et al.*, 1988b). These inhibitors are suggested to inactivate the enzyme during the uncoupled reaction in place of ascorbate, because they generate semiquinone radicals only with the Fe(III) state of iron (which is the same form that ascorbate specifically acts on). In human skin fibroblast cultures, these compounds exhibit 50% inhibition at $1 \mu M$ (Sasaki *et al.*, 1987). Use of these anthracyclines is, however, associated with cardiotoxicity (Wallace, 2003), which limits their use as potential anti-fibrotic therapeutics.

1.1.4.3 α -Ketoglutarate Mimics

Inhibitors of P4H based on the α -KG structure offer the most effective strategies to date. The pyridine dicarboxylic acids, pyridine-2,5-dicarboxylate (**1.6**) and pyridine-2,4-dicarboxylate (**1.7**), act as reversible inhibitors of P4H by mimicking important structural features of α -KG. The pyridine ring nitrogens and the C2 carboxylate oxygens of **1.6** and **1.7** present essential elements for cationic iron binding in the enzymic active site, while the C5 or C4 carboxylate groups satisfy the need for a Lys493 binding partner on the other end of the α -KG binding site. The 2,4-dicarboxylate **1.7** is a close mimic of α -KG, while the 2,5-dicarboxylate **1.6** has one less carbon atom than does α -KG between its cationic iron binding element and carboxylate tail. Compound **1.6** displays nearly three-fold more potency than does compound **1.7**; the K_i values are 0.8 μ M and 2.1 μ M for **1.6** and **1.7**, respectively (Majamaa *et al.*, 1984). *In vivo*, compounds **1.6** and **1.7** inhibited proline hydroxylation in fibroblast cultures with IC_{50} values of 2.2 mM and 5 mM, respectively. These data are surprising considering the structural similarities that the 2,4-dicarboxylate **1.7** shares with α -KG. Majamma *et al.* suggest that this discrepancy in structural similarity to α -KG and activity can be explained by steric hinderance in the α -KG binding site. The ring C6 of the 2,5-dicarboxylate **1.6** could force the C5-carboxylate group into a favorable alignment with Lys493 in the α -KG binding site, while the same interaction could drive the C4-carboxylate of the 2,4-dicarboxylate **1.7** away from the key contact with Lys493 in the binding site. When these compounds were studied in isolated bone microsomes, **1.7** exhibited a more potent inhibition than did **1.6**, with K_i values of 5 μ M and 100 μ M for **1.7** and **1.6**, respectively. The higher K_i value in microsomes of **1.7**

than 1.6 suggests that a specific transport system exists for α -KG in the ER (Tschank *et al.*, 1988).

Oxalylglycine (1.8) is the most potent aliphatic α -KG analog directed towards P4H inhibition yet reported, with a K_i value of 0.51 μ M (Franklin *et al.*, 1991; Cunliffe *et al.*, 1992; Baader *et al.*, 1994). Its structure is identical to α -KG with the exception of a NH group replacing the native C3 methylene. Oxalylglycine does not act as a substrate for P4H because the amide resonance donates additional electron density to the C2 carbon compared to α -KG, which prevents nucleophilic attack by the Fe-superoxide species at C2 during P4H catalysis. Heterocyclic carbonyl glycines also inhibit P4H and are more potent than oxalylglycine. These compounds include 4-hydroxycinnoline-3-carbonyl glycine (1.9), which exhibits an *in vitro* IC_{50} value of 0.02 μ M, and 4-hydroxy-isoquinoline-3-carbonyl glycine (1.10), which exhibits an IC_{50} value of 0.19 μ M *in vitro* and 20 μ M *in vivo* (Franklin *et al.*, 1991). These results with variants of oxalylglycine suggest that preorganization of the Fe-binding domain using an intramolecular hydrogen bond likely provides additional potency.

Several other heterocyclic compounds that compete with α -KG binding have also been developed to inhibit P4H activity. Most recently, a novel series of phenanthrolinones were identified to inhibit P4H (Franklin *et al.*, 2001). The most effective member of this group (1.11) contained a carboxylate on one end and a nitro group at the other end, while presumably chelating the iron center through the ring nitrogens. These phenanthrolinones displayed sub-micromolar inhibition constants in both *in vitro* and *in vivo* assays, and represent the only recent novel advances in this field.

Coumalic acid (**1.12**) is also an α -KG mimic and is the only known inhibitor of this class that acts irreversibly with P4H (Gunzler *et al.*, 1987). This compound, however, shows lower activity against human-derived P4H than chick-embryo derived P4H enzyme. In addition, successful uptake of **1.12** into cells has not been shown.

1.1.4.4 Peptide Mimics

Vertebrate P4H enzymes recognize Xaa-Pro-Gly sequences in their collagen substrates. Therefore, peptide substrate mimics have also been successful inhibitors of P4H. Long chains of polyproline residues inhibit the human P4H enzyme, but they act as substrates for P4H derived from *Caenorhabditis elegans* or green algae plant sources (Prockop & Kivirikko, 1969). In addition, peptides containing 5-oxaproline (**1.13**) function as irreversible inhibitors of P4H (Gunzler *et al.*, 1988a; Karvonen *et al.*, 1990; Wu *et al.*, 1999; Moon & Begley, 2000). These peptides can specifically trap radical intermediates through β -scission of the weak N-O bond. They behave in a syncatalytic manner by taking advantage of the radical mechanism of the enzyme.

1.1.5 The Role of Prolyl 4-Hydroxylase in the Hypoxia Signaling Cascade

In addition to collagen biosynthesis, P4H has also been implicated in the hypoxia signaling pathway, wherein P4H acts as an oxygen sensor (Bruick & McKnight, 2001; Ivan *et al.*, 2001; Jaakkola *et al.*, 2001). Under normal oxygen conditions (normoxia), a specialized, oxygen-sensing P4H enzyme hydroxylates the hypoxia inducible factor α (HIF- α), which is then recognized by the von Hippel-Lindau (VHL) tumor suppressor gene, ubiquitinated, and degraded by the proteasome. Under low oxygen conditions

(hypoxia), the HIF P4H cannot hydroxylate HIF- α , but is instead recognized by HIF- β . The α and β factors form a dimer that is translocated to the nucleus, where it binds to HIF-responsive elements (HREs) in hypoxia-inducible genes and promotes transcription (Bruick, 2003; Hewitson *et al.*, 2003). Collagen P4H enzymes do not act on HIF α , and the HIF P4H enzymes share little sequence identity to collagen P4H enzymes except for active-site residues (Myllyharju, 2003). Known inhibitors of P4H, such as dimethyloxalylglycine, cause heart cells to mimic hypoxic conditions and offer protection from metabolic inhibitors, suggesting a pharmacological strategy to induce heart protection (Wright *et al.*, 2003). Several research groups have demonstrated that P4H inhibitors have activity against this new class of HIF P4H enzymes (Ivan *et al.*, 2002; Mole *et al.*, 2003; Schlemminger *et al.*, 2003).

It is evident from the list of fibrotic diseases associated with overproduction of collagen that there is a need for specific inhibitors of P4H. The newly discovered role of P4H in hypoxia and the potential role for P4H inhibitors in tissue protection also highlight the need for continued pursuit of bioavailable inhibitors of P4H. The requirement that inhibitors cross both the cellular membrane and the ER membrane also presents a challenge to inhibitor design. The current inhibitors have not addressed the need to sustain inhibition and overcome the eventual restoration of P4H activity. Therefore, new approaches to P4H inhibition are necessary.

We have identified a bioavailable and irreversible inhibitor that addresses the problems of crossing the cellular and ER membranes, and addresses the problem of sustained inhibition by irreversible binding in the active-site of the P4H enzyme. In

addition, our inhibitor can be specifically immobilized for proteomic studies that may identify additional roles for prolyl 4-hydroxylase activity. These results are described in Chapter 2.

1.2 Metal-Mediated Inhibition of Microbial Ribonucleases

Recently, Katz *et al.* discovered a new strategy for the metal ion, Zn^{2+} , in mediating the interactions of inhibitors with enzymic active sites. These workers found that recruitment of a non-endogenous metal increased the potency of the serine protease inhibitor, bis(5-amidino-2-benzimidazolyl)methane (BABIM, **1.14**, Figure 1.3) (Katz *et al.*, 1998; Katz & Luong, 1999). By tetrahedrally coordinating to two catalytic residues and the two benzimidazole nitrogens, the metal ion, Zn^{2+} , increases the affinity of BABIM to the serine protease by 3800-fold. This result portends a new strategy to inhibit enzymes (Schirmeister, 1998; Thorp, 1998; Louie & Meade, 1999).

1.2.1 Ribonucleases

Ribonucleases, which catalyze RNA cleavage, are among the best-characterized enzymes (D'Alessio & Riordan, 1997). They are an ideal class of enzymes to study as their three-dimensional structures have been solved by x-ray diffraction studies and they are readily available in large quantity through recombinant expression in *Escherichia coli*. Various active-site variants have been produced to illuminate mechanistic details of binding and catalysis as well as substrate specificities.

The reaction mechanism of ribonucleases is well understood. They catalyze the hydrolysis of the P–O^{5'} bonds in RNA in two steps: transphosphorylation followed by

hydrolysis (Yoshida, 2001). An amino acid side chain acts as a base to abstract a proton from the 2'-hydroxyl group of the substrate RNA molecule which facilitates attack on the phosphorous atom (Figure 1.6). A second amino acid side chain acts as an acid to protonate the 5''-oxygen, which facilitates the displacement of the cleaved nucleoside. In a separate step, the resulting 2',3'-cyclic phosphodiester is released to solvent and slowly hydrolyzed by the enzyme.

The ribonuclease angiogenin fosters neovascularization through its ribonucleolytic activity (Shapiro & Vallee, 1989). Inhibition of this enzyme suppresses tumor growth (Riordan, 1997). Inhibitors of secretory ribonucleases are essential for laboratory studies of RNA, providing further motivation for the development of new ribonuclease inhibitors. Ribonuclease inhibitor protein (RI) is a potent natural inhibitor of mammalian secretory ribonucleases, but is extremely unstable in oxidative environments (Shapiro, 2001). Therefore, the development of small-molecule ribonuclease inhibitors could lead to novel therapeutics and superior laboratory reagents.

1.2.2 Microbial Ribonucleases

Microbial ribonucleases from the RNase T₁ family (EC 3.1.27.3) consist primarily of guanyl-specific endonucleases using the catalytic acid/base pair of His and Glu (Irie, 1997). The RNase T₁ family represents a group of enzymes with diverse disulfide-bonding patterns that are well characterized for their protein folding behavior. Members of this family include RNase Bi (Binase), RNase T1, and RNase Sa. Binase is secreted from the bacteria *Bacillus intermedius* and contains no disulfide bonds, which makes it a strong model system for studying non-oxidative protein folding. RNase T1 is secreted by

the mold fungus, *Aspergillus oryzae*. Unlike Binase, RNase T1 possesses two disulfide bonds. Finally, RNase Sa is a secreted ribonuclease from the bacteria *Streptomyces aureofaciens*. RNase Sa contains one disulfide bond and acts as an evolutionary bridge between the simple ribonucleases of *Bacillus* and the more complex ribonucleases from *Aspergillus* (Hartley, 1997).

Interestingly, the sequence identity between members of the RNase T₁ family does not extend much further than their catalytic residues (Sevcik *et al.*, 1990). In fact, the isoelectric points for the different family members are drastically different. RNase Sa and T1 are negatively charged ribonucleases exhibiting pI values of 3.5 and 4.5, respectively, while Binase is a positively charged ribonuclease exhibiting a pI value of 9.6 (Pace *et al.*, 1991; Hartley, 1997).

1.2.3 Small-Molecule Ribonuclease Inhibitors

Current evidence indicates that the enzymatic properties of various ribonucleases derived from different species are similar and that compounds with activity against a particular ribonuclease will likely inhibit other distinct ribonucleases (Russo *et al.*, 2001). Early work on small-molecule inhibitors of ribonucleases revealed that mononucleotides and dinucleotides mimicking substrate or product analogs exhibited inhibitory activity. Compounds such as thymidine 3',5'-diphosphate (**1.15**) and adenosine 3',5'-diphosphate (**1.16**) display low micromolar inhibition constants (Figure 1.5) (Sawada & Irie, 1969; Iwahashi *et al.*, 1981). These compounds illuminated important nucleobase- and phosphoryl group-binding specificity.

Bioinorganic compounds such as uridine 2',3'-cyclic vanadate (U>v, **1.17**) also inhibit ribonucleases (Lindquist *et al.*, 1973). In the case of RNase A, this complex coordinates active-site histidines to vanadium-bound oxygens in a complex that was designed to mimic the enzymic transition state. The U>v complex exhibits a K_i value of 0.45 μM , which is 10,000-fold less than that of the K_m value for the reaction intermediate uridine cyclic phosphate (U>p) (Leon-Lai *et al.*, 1996). Despite this relatively strong affinity, only 80% of RNase A is bound by U>v at 10 mM uridine and 100 μM vanadate at pH 7 (Lindquist *et al.*, 1973).

Uridine 3'-[4-(fluoromethyl)phenyl] phosphate (UpOC₆H₄-*p*-CH₂F, **1.18**) acts as an irreversible mechanism-based inactivator of RNase A (Stowell *et al.*, 1995). The quinone methide product of UpOC₆H₄-*p*-CH₂F turnover by RNase A alkylates side-chain residues of the enzyme. Unfortunately, this inactivation only proceeds to 66% completion.

Adenosine 5'-pyrophosphate derivatives represent a new class of nucleotide inhibitors with high affinity for ribonucleases. These pyrophosphate-bridged nucleotides bind to multiple nucleobase- and phosphoryl group-binding subsites, which contribute to their increased potency (Leonidas *et al.*, 1997; Russo *et al.*, 1997). From this series, the 5'-phospho-2'-deoxyuridine 3'-pyrophosphate P'→5' ester with adenosine 3'-phosphate (pdUppAp, **1.19**) emerged as the most potent known small-molecule inhibitor of a ribonuclease with a K_i value of 0.22 μM (0.2 M Hepes buffer, pH 7.0, with no added salt) for the inhibition of RNase A (Russo & Shapiro, 1999).

Our extensive understanding of the chemical, physical, and functional properties of microbial ribonucleases of the RNase T₁ family makes them a good model to study inhibitors of ribonucleases. In addition, the availability of active-site variants of microbial ribonucleases from recombinant DNA expression makes it possible to reveal the mechanism of inhibition.

Hydroxamic acids coordinate strongly with metal ions, particularly Zn²⁺ (Babine & Bender, 1997). This motif is the most effective zinc(II)-binding functional group in inhibitors of matrix metalloprotease enzymes, including carboxypeptidase A (Levy *et al.*, 1998; Yamamoto *et al.*, 1998; Mock & Cheng, 2000). Furthermore, zinc(II)-containing histone deacetylases undergo rapid inhibition in the presence of hydroxamic acid inhibitors (Miller *et al.*, 2003). The hydroxamate group binds transition metals such as zinc(II), through bidentate ligation primarily as a deprotonated *O*-acid (Babine & Bender, 1997). In solution, the terminal OH groups of hydroxamic acids display p*K*_a values in the range of 8–10. The *N*-hydroxyurea is known to bind zinc(II) in the same manner as a hydroxamic acid and is also used in zinc(II)-binding inhibitors (Greco *et al.*, 1992; Connolly *et al.*, 1999; Chung & Kim, 2001).

Zinc(II) is the second most abundant trace metal in the body after iron, and the average human contains nearly 2.3 g of zinc(II) (McCall *et al.*, 2000). Although its filled *d*-orbital renders this transition metal redox-inactive, it can function as a Lewis acid to accept a pair of electrons. Moreover, it can adopt several coordination geometries without energetic barriers between them, and it is this property that allows metalloenzymes to

tune the reactivity of this metal through changes in its ligand conformations. Therefore, zinc(II) can act as a versatile, redox-stable ion catalyst in fluctuating environments.

We have developed a novel inhibitor of ribonucleases that uses a Zn^{2+} ion and an *N*-hydroxyurea. Our strategy was to combine a metal with a chelating functional group and demonstrate exogenous metal inhibition of non-metalloenzymes other than proteases. Our knowledge from inhibitor design in the P4H system has allowed us to apply what we learned to the development of a metal-dependent inhibitor of ribonucleases. These results are described in Chapters 3 and 4.

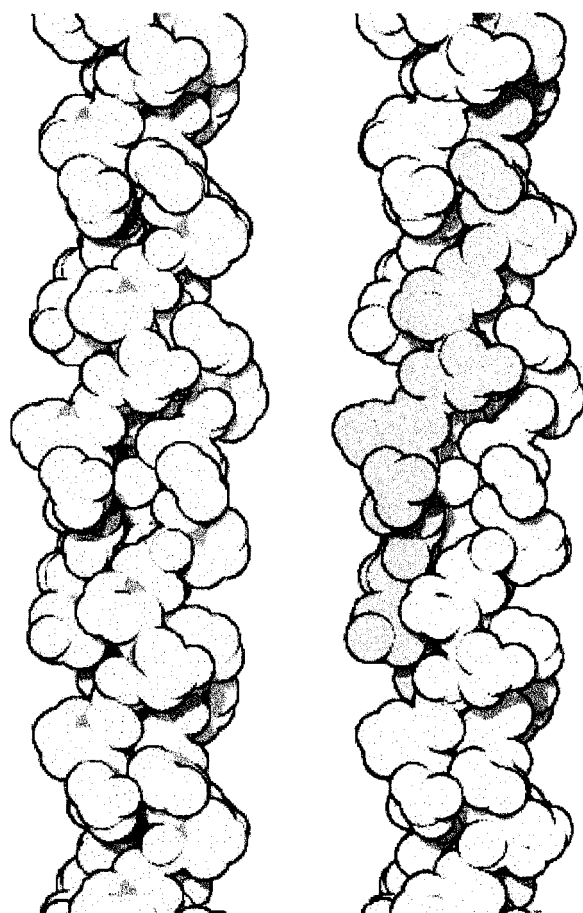


Figure 1.1 Structure of crystalline collagen triple helices from a peptide containing repeats of Pro-Hyp-Gly. On the left, the Hyp hydroxyl groups are shown in red. On the right, each of the three α -chains is shown in a different color. (PDB ID: 1CAG (Kramer *et al.*, 1999))

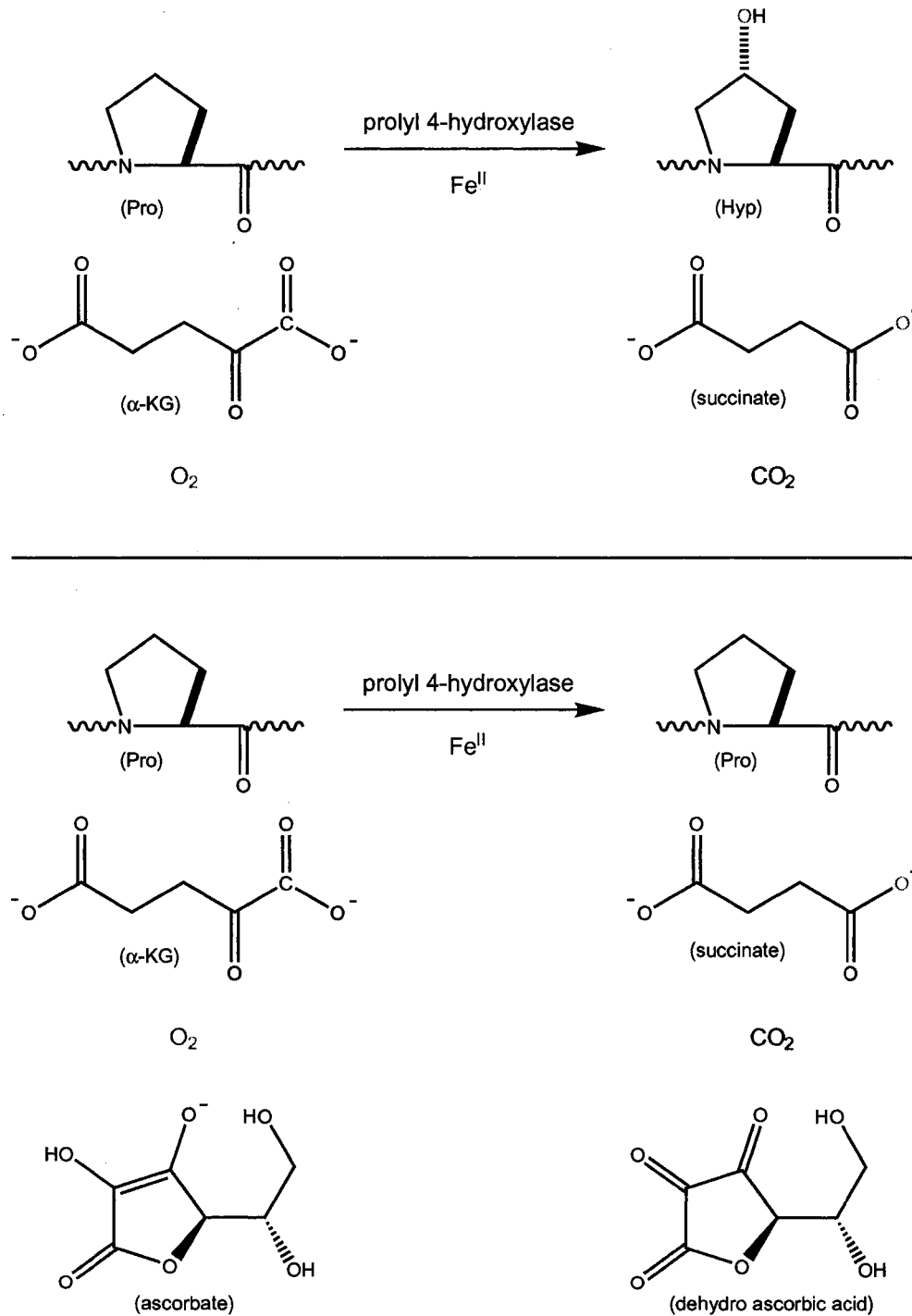


Figure 1.2 Top: the hydroxylation reaction catalyzed by prolyl 4-hydroxylase. Below: the α -KG uncoupled decarboxylation reaction associated with prolyl 4-hydroxylase in which ascorbate is oxidized and the cationic iron is reduced back to its resting state.

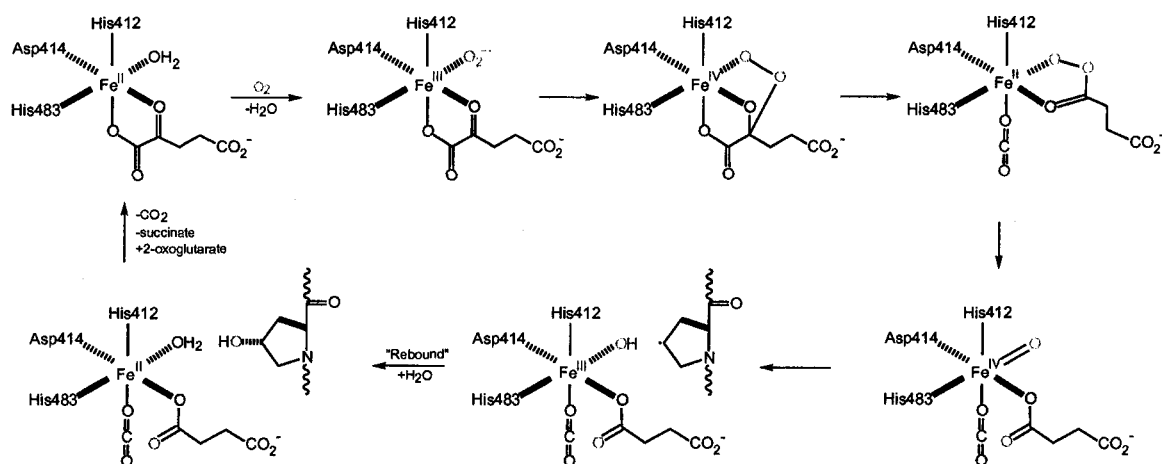


Figure 1.3 Proposed mechanism of proline hydroxylation by P4H. Derived from (Costas *et al.*, 2004)

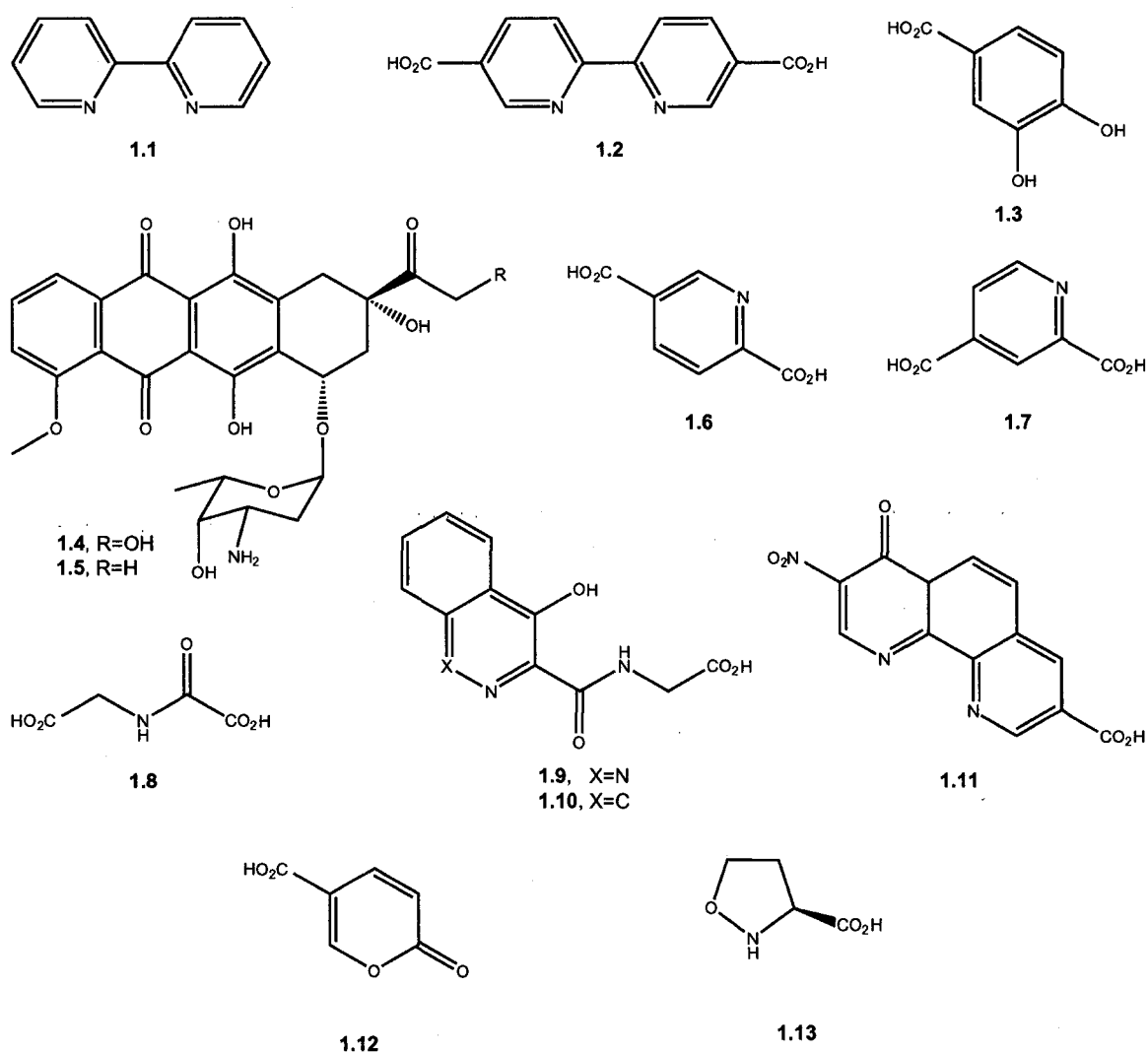


Figure 1.4 Examples of known inhibitors of P4H.

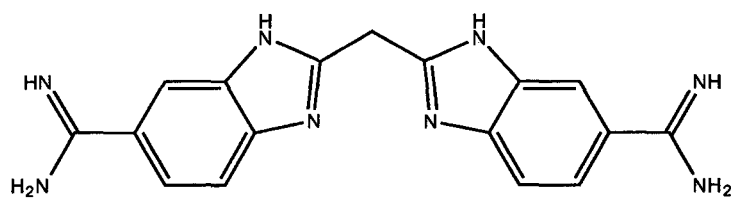


Figure 1.5 bis(5-amidino-2-benzimidazolyl)methane (1.14, BABIM)

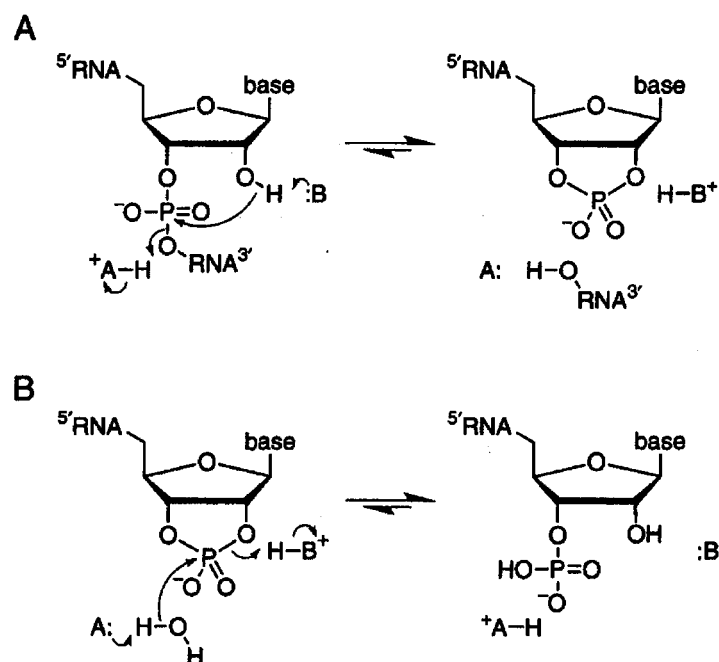


Figure 1.6 A. Putative mechanism of ribonuclease transphosphorylation. B. Putative mechanism of ribonuclease hydrolysis. For microbial RNases "A" is histidine and "B" is glutamate. Adapted from (Raines, 1998).

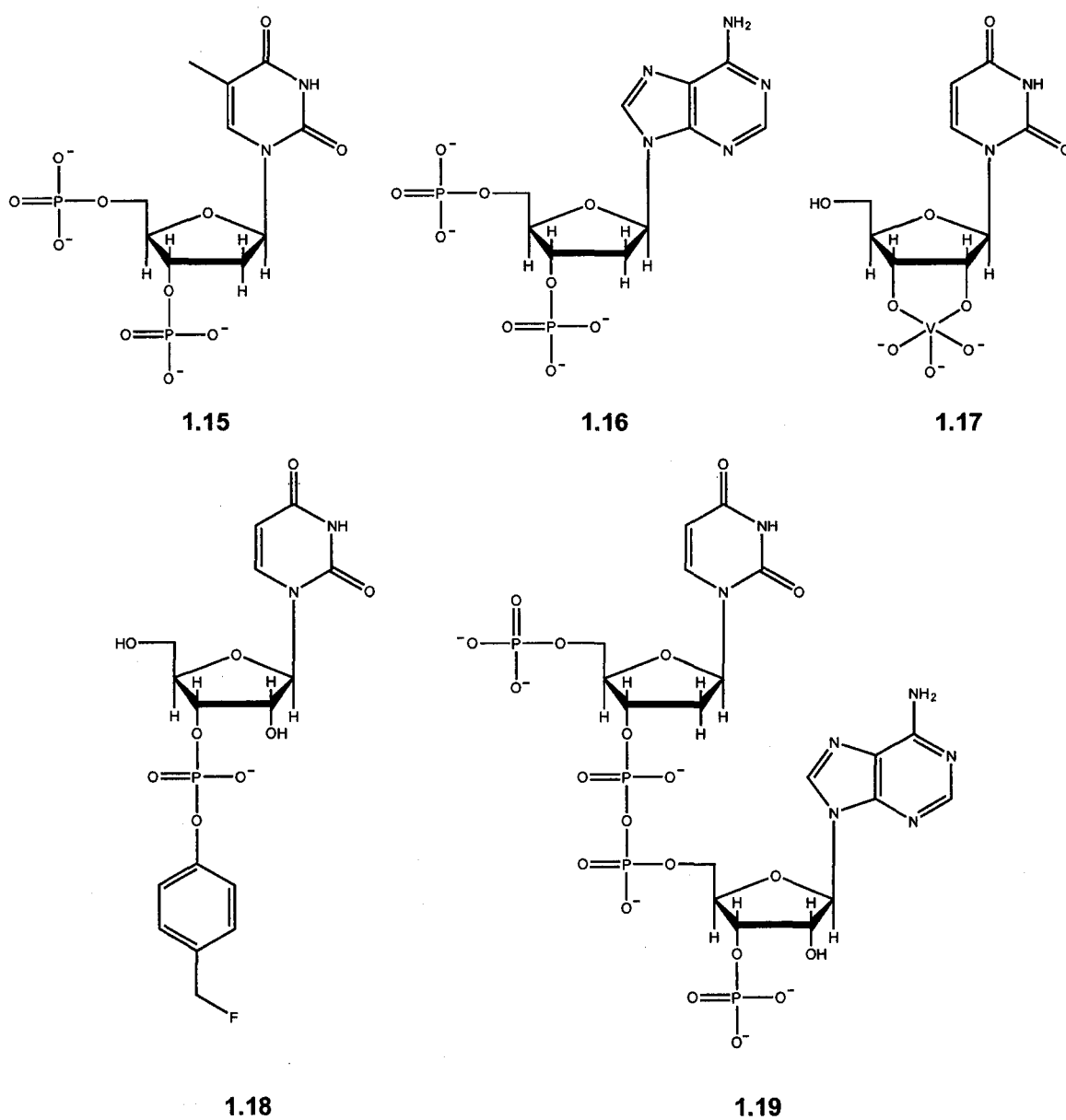


Figure 1.7 Examples of small-molecule ribonuclease inhibitors.

Chapter Two

Bioavailable Inhibitors of Prolyl 4-Hydroxylase

2.1 Abstract

Collagen is the most abundant protein in animals. The hydroxyl groups of the prevalent 4(*R*)-hydroxyproline residues contribute greatly to the conformational stability of collagen. These hydroxyl groups arise from the post-translational modification of proline residues by the iron-dependent enzyme prolyl 4-hydroxylase (P4H). Inhibitors of P4H diminish collagen stability and could be used to treat scarring, fibrosis, and fibroproliferative disorders in humans. Reverse genetics can reveal the phenotype of a mutant organism that lacks a specific protein. A small molecule that mimics that phenotype is likely to be a ligand of the protein. We have developed a sensitive *in vivo* assay for bioavailable inhibitors of P4H. The assay uses the nematode *Caenorhabditis elegans*, which is the best characterized animal. A *C. elegans* mutant that lacks one of the two genes that encode P4H is viable, but its progeny die when exposed to low levels of P4H inhibitors. This assay was used to screen new inhibitors based on α -ketoglutarate, which is a cosubstrate of P4H. We discovered an epoxy ketone that binds covalently to P4H and inhibits the enzyme *in vivo* and irreversibly inactivates the enzyme *in vitro*.

2.2 Introduction

Collagen is the most abundant protein in animals (Prockop & Kivirikko, 1995; Kivirikko & Pihlajaniemi, 1998; Myllyharju & Kivirikko, 2001; Jenkins & Raines, 2002). This protein plays a critical role in maintaining the structural integrity of various connective tissues. The overproduction and overaccumulation of collagen is associated with fibrotic diseases, such as scleroderma, organ fibrosis, cirrhosis, keloids, and scarring (Hanauske-Abel & Guenzler, 1982; Franklin *et al.*, 1991; Cunliffe *et al.*, 1992; Franklin, 1995; Bickel *et al.*, 1998; Kim *et al.*, 2000; Franklin *et al.*, 2001). The stability of collagen is derived from its triple helical structure and several important post-translational modifications. The enzyme P4H hydroxylates proline residues in procollagen, which increases the conformational stability of the triple helix (Berg & Prockop, 1973b; Rosenbloom *et al.*, 1973). P4H is a $\alpha_2\beta_2$ tetramer located in the lumen of the endoplasmic reticulum (ER) and has been studied in humans, mice, chickens, and worms (Guzman, 1998; Kivirikko & Pihlajaniemi, 1998; Myllyharju, 2003; Myllyharju & Kivirikko, 2004). Inhibitors of P4H thus present a viable therapeutic approach to treating collagen-related diseases.

Although various small molecules have been shown to inhibit P4H, many do not display strong *in vivo* activity. P4H resides in the ER; therefore, inhibitors must traverse both the cell membrane and the ER membrane. In order to pass through the cell membrane, compounds must exhibit general lipophilicity. Conversely, compounds traversing the ER membrane must meet the requirements of a specific transport system, which are under investigation (Tschank *et al.*, 1988). One solution to this challenge

utilizes a pro-drug strategy (see Figure 2.1 for examples of prodrugs). For example, diethyl pyridine-2,4 dicarboxylate (**2.1**), a prodrug form of pyridine-2,4-dicarboxylate (see Chapter 1), crosses the cellular membrane and is thought to be deesterified by nonspecific esterases in the cytoplasm (Bundgaard, 1985; Silverman, 1992). Interestingly, the IC_{50} for **2.1** is 65-fold greater than its parent form when tested *in vitro* (Tschank *et al.*, 1991). Additionally, dimethyloxalylglycine (**2.2**), an ester prodrug form of oxalylglycine (see Chapter 1), exhibits at least 100-fold more activity than its parent drug *in vivo* (Baader *et al.*, 1994).

Unlike the ester prodrug, the amide prodrug, HOE 077 (pyridine-2,4-dicarboxylic-di-(2-methoxyethyl)amide; Lufironil; **2.3**) is stable to blood plasma and was the first P4H inhibitor based on α -KG to enter clinical trials (Bickel *et al.*, 1991; Boeker *et al.*, 1991; Sakaida *et al.*, 1994). In animal studies, HOE 077 (**2.3**) reduces hepatic collagen content in CCl_4 -induced fibrosis, bileduct ligation fibrosis, and choline-deficient diet induced fibrosis. In the liver, HOE 077 is converted to a number of metabolites, including pyridine-2-carboxylate, which is known to give weak inhibition of P4H *in vitro* (Kellner *et al.*, 1991). Surprisingly, the assumed active species, pyridine-2,4-dicarboxylate, was not identified as a metabolite.

Based on the different activities observed *in vitro* and *in vivo*, we decided to develop an *in vivo* assay system that would identify inhibitors that both inhibit P4H specifically and are bioavailable. *Caenorhabditis elegans*, the most well characterized animal model system, provides an excellent vehicle to study collagen biosynthesis. Simple body morphology with known cellular lineage and the completely sequenced

genome of this nematode provide an ideal background for detailed *in vivo* studies (Wood, 1988; The *C. elegans* Sequencing Consortium, 1998).

C. elegans contains two genes that code for collagen P4H α subunits. The *dpy-18* (also known as *phy-1*) gene codes for an α subunit that is essential for body morphology, while the *phy-2* gene has no apparent essential function (Friedman *et al.*, 2000). The *dpy-18* deletion mutant worm displays a dumpy phenotype (a short, squat, and deformed body shape), while the *phy-2* deletion mutant worm has no apparent phenotype (Figure 2.2). These two forms of the α -subunit share 56.5% amino acid sequence identity with each other, and share about 50% sequence identity with their human counterparts. The main form of P4H in wild-type *C. elegans* exists as a DPY-18/PHY-2/PDI₂ mixed tetramer (Myllyharju *et al.*, 2002). In the absence of either the DPY-18 or the PHY-2 form of the α -subunit, an $\alpha\beta$ dimer consisting of DPY-18/PDI or PHY-2/PDI provides the P4H activity essential for cuticle development (Friedman *et al.*, 2000; Myllyharju *et al.*, 2002). The deletion of both the *dpy-18* and the *phy-2* genes results in embryos that grow to the twofold stage, but are unable to maintain their shape and consequently explode (Figure 2.3)(Friedman *et al.*, 2000). We have utilized this phenotype to develop a sensitive assay to screen for bioavailable inhibitors of P4H.

A key component of our assay is the sensitivity inherent in the mutant animal, *dpy-18*. In this mutant animal, a significant fraction of P4H activity is missing. Therefore, chemical inhibitors can readily eliminate remaining P4H activity (which arises from only one enzyme), and thereby mimic the phenotype of the double deletion (Figure 2.3). The stringent requirements of this assay rely on the ability of a compound to enter the worm

by either oral ingestion or dermal diffusion, and interact with the target protein in the embryos. This chemical genetics approach to drug discovery using whole animal model systems such as zebrafish, *Arabidopsis*, and drosophila is gaining acceptance as a tool for drug discovery (Crews & Splittgerber 1999; Zhao *et al.*, 2003 Peterson *et al.* 2004). This approach offers an easy method to screen libraries of bioavailable inhibitors of P4H.

Studying P4H presents certain problems. First, a source of purified enzyme is not readily available, which makes assaying this enzyme for *in vitro* inhibitor activity difficult (Vuori *et al.*, 1992). Second, the *in vitro* assays are very complex, as they involve multiple reaction components. The most common method for measuring hydroxylation is a discontinuous indirect assay that measures CO₂ production as opposed to proline hydroxylation (Berg & Prockop, 1973a; Kivirikko & Myllylae, 1982). In addition, *in vivo* studies usually involve measuring tissues for collagen production or measuring Hyp/Pro ratios in collagen after protein extraction and purification. These two assays tend to be inexact and non-reproducible (Baader *et al.*, 1994).

The need for specific inhibitors of P4H is evident from the list of fibrotic diseases associated with overproduction of collagen. In addition, the newly discovered role of P4H in hypoxia and the potential role for P4H inhibitors in tissue protection highlight the need for new effective therapeutics (Ivan *et al.*, 2002; Mole *et al.*, 2003; Schlemminger *et al.*, 2003; Wright *et al.*, 2003). The difficulty of finding inhibitors that can cross both the cellular membrane and the ER membrane also presents a challenge. The current inhibitors do not address the need for long-lasting effectiveness to sustain inhibition and overcome the eventual restoration of P4H activity. We have developed both a method to

screen for bioavailable inhibitors using the *dpy-18* mutant nematode and an *in vitro* assay to monitor the hydroxylation of proline residues in a time-dependent manner. Using these tools, we have identified bioavailable inhibitors of P4H that provide a starting point for the development of effective chemotherapeutics based on the control of P4H activity.

2.3 Results and Discussion

2.3.1 Development of an Assay for Bioavailable Inhibitors of P4H Using *C. elegans*

In order to identify bioavailable inhibitors of P4H, an *in vivo* assay using the animal model, *C. elegans*, was developed (Friedman *et al.*, 2000). *C. elegans* contains two genes encoding collagen P4H. The assay utilizes two distinct mutant nematodes in which only one of the two genes is expressed (Friedman *et al.*, 2000). The *dpy-18* gene is expressed in the cuticle, which constrains the animal's body morphology. Its deletion results in a dumpy phenotype where the body shape is generally short and fat compared to a wild-type animal (Figure 2.2). The *phy-2* gene is expressed in the basement membranes and its deletion has a wild-type phenotype (Figure 2.2). The double-deletion animal, however, displays a phenotype in which the progeny are not viable due to incomplete cuticle development, indicating no production of P4H (Figure 2.3).

We hypothesized that complete chemical inhibition of the P4H enzyme using known inhibitors in the nematode system should result in the same phenotype as the double-deletion animal (that is, inviable progeny). Therefore, the α -KG mimics, diethyl-2,4-pyridine dicarboxylate (2.1) and dimethyloxalylglycine (2.2) were synthesized (Tschank *et al.*, 1991; Cunliffe *et al.*, 1992; Baader *et al.*, 1994). They are two well-

studied, bioavailable inhibitors that have been shown to be active against P4H *in vivo* and in whole cell assays (Tschank *et al.*, 1991; Baader *et al.*, 1994). As ester prodrugs, their translocation through cellular membranes is expected, in contrast to the active form of the drugs, which are anionic at physiological pH. Upon translocation, nonspecific esterases within the cell hydrolyze the prodrugs to their active forms, and these carboxylate compounds inhibit the P4H enzyme at low micromolar concentrations *in vitro* (Tschank *et al.*, 1987; Baader *et al.*, 1994).

To expose nematode animals to the known P4H inhibitors, plates containing growth medium were soaked with inhibitor compounds (see figure 2.4). L4-stage worms were then placed onto the media and allowed to mature and lay eggs. After sufficient time had elapsed for embryos to hatch, lethality was assessed by determining the ratio of hatched to unhatched (that is, dead) eggs. These ratios enable the determination of an LC₅₀ value based on the concentration of inhibitor in the growth media plate. (The concentration of inhibitor in the animals or embryos is not determined.)

When the *dpy-18* nematodes were treated with diethyl 2,4-pyridine dicarboxylate or dimethyloxalylglycine, they did indeed exhibit the same phenotype as the double deletion animal (Figure 2.3). These data indicate that the embryonic lethality is due to P4H inhibition and not to the general toxicity of the compounds, as most of the adult worms remain viable. In addition, when other *C. elegans* animals containing different collagen related gene deletions were tested against these inhibitors, they exhibited the same dose-response curves as did the wild-type animals (Friedman *et al.*, 2000). Again, these results suggest that the response observed is due to specific inhibition of P4H. To

demonstrate further that the observed embryonic lethality is due to P4H inhibition, we also compared the responses of the wild-type and the *phy-2* deletion animal. If inhibition is specific to P4H, the deletion animals should display increased sensitivity. Indeed, upon exposure, the *phy-2* deletion animals showed more susceptibility to the inhibitors than did the wild-type animals. Moreover, the *dpy-18* deletion animal displayed about 10-fold greater sensitivity to the inhibitors than the wild-type, but the *phy-2* deletion animal displayed only about twofold greater sensitivity to the inhibitors than the wild-type animal (Figure 2.5). This result is consistent with the phenotypes of the single-deletion animals. Therefore, in subsequent experimentation, inhibitors were tested only against the *dpy-18* deletion animal, and the apparent LC₅₀ values from compounds **2.1** and **2.2** were used as benchmarks for bioavailable inhibitory activity.

2.3.2 Development and Screening of Novel α -Ketoglutarate Mimics in *C. elegans*

2.3.2.1 Library of N-Branched Oxalylglycine Compounds

P4H requires α -KG as a necessary cosubstrate for enzymatic activity. Oxalylglycine, an α -KG mimic, strongly inhibits enzyme activity *in vitro* and *in vivo* (Cunliffe *et al.*, 1992). In contrast, other oxalyl-amino acids with varying α -branched functionalities (corresponding to the C4 position on α -KG) exhibit little activity against P4H (Franklin *et al.*, 1991; Baader *et al.*, 1994). This series of compounds explored only one side of the corresponding binding pocket and indicated that the putative α -KG-backbone binding subsite does not tolerate branching off of the α -carbon of the oxalylglycine (Majamaa *et al.*, 1984). Accordingly, a series of *N*-branched oxalylglycine

compounds were designed to explore contacts on the opposite side of the binding pocket (corresponding to the C3 position of α -KG).

The strategy involved a library based on *N*-branched oxalylglycine, and was comprised of three components. First, glycine attached to solid support was coupled to various aldehydes to form the corresponding imines (Scheme 2.1). Reductive amination of the imine intermediates resulted in secondary amines that were capped subsequently by an oxalyl group to form derivatives of **2.2**. Finally, cleavage of the compounds was followed by thionyl chloride esterification of the free carboxylic acid groups. This resin based-strategy yielded products of high purity, as most of the impurities were removed by three distinct wash steps. In total, 25 compounds (Figure 2.6) were synthesized in parallel, with a model compound (**2.4**) characterized by ^1H NMR spectroscopy, and its purity assessed to be $\geq 95\%$. The NMR spectroscopic analysis of our model compound revealed two nearly equal populations of species due to rotation about the tertiary amide bond.

Each compound was assayed against the *dpy-18* deletion animal at various concentrations up to 1 mM. Unfortunately, none of the compounds exhibited the characteristic activity of P4H inhibition in this assay. These data indicate that the α -KG pocket or the specific uptake system does not tolerate branching at the *N*-position of oxalylglycine. In addition, the backbone rigidity of the molecule could play an important role in binding as shown by **2.1** and 4-hydroxyisoquinoline 3-carboxylate (see Chapter 1), which are both strong inhibitors of P4H (Franklin *et al.*, 1991). The structure of these

molecules forces them into constrained conformations, unlike the library developed herein.

2.3.2.2 Dimethyl-6-hydroxy-2,4-pyridine dicarboxylate

The potent P4H inhibitor, diethyl 2,4-pyridine dicarboxylate (**2.1**) crosses through the cellular membrane and undergoes ester hydrolysis in the cytosol. It has been suggested that the resulting 2,4-pyridine dicarboxylate crosses the ER membrane via a selective uptake mechanism (Tschank *et al.*, 1991) to display strong inhibition against P4H in the ER. Based on this result, we sought to develop a pyridine dicarboxylate derivative that would increase the affinity for the active-site Fe(II) and yet maintain the same bioavailability. Because **2.1** is thought to chelate the active site iron center through the ring nitrogen and C2 carbonyl (Tschank *et al.*, 1987), increasing the electron density on the nitrogen is expected to enhance cationic iron binding. Therefore, we designed dimethyl-6-hydroxy-2,4-pyridine dicarboxylate (**2.6**) to enhance the electron density on the nitrogen through resonance.

Compound **2.6** was synthesized using the enzymatic oxidation of asparagine to 6-hydroxy-2,4-pyridine dicarboxylate (Stephani & Meister, 1971) followed by esterification with thionyl chloride in methanol. At 290 μ M, this compound displayed no activity against the *dpy-18* nematode. Again, there are several possible explanations for these results. The addition of a hydroxyl group could render this compound too large to fit in the α -KG binding site. Additionally, the selective uptake system may not recognize **2.6** as α -KG and exclude it from the target P4H enzyme. The selective uptake system is very specific to α -KG-like molecules, facilitating transport of 2,4-pyridine dicarboxylate

but not 2,5-pyridine dicarboxylate (Tschank *et al.*, 1987; Hanauske-Abel, 1991; Tschank *et al.*, 1991). The hydroxyl group on **2.6** represents an additional deviation from α -KG compared to 2,4-pyridine dicarboxylate. This deviation could prevent its uptake into the ER, as the exact substrate specificity for the uptake mechanism is unknown.

2.3.2.3 Hydroxamic Acid Analog of α -Ketoglutarate

Hydroxamic acids provide excellent metal binding ligands and are common inhibitors of metalloenzymes (Sigel & Sigel, 1998; Farkas *et al.*, 2000b; Mock & Cheng, 2000). We chose to develop a hydroxamic acid inhibitor of P4H that mimics the structure of α -KG. The structure of our inhibitor, *N*-hydroxy-succinamic acid ethyl ester (**2.7**), varies from α -KG by two atoms. Instead of the acid carbonyl C=O of α -KG, we have added an N-H in **2.7**. This hydroxamic acid is also a good mimic of the peracid intermediate that has been proposed in the catalytic mechanism of α -KG-dependent iron oxidases (Scheme 4.2)(Valegard *et al.*, 2004).

Compound **2.7** was synthesized from ethyl succinyl chloride and hydroxyl amine. When the hydroxamic acid inhibitor **2.7** was tested in the nematode assay at concentrations up to 7 mM, no inhibition was detected.

2.3.2.4 Electrophilic α -Ketoglutarate Analogs

Several α -KG analogs were explored that could bind irreversibly to P4H after attack by an active-site nucleophile. Thus, dehydro α -KG (**2.10**) was synthesized to serve several purposes. First, it could act as a Michael acceptor, binding irreversibly to the active site if a nucleophilic amino acid side chain were to attack through a 1,4 addition. Second, it exhibits more rigidity than α -KG, similar to that of dimethyloxalylglycine

(2.2). In addition, we examined an intermediate in the chemical synthesis of dehydro α -KG because it could also serve as an irreversible inhibitor. Dimethyl 3-bromo-2-oxoglutarate (2.9) is susceptible to nucleophilic attack by an enzymic side chain which could displace bromine and bind to the enzyme irreversibly. Furthermore, dimethyl 3,4-dibromo-2-oxoglutarate (2.11) can be prepared by a simple conversion from 2.10. Esterification followed by bromination of α -KG yields dimethyl 3-bromo-2-oxoglutarate (2.9). Elimination of HBr from 2.9 gives dimethyl 3,4-dehydro-2-oxoglutarate (2.10) (Carrigan *et al.*, 2002), and bromination of 2.10 generates 2.11 (scheme 2.2).

Each electrophilic analog of α -KG (2.9, 2.10, and 2.11) was tested with the nematode *dpy-18* mutant nematode for bioavailable P4H inhibition. Again, these compounds displayed no *in vivo* activity when assayed at concentrations between 0.5 mM and 1.0 mM. One possible explanation for these results is that each of these three inhibitors acts as a substrate for P4H by mimicking α -KG. If the rate of enzymatic turnover and product release is faster than that of nucleophilic attack, then no inhibition would be detected. These compounds are very electrophilic and may not be stable to the assay conditions. Additionally, it remains unknown whether these compounds are substrates for selective uptake into the endoplasmic reticulum.

2.3.2.5 Epoxy Ketone Analog of α -Ketoglutarate

The design of an epoxide-based α -KG mimic (2.13) could be used to explore and exploit the region near the active site Fe(II) of P4H for nucleophilic residues. Specifically, epoxide 2.13 could bind Fe(II) using its ketone and epoxide oxygens, while maintaining a carboxylate to bind to Lys493. If a nucleophilic side chain resides near the

iron-binding region, the epoxide should be susceptible to attack. The coordination of the epoxide to the iron center would activate the epoxide for nucleophilic attack specifically in the active site. Although this compound was originally reported to display competitive inhibition with 5-aminolaevulinic acid dehydratase, which like P4H is a metal-dependent enzyme, it has not been shown to act as an irreversible inhibitor (Appleton *et al.*, 1998).

Reaction of ethyl 4-chlorooxobutylate with tributylvinyltin and a palladium catalyst produced ethyl 4-oxo-5-hexenoate (**2.12**) according to the method of Milstein and Stille (Milstein & Stille, 1979). Its treatment with hydrogen peroxide formed the epoxide product **2.13** (Scheme 2.3) (Appleton *et al.*, 1998). When this compound was tested for P4H inhibition against *dpy-18* animals, concentration dependent embryonic lethality was observed (Figure 2.8). Determination of the approximate LC₅₀ value indicated that at 65 μ M epoxy ketone **2.13** in the growth medium, half of the nematode progeny were not viable. These data compare favorably to that of diethyl pyridine dicarboxylate **2.1** and dimethyloxalylglycine **2.2**, which exhibit LC₅₀ values of 90 μ M and 74 μ M, respectively.

Given that **2.13** showed strong activity *in vivo*, we sought to characterize the extent and mode of binding of the carboxylate derivative (**2.19**) of epoxy ketone **2.13** *in vitro*.

2.3.3 In Vitro Characterization of the Epoxy Ketone as an Irreversible Inhibitor

2.3.3.1 Development of a Simple in vitro Assay for Prolyl 4-Hydroxylase

Characterization of the epoxide inhibitor **2.19** (Scheme 2.3) required *in vitro* analysis with purified P4H. Current strategies monitor the release of radiolabeled CO₂

from α -KG as an indirect measurement of proline hydroxylation (Berg & Prockop, 1973a; Kivirikko & Myllylae, 1982). This assay has a number of disadvantages. For example, it cannot distinguish between hydroxylation-coupled decarboxylation and the uncoupled decarboxylation that occurs even in the presence of the peptide substrate. Several control reactions must be preformed simultaneously to subtract out the effects from this unproductive decarboxylation. In addition, the assay requires the use of radioactive substrates and analysis of a gaseous product. Therefore, we sought to develop an alternative method to analyze P4H hydroxylation using direct observation of the Hyp product using a chromophore-tagged substrate (**2.20**) and its hydroxylated product (**2.21**).

Begley and coworkers illustrated that a small peptide could serve as a substrate for P4H (Tandon *et al.*, 1998; Wu *et al.*, 1999; Moon & Begley, 2000; Wu & Begley, 2000). Based on these studies, we synthesized dansyl-Gly-Phe-Pro-Gly-OEt (**2.20**) and dansyl-Gly-Phe-Hyp-Gly-OEt (**2.21**) using standard solution and solid phase peptide synthesis strategies (Scheme 2.4). Chromatographic conditions to separate substrate and product were developed using a reversed-phase C18 column on an HPLC equipped with autosampler capabilities. Baseline resolution between the two peptide species was achieved within 10 min (Figure 2.9). This assay allowed direct detection of hydroxylated products at specific time points along the enzymatic reaction course. The use of a dansyl group appended to the peptide substrate allowed observation of the peptide at 337.5 nm without interference from other reaction components.

To validate this assay we determined the kinetic parameters of substrate **2.20** using human P4H enzyme produced in baculovirus insect cells (Vuori *et al.*, 1992) which

was received as a generous gift from J. Myllyharju (University of Oulu, Finland). Enzymatic reaction mixtures contained P4H (0.43 μM), FeSO_4 (50 μM), ascorbate (2 mM), $\alpha\text{-KG}$ (0.5 mM), catalase (0.1 mg/ml), DTT (0.1 mM), BSA (1 mg/ml), and substrate **2.20** (0.5 mM) in 50 mM Tris-HCl, pH 7.8 (Kaule & Guenzler, 1990). FeSO_4 provides the cationic iron source for the enzymic active site, while ascorbate serves to maintain the cationic iron in the correct oxidation state. Catalase preserves the oxygen content within the solution, and DTT maintains the solution in a reducing environment. Because the stability of the P4H enzyme is diminished in dilute solution, added BSA helps maintain the viscosity of the solution. The reaction was initiated by the addition of peptide substrate (**2.20**), and aliquots were removed at known times and quenched by boiling for 30 s. At increasing peptide substrate concentrations, P4H exhibited first-order kinetics (Figure 2.11). The values for V_{max} and K_{m} were determined to be 0.04 μM Hyp/sec and 0.09 mM respectively. Determination of k_{cat} revealed a value of 0.09 s^{-1} . It should be noted that these parameters could be lower limits due to some degradation of the enzyme during prolonged storage at $-20\text{ }^{\circ}\text{C}$.

The gift of recombinant enzyme from J. Myllyharju provided insufficient quantities to complete the necessary studies to fully characterize the epoxide inhibitor **2.19**. Therefore, a method was developed to produce large quantities of human P4H enzyme in *Escherichia coli* (E.A. Kersteen and R.T. Raines, unpublished results). Kinetic assays of this enzyme were performed using the same reaction conditions as was used to test the P4H produced in baculovirus. First-order kinetics with respect to the peptide substrate **2.20** was again observed (Figure 2.10). Determination of V_{max} and K_{m} revealed

values of 0.4 μM Hyp/sec and 0.05 mM respectively. The k_{cat} value was 0.7 s^{-1} , which was approximately 10-fold higher than that determined for the enzyme produced in baculovirus (*vide supra*). The K_{m} values, however, appear to agree. Therefore, the enzyme purified from *E. coli* was utilized in all subsequent experiments.

2.3.3.2 Assessment of *in vitro* Inactivation of P4H by Epoxy Ketone Inhibitor

The carboxylic acid derivative of our epoxy ketone inhibitor (**2.19**) is expected to act as an irreversible inhibitor of P4H. As such, time- and concentration-dependent inactivation should be observed. Because the deesterification of **2.13** with NaOH gave a mixture of products, the sodium salt and free acid of the derivatives of **2.13** were synthesized from a benzyl ester of the epoxy ketone (see scheme 2.5). Benzyl 4-chlorooxobutyrate (**2.15**) was synthesized according to Abell *et al.* (Abell *et al.*, 1990) from benzyl succinate (**2.14**) (Linstead *et al.*, 1955). The benzyl 4-oxo-5-hexenoate intermediate (**2.16**) and benzyl 5,6-epoxy-4-oxohexanoate (**2.17**) were synthesized in the same manner as were the ethyl esters. The benzyl group was removed by hydrogenation to give the free acid of the epoxy ketone (**2.18**), and its reaction with NaHCO_3 gave the sodium salt (**2.19**). To measure inactivation, enzyme (19 μM), FeSO_4 (2.2 mM), and increasing concentrations of **2.19** (between 33 mM and 356 mM) were pre-incubated for various time periods (between 2.5 and 20 min), and P4H activity was measured as before. Data were plotted as relative activity on a log scale versus pre-incubation time (Figure 2.10). These data do reveal first order time- and substrate concentration-dependent inactivation of P4H activity. Using these data, half-times for inactivation ($t_{1/2}$) were calculated and used to create a linear Kitz and Wilson plot (Figure 2.12) (Kitz & Wilson,

1962). From this plot, the binding constant (K_I) and the rate of inactivation (k_{inact}) of epoxy ketone **2.19** for human P4H were determined to be 0.36 M and 2 min⁻¹, respectively. Coumalic acid (see Chapter 1), the only other known α -KG-mimicking inactivator of P4H, has a second order rate constant of $k_{\text{inact}}/K_I = 0.09 \text{ M}^{-1}\cdot\text{s}^{-1}$ against chicken P4H (Gunzler *et al.*, 1987). The value of k_{inact}/K_I for epoxy ketone **2.19** compares favorably with that of coumalic acid. These analyses indeed provide substantial evidence that **2.19** is a potent inactivator of P4H. We wanted to demonstrate further that **2.19** mimics α -KG by sharing its binding site.

A competition experiment should elucidate the binding mode of epoxy ketone **2.19**. Increasing concentrations of α -KG were pre-incubated with FeSO₄, P4H, and **2.19**. The concentration of **2.19** and time of pre-incubation were chosen to give greater than 50% inactivation as compared to control reactions (*i.e.*, those with no inhibitor present). When α -KG was added to the reaction mixture, protection of P4H activity was observed in a concentration-dependent manner (Figure 2.13). These data indicate that **2.19** competes with α -KG for binding in the active site of P4H.

2.3.3.3 Determination of Chiral Preference for Inactivation of P4H by Epoxy Ketones

The syntheses of epoxides **2.13** and **2.19** result in racemic mixtures at C5. Because enzymic active sites are chiral environments, they usually recognize and bind one stereoisomer preferentially over the other. To determine if P4H preferentially reacts with one enantiomer of epoxy ketone **2.19** over the other, a pure sample of each enantiomer was required. Synthetic procedures using a (salen)Co^{III} complex for hydrolytic kinetic resolution of selective epoxide ring opening did not react completely

(Schaus *et al.*, 2002), and only partially enriched mixtures could be obtained. Therefore, we utilized chiral HPLC methods to separate and collect each enantiomer of the ethyl (2.13) and benzyl (2.17) esters of the epoxide. The absolute configuration of each purified enantiomer was assigned from chiral HPLC analysis of the incomplete reactions of the (salen)Co^{III} complex. The epoxide benzyl ester 2.17 treated with the (*R,R*) catalyst yielded the (*S*) epoxide and showed an increase in the relative area of the peak displaying a shorter retention time. Likewise, epoxide treated with the (*S,S*) catalyst yielded the (*R*) epoxide and showed an increase in the relative area of a peak with a longer retention time. Following HPLC separation, the enantiomeric purity of the (*S*)-2.17 was $\geq 95\%$, while the enantiomeric purity of the (*R*)-2.17 was 87%.

The two ethyl ester compounds were purified in the same manner as the benzyl esters and tested *in vivo* utilizing the *dpy-18* nematode assay. These data indicate that the apparent LC₅₀ for the epoxide (*S*)-2.13 was approximately 0.09 mM while the LC₅₀ for the epoxide (*R*)-2.13 was 0.12 mM suggesting that the (*S*)-epoxide exhibited nearly 20% more inactivation than did the (*R*)-epoxide (Figure 2.14). As expected, the racemate 2.13 displays activity between that of the (*R*) and (*S*)-epoxide inhibitors (Figure 2.14). In addition to the *in vivo* data, *in vitro* analysis also confirms the preference of P4H for the (*S*)-epoxide. Relative rate measurements indicated that the (*S*) enantiomer gives about 15% more inactivation than did the (*R*) enantiomer.

2.3.4 Identification of Enzyme Residue Targeted by Epoxy Ketone Inhibitor

The three-dimensional structure of P4H (human or otherwise) is unknown. Inactivation of human P4H by the epoxide 2.19 should result in the covalent modification

of a residue near the binding site of α -KG. To identify the active-site nucleophile, the enzyme was incubated with inhibitor and then digested with trypsin, which catalyzes the cleavage of peptide bonds after arginine and lysine residues. The resulting fragments were subjected to mass spectrometric analysis and compared to the predicted proteolytic fragments. Those that differed by the molecular weight of the inhibitor (144 Da) comprised our pool of possible nucleophiles. Two fragments were identified that met these criteria. Overlapping fragments corresponding to residues 244-257 (SASDDQSDQKTTPK) and 244-258 (SASDDQSDQKTTPKK) displayed masses equal to that of the fragment plus the inhibitor. In these cases, the protease did not appear to cleave after Lys253; no masses corresponding to a fragment 244-253 were detected. Modification of the amino group in the side chain of Lys253 should prevent cleavage by blocking binding to trypsin. Furthermore, these data were reproduced with human P4H produced in baculovirus. These data indicate that the side-chain amino group of Lys253 is the nucleophile in epoxide-mediated inactivation of P4H.

2.3.5 Immobilization of Prolyl 4-Hydroxylase by Epoxy Ketone Inhibitor

To examine further the irreversibility of epoxide inhibitor **2.19** binding, the available ketone functionality within **2.19** was derivatized with a lysine hydrazide (biocytin hydrazide). If covalent modification does exist, then the ketone functionality will be susceptible to attack by biocytin hydrazide. This three-component covalent complex should bind specifically to streptavidin-coated plates and could then be detected using an antibody directed against the human P4H α subunit.

Epoxide **2.19** was incubated with P4H in the presence of FeSO_4 , and the mixture was treated with biocytin hydrazide. The acylhydrazone formed between the hydrazide and inhibitor-ketone was then reduced to the more stable secondary amine using NaBH_4 (Scheme 2.6). The enzyme-inhibitor-biotin complex was separated from unreacted small molecules by gel filtration chromatography using a NICK™ column. The complex was then bound to streptavidin plates and washed before the addition of a monoclonal antibody to the P4H α subunit. Visualization of P4H antibody by a secondary antibody conjugated to horseradish peroxidase revealed that P4H is associated with the streptavidin plates only in the presence of epoxide inhibitor **2.19** (Figure 2.15). These data indicate that the P4H enzyme is indeed covalently modified by the epoxide.

2.4 Conclusion

A bioavailable irreversible inhibitor of P4H was identified with an animal model system. Our epoxy ketone inhibitor binds in the α -KG binding site of P4H and inactivates the enzyme. This compound likely would not have been identified in traditional *in vitro* studies because it requires relatively high concentrations to show its effects *in vitro*. It displays high efficacy *in vivo* however, due to its irreversible mode of action. This compound provides a new approach in the treatment of P4H-related fibrotic diseases. Another application for this epoxide is as a tool to identify (and inhibit) new P4H enzymes and other α -KG dependent enzymes with unknown function.

2.5 Future Directions

Other potential P4H inhibitors directed at the α -KG binding site could include an episulfide analog of **2.13**. This compound should exhibit affinity to the active-site iron center and may be able to inactivate the iron center via its reduction (Wright & Nelson, 1992). Initial attempts at the direct conversion of the epoxide to the episulfide were unsuccessful, probably because of the electron withdrawing influence of the ketone adjacent to the epoxide. As several inhibitors of P4H have shown that the enzyme tolerates bulk in the iron-binding site (Franklin *et al.*, 2001), branched epoxides could be used to explore the binding pocket beyond the iron-binding domain of the inhibitor. This approach could decrease the reactivity of the epoxide, while increasing the specificity for the enzyme target (Way, 2000). Furthermore, an oxiranecarbonyl glycine could add rigidity and increase electron density to the carbonyl oxygen and could produce a tighter binding inhibitor. This compound suffers from the lack of the ketone functionality (which is necessary for the proteomics approach described above) but could be a better inhibitor of catalysis by P4H. Finally, in order to develop a collagen-specific inhibitor, a single compound that mimics both α -KG and a peptide substrate could produce strong and specific inhibition P4H.

2.6 Materials and Methods

General. BakerDry™ solvents DMF ≤ 20 ppm water, CH₂Cl₂ ≤ 30 ppm water, and THF ≤ 10 ppm water in cyclotainers™ were purchased from the J.T. Baker (Phillipsburg, NJ). All other chemicals unless noted otherwise, were purchased from Aldrich (Milwaukee,

WI), Fisher Scientific (Pittsburgh, PA), NovaBiochem (San Diego, CA), or other commercial sources and were used without further purification. NMR spectra were obtained using a Bruker AC+ 300 MHz spectrometer. Mass spectra were obtained using a Micromass LCT electrospray ionization, time-of-flight analyzer and Matrix-Assisted Laser Desorption/Ionization, time-of-flight (MALDI-TOF) spectrometers (Bruker REFLEX II, Bruker BIFLEX III, or Perkin - Elmer Voyager). HPLC analysis was performed using a Waters (Milford, MA) system controlled using the Millennium³² (version 3.20) software package and equipped with two 515 pumps, a 717plus autosampler, and a 996 photodiode array detector.

2.1 2,4-Diethylpyridine dicarboxylate. 2,4-Diethylpyridine dicarboxylate was synthesized according to Tschank *et al.* and summarized below (Tschank *et al.*, 1991). Pyridine-2,4-dicarboxylic acid (1g, 6.0 mmol) and SOCl₂ (2.81 ml, 4.3 g, 36 mmol) were heated to reflux in ethanol (10 ml) for 4 h. The product was extracted into EtOAc (75 ml) from satd NaHCO₃ (100 ml) and concentrated by rotary evaporation. ¹H NMR (CDCl₃, 300 MHz) δ 8.92 (dd, *J* = 1, 5 Hz, 1H), 8.65 (dd, *J* = 1, 2 Hz, 1H), 8.04 (dd, *J* = 2, 5 Hz, 1H), 4.52 (q, *J* = 7 Hz, 2H), 4.46 (q, *J* = 7 Hz, 2H), 1.47 (t, *J* = 7 Hz, 3H), 1.44 (t, *J* = 7 Hz, 3H). ¹³C NMR (CDCl₃, 75 MHz) δ 164.8, 164.5, 150.8, 149.5, 139.3, 126.1, 124.4, 62.4, 62.3, 14.5, 14.4.

2.2 Dimethyloxalylglycine. Dimethyloxalylglycine was synthesized according to Baader *et al.* and summarized below (Baader *et al.*, 1994). Glycine methyl ester•HCl (1.0 g, 8.0 mmol), TEA (2.23 ml, 16 mmol) and DMAP (1.95 g, 16 mmol) were dissolved in CH₂Cl₂ (20 ml) and methyl oxalylchloride (0.73 ml, 0.975g, 8.0 mmol) was dripped slowly into

the reaction mixture and allowed to stir at RT overnight. The reaction mixture was extracted with satd aq NaHCO₃ (50 ml) and the organic layer was concentrated by rotary evaporation. The product was purified by silica gel chromatography eluting with 5:1 (v/v) EtOAc/MeOH. ¹H NMR (CDCl₃, 300 MHz) δ 7.53 (br s, 1H), 4.14 (d, *J* = 6 Hz, 2H), 3.93 (s, 3H), 3.80 (s, 3H). ¹³C NMR (CDCl₃, 75 MHz) δ 160.6, 139.1, 54.0, 52.9, 41.6.

2.4 *N*-branched oxlalyglycine library. The *N*-branched oxlalyglycine library was synthesized in parallel. The synthesis and characterization of a library member and model compound, *N*-benzyloxalylglycine is summarized below. All of the reactions steps on solid support were run in 10 ml disposable Poly-Prep column from Bio-Rad at RT. Fmoc-Gly resin (223 mg, 0.6 mmol/g) was deprotected with 20% (v/v) piperidine in DMF (3 x 10 ml, 5 min), washed with DMF (3 x 10 ml) and CH₂Cl₂ (3 x 10 ml), and dried under vacuum. The resin was resuspended in trimethylorthoformate (2 ml), and benzaldehyde (0.041 ml, 0.4 mmol, 3 eq.) was added. The reaction mixture was agitated on a rocking platform shaker for 2 h then filtered, resubjected to the aldehyde (0.028 ml, 0.4 mmol, 3 eq.), and agitated overnight. The reaction mixture was filtered and the resin was washed with MeOH (3 x 10 ml) and dried under vacuum. The resin was resuspended in CH₂Cl₂ (2 ml), and sodium triacetoxy borohydride (40 mg, 0.19 mmol), NaCNBH₃ (25 mg, 0.40 mmol), and acetic acid (10 μl) were added. The reaction mixture was agitated overnight. Additional triacetoxy borohydride (40 mg, 0.19 mmol) was added, and the reaction mixture was agitated for an additional 4 h. The resin was then filtered and washed with CH₂Cl₂ (3 x 10 ml) and MeOH (3 x 10 ml) and CH₂Cl₂ (3 x 10 ml), and dried under vacuum. The resin was resuspended in CH₂Cl₂ (2 ml), and pyridine (100 μl) and

methyloxalylchloride (50 μ l) were added, then the reaction mixture was agitated overnight. The resin was filtered, washed with CH_2Cl_2 (3 x 10 ml), and dried under vacuum. The product was cleaved from the resin with 50% (v/v) TFA in CH_2Cl_2 (4 ml) for 1 h, then the resin was filtered washed with CH_2Cl_2 (3 x 10 ml). The combined filtrate was concentrated by rotary evaporation and dried under vacuum. The cleaved product was dissolved in MeOH (10 ml), and SOCl_2 (100 μ l) was added, and the reaction mixture was stirred overnight at RT. The final product was dried under vacuum and used without further purification (overall yield 30 mg, 84%). ^1H NMR (CDCl_3 , 300 MHz) δ 7.34 (m, 5H), 4.73 (s, 0.7H), 4.58 (s, 1.3H), 4.08 (s, 0.8H), 4.01 (s, 1.2H), 3.91 (s, 1.8H), 3.87 (s, 1.2H), 3.73 (s, 1.8 H), 3.72 (s, 1.2H).

2.5 6-Hydroxy-pyridine-2,4-dicarboxylic acid. 6-Hydroxy-pyridine-2,4-dicarboxylic acid was synthesized according to Stephani and Meister and summarized below (Stephani & Meister, 1971). L-Asparagine (5g, 37.8 mmol) was incubated with L-amino acid oxidase (300 mg) in H_2O (50 ml). The pH was adjusted to 7.2 with 2 M NaOH. Additional H_2O was added to adjust the total reaction volume to 100 ml. $\text{O}_2(\text{g})$ was bubbled through the solution at 37 $^\circ\text{C}$ overnight, and a small amount of octanol (~1 ml) was added to control foaming. The reaction mixture was dialyzed in H_2O (2000 ml) to remove enzyme. The H_2O containing the product was concentrated by rotary evaporation to approximately 50 ml. The product was purified by cation-exchange chromatography using Dowex 50 resin charged with Na^+ . The fractions containing the product were treated with decolorizing charcoal and the volume was reduced to 50 ml, to which acetone (250 ml) was added. The solution was then cooled to -20 $^\circ\text{C}$ for 24 h. The

precipitate was filtered and added to 1 M HCl (50 ml), and this reaction mixture incubated at 37 °C for several days. The resultant solid was filtered to yield 4.7g (84%) of the free acid. ^1H NMR (CDCl_3 300 MHz) δ 7.10 (s, 1H), 7.09 (s, 1H), 2.51 (q, J = 2 Hz, 1H).

2.6 Dimethyl-6-hydroxy-2,4-pyridine dicarboxylate. 6-Hydroxy-pyridine-2,4-dicarboxylic acid (53 mg, 0.29 mmol) and SOCl_2 (100 μl , 1.4 mmol) were added to MeOH (1.5 ml) and heated at reflux for 1 h. The solvent was removed by rotary evaporation, and the product was extracted into EtOAc from aq HOAc (50 mM). The organic solvent was removed by rotary evaporation, and the residue was dried under vacuum to yield 55 mg (90%) of the dimethyl ester. ESI MS m/z : $[\text{M} + \text{H}]^+$ 212.0, calcd. 212.0. ^1H NMR (CDCl_3 , 300 MHz) δ 7.47 (s, 2H), 4.01 (s, 3H), 3.96 (s, 3H). ^{13}C NMR (CDCl_3 , 75 MHz) δ 164.4, 161.2, 141.6, 134.6, 128.8, 108.5, 53.7, 53.3.

2.7 N-Hydroxy-succinamic acid ethyl ester. Ethyl succinyl chloride (2.46 ml, 17 mmol) and hydroxyl amine hydrochloride (1 g, 14 mmol) were dissolved in CH_2Cl_2 (10 ml) at 0 °C. Pyridine (2.33 ml, 29 mmol) was added, and the reaction mixture was allowed to warm to RT. CH_2Cl_2 (50 ml) and pyridine (2 ml) were added to keep all salts in solution. The reaction mixture was stirred overnight. The solvents were removed by rotary evaporation, and the product was purified by reversed-phase C18 HPLC using a gradient of 0-20% (v/v) aq. acetonitrile to yield 113 mg (19.5%) of product. ^1H NMR (CDCl_3 , 300 MHz) δ 10.44 (br s, 1H), 4.04 (q, J = 7 Hz, 2H), 2.50 (t, J = 7 Hz, 2H), 2.23 (t, J = 7 Hz, 2H), 1.17 (t, J = 7 Hz, 3H).

2.8 Dimethyl 2-oxoglutarate. Dimethyl 2-oxoglutarate was synthesized according to Carrigan *et al.* and summarized below (Carrigan *et al.*, 2002). α -Ketoglutaric acid (5g, 34 mmol) was dissolved in MeOH (40 ml) and cooled to -5 °C. SOCl_2 (5 ml, 69 mmol, 2eq) was added slowly to the reaction mixture. Immediately after the addition of SOCl_2 , the reaction mixture was concentrated by rotary evaporation to yield 5.2 g (88%) of product as a clear viscous liquid. ESI MS EMM m/z : $[\text{M} + \text{CH}_3\text{OH} + \text{Na}]^+$ 229.0698, calcd. 229.0688. ^1H NMR (CDCl_3 , 300 MHz) δ 3.90 (s, 3H), 3.70 (s, 3H), 3.18 (t, $J = 7$ Hz, 3H), 2.69 (t, $J = 7$ Hz, 3H).

2.9 Dimethyl 3-bromo-2-oxoglutarate. Dimethyl 3-bromo-2-oxoglutarate was synthesized according to Carrigan *et al.* and summarized below (Carrigan *et al.*, 2002). Dimethyl 2-oxoglutarate (1 g, 6 mmol) was dissolved in CH_2Cl_2 (30 ml). Br_2 (0.46 ml, 9 mmol) was then added, and the resulting solution was heated at reflux for 3 h. The solvent was removed by rotary evaporation to give 1.44 g (99%) of a yellow solid judged to be about 75% pure by ^1H NMR spectroscopy. ESI MS EMM m/z : $[\text{M} + \text{Na}]^+$ 306.9785, calcd. 306.9793. ^1H NMR (CDCl_3 , 300 MHz) δ 5.40 (dd, $J = 6, 9$ Hz, 1H), 3.96 (s, 3H), 3.72 (s, 3H), 3.35 (dd, $J = 9, 17$ Hz, 1H), 3.06 (dd, $J = 6, 17$ Hz, 1H).

2.10 Dimethyl dehydro-2-oxoglutarate. Dimethyl dehydro-2-oxoglutarate was synthesized according to Carrigan *et al.* and summarized below (Carrigan *et al.*, 2002). Dimethyl 3-bromo-2-oxoglutarate (1.16 g, 4.6 mmol) was dissolved in diethyl ether (30 ml). TEA (0.71 ml) was added, and the reaction mixture was stirred for 30 min at RT. The reaction mixture then was filtered through a pad of Celite to remove TEA-HBr salts. The solvent was removed by rotary evaporation, and the product was dried under vacuum.

to yield 624 mg (80%) of a yellow solid. ESI MS EMM m/z : $[M + Na]^+$ 227.0521, calcd. 227.0532. 1H NMR ($CDCl_3$, 300 MHz) δ 7.64 (d, J = 16 Hz, 1H), 6.98 (d, J = 16 Hz, 1H), 3.94 (s, 3H), 3.85 (s, 3H).

2.11 Dimethyl 3,4-dibromo-2-oxoglutarate. Dimethyl dehydro-2-oxoglutarate (335 mg, 1.9 mmol) was dissolved in CH_2Cl_2 (~100 ml) and Br_2 (0.1 ml, 20 mmol) was added. After stirring overnight, additional Br_2 (0.1 ml, 20 mmol) was added, and the reaction mixture was stirred for an additional 24 h. The solvent was removed by rotary evaporation, and the residue was dried under vacuum to yield 558 mg (84%) of the product. ESI MS EMM m/z : $[M + CH_3OH + Na]^+$ 384.8902, calcd. 384.8898. 1H NMR ($CDCl_3$, 300 MHz) δ 5.58 (d, J = 11 Hz, 0.8H), 5.43 (d, J = 10 Hz, 0.2H), 4.83 (d, J = 11 Hz, 0.8H), 4.71 (d, J = 10 Hz, 0.2H), 3.98 (s, 2.3H), 3.97 (s, 0.7H), 3.89 (s, 2.3H), 3.80 (s, 0.7H).

2.12 Ethyl 4-oxo-5-hexenoate. Ethyl 4-oxo-5-hexenoate was synthesized according to Milstein and Stille and summarized below (Milstein & Stille, 1979). Ethyl 4-chlorooxobutyrates (2.5 g, 15.2 mmol) was dissolved in HMPA (10 ml). Tributylvinyltin (5.0 g, 15.2 mmol) and benzylchlorotriphenylphosphine palladium II (52 mg) were added, and the reaction mixture was heated open to air to 65 °C for 5 min, at which time the reaction mixture turned black. The reaction was allowed to cool to RT. H_2O (50 ml) and NaCl (1.0 g) were added, and the reaction mixture was stirred for 5 min. The reaction mixture was extracted with diethyl ether (3 x 60 ml). The combined organic layers were washed with H_2O (4 x 60 ml), and the organic layer was dried over anhydrous $MgSO_4$ and concentrated by rotary evaporation to approximately 20 ml. Half-saturated KF in

MeOH (25 ml) was added to precipitate the SnBu_3F , which was filtered out through Celite. The product was concentrated by rotary evaporation to an oil and purified by silica gel chromatography, eluting with 10% (v/v) ethyl acetate/ CH_2Cl_2 to give 1.944 g (81.9%) of ethyl 4-oxo-5-hexenoate. ESI MS m/z : $[\text{M} + \text{Na}]^+$ 179.0, calcd 179.1. ^1H NMR (CDCl_3 , 300 MHz) δ 6.39 (dd, $J = 10, 18$ Hz, 1H), 6.27 (dd, $J = 1, 18$ Hz, 1H), 4.14 (q, $J = 7$ Hz, 2H), 2.93 (t, $J = 7$ Hz, 2H), 2.63 (t, $J = 3$ Hz, 2H), 1.26 (t, $J = 7$ Hz, 3H).

2.13 Ethyl 5,6-epoxy-4-oxohexanoate. Ethyl 5,6-epoxy-4-oxohexanoate was synthesized according to Appleton *et al.* and summarized below (Appleton *et al.*, 1998). 30% H_2O_2 (1.75 ml) and ethyl 4-oxo-5-hexenoate (1.107 g, 7.09 mmol) were dissolved in $t\text{BuOH}$ (11.81 ml) and H_2O (5.9 ml) and cooled to 0 °C. Saturated aqueous K_2CO_3 (606 μl) was slowly added at 0 °C and the reaction mixture was stirred for 1 h, after which time it was allowed to warm to RT and stirred for 3 additional h. The reaction was diluted with H_2O (100 ml) and extracted with diethyl ether (3 x 30 ml). The combined organic extracts were dried over anhydrous MgSO_4 and concentrated by rotary evaporation. The product was purified by silica gel chromatography, eluting with 10% (v/v) ethyl acetate/ CH_2Cl_2 to give 1.04 g (85.2%) of ethyl 5,6-epoxy-4-oxohexanoate. NMR spectra show some HMPA contamination. ESI MS m/z : $[\text{M} + \text{Na}]^+$ 195.0, calcd 195.1. ^1H NMR (CDCl_3 , 300 MHz) δ 4.11 (q, $J = 7$ Hz, 2H), 3.48 (dd, $J = 3, 4$ Hz, 1H), 3.03 (dd, $J = 4, 6$ Hz, 1H), 3.01 (dd, $J = 3, 6$ Hz, 1H), 2.66 (m, 4H), 1.25 (t, $J = 7$ Hz, 3H). ^{13}C NMR (CDCl_3 , 75 MHz) δ 206.3, 172.6, 60.9, 53.7, 46.3, 31.3, 27.5, 14.3.

2.14 Benzyl succinate. Benzyl succinate was synthesized according to Linstead *et al.* and summarized below (Linstead *et al.*, 1955). Succinic anhydride (30g, 300 mmol) was dissolved in benzyl alcohol (31.6 ml, 33g, 300 mmol) and heated to reflux for 4 h. The reaction mixture was dissolved in ether (100 ml), and the insoluble succinic acid was removed by filtration. The organic filtrate was extracted with satd aq Na₂CO₃ (3 x 100 ml), and the combined aqueous layers were acidified with 2 M HCl (2000 ml). The precipitate was filtered and dried under vacuum to give 30 g (48%) of product. ¹H NMR (CDCl₃, 300 MHz) δ 7.35 (m, 5H), 5.15 (s, 2H), 2.70 (m, 4H). ¹³C NMR (CDCl₃, 75 MHz) δ 177.7, 172.1, 128.8, 128.5, 128.4, 66.9, 29.1, 29.0.

2.15 Benzyl 4-chlorooxobutyrates. Benzyl 4-chlorooxobutyrates were synthesized according to Abell *et al.* and summarized below (Abell *et al.*, 1990). Benzyl succinate (4.14 g, 20 mmol) was dissolved in CH₂Cl₂ (150 ml), and the resulting solution was cooled to 0 °C. Oxalyl chloride (99+%, 13.8 g, 109 mmol) was added slowly, and the reaction mixture was stirred at 0 °C for 5 min. The reaction mixture was allowed to warm to 15 °C and was stirred for an additional 30 min. The solvent was removed by rotary evaporation, and the residue was dissolved in benzene. The benzene was removed by rotary evaporation to give 4.5 g (99%) of product as a clear viscous liquid. ¹H NMR (CDCl₃, 300 MHz) δ 7.34 (m, 5H), 5.13 (s, 2H), 3.19 (t, *J* = 7 Hz, 2H), 2.69 (t, *J* = 7 Hz, 2H). ¹³C NMR (CDCl₃, 75 MHz) δ 173.2, 170.9, 135.6, 128.8, 128.6, 128.4, 67.1, 41.9, 29.5, 28.5.

2.16 Benzyl 4-oxo-5-hexenoate was synthesized in the same manner as ethyl 4-oxo-5-hexenoate from benzyl 4-chlorooxobutyrates in 82% yield. ¹H NMR contains EtOAc

contamination. ^1H NMR (CDCl_3 , 300 MHz) δ 7.35 (m, 5H), 6.38 (dd, $J = 10, 18$ Hz, 1H), 6.26 (dd, $J = 1, 18$ Hz, 1H), 5.86 (dd, $J = 1, 10$ Hz, 1H), 5.13 (s, 2H), 2.94 (t, $J = 7$ Hz, 2H), 2.70 (t, $J = 7$ Hz, 2H).

2.17 Benzyl 5,6-epoxy-4-oxohexanoate was synthesized in the same manner as ethyl 4-chlorooxobutyrate in 98% yield. ^1H NMR (CDCl_3 , 300 MHz) δ 7.34 (m, 5H), 5.10 (s, 2H), 3.46 (dd, $J = 2, 5$ Hz, 1H), 2.99 (dd, $J = 5, 6$ Hz, 1H), 2.94 (dd, $J = 2, 6$ Hz, 1H), 2.64 (m, 4H). ^{13}C NMR (CDCl_3 , 75 MHz) δ 206.1, 172.4, 135.9, 128.7, 128.5, 128.4, 66.6, 53.7, 46.3, 31.3, 27.5.

2.18 5,6-epoxy-4-oxohexanoic acid. Benzyl 5,6-epoxy-4-oxohexanoate (340 mg, 1.45 mmol) was dissolved in EtOAc (20 ml). Pd/C (40 mg, 10 wt. %) was added, and the reaction mixture was stirred under H_2 balloon for 4 h. The reaction mixture was filtered through celite, and the solvent was removed by rotary evaporation to give 183 mg (99%) of product. ESI MS EMM m/z : $[\text{M} - \text{H}]^-$ 143.0340, calcd. 143.0344. ^1H NMR (CDCl_3 , 300 MHz) δ 10.74 (br s, 1H), 3.48 (dd, $J = 2, 5$ Hz, 1H), 3.03 (dd, $J = 5, 5$ Hz, 1H), 2.96 (dd, $J = 2, 5$ Hz, 1H), 2.64 (m, 4H). ^{13}C NMR (CDCl_3 , 75 MHz) δ 178.3, 53.7, 46.4, 31.1, 27.2.

2.19 Sodium 5,6-epoxy-4-oxohexanoate. 5,6-Epoxy-4-oxohexanoic acid (206 mg, 1.4 mmol) was dissolved in aq NaHCO_3 (3.6 ml, 400 mM), and the resulting solution was stirred for 1 h. The reaction mixture was concentrated to dryness by Speed-vac at 35 $^\circ\text{C}$. NMR analysis shows some decomposition of the product from Speed-vac concentration. ^1H NMR (D_2O , 300 MHz) δ 3.77 (dd, $J = 3, 5$ Hz, 1H), 3.08 (t, $J = 5$ Hz, 1H), 2.898 (dd,

$J = 3, 6$ Hz, 1H), 2.77 (m, 4H), 2.54 (q, $J = 7$ Hz, 1H), 2.42 (m, 4H), 1.35 (d, $J = 7$ Hz, 1H), 0.97 (t, $J = 7$ Hz, 1H).

Resolution of (*R*) and (*S*) enantiomers of ethyl 5,6-epoxy-4-oxohexanoate and benzyl 5,6-epoxy-4-oxohexanoate. Enantiomers of ethyl 5,6-epoxy-4-oxohexanoate and benzyl 5,6-epoxy-4-oxohexanoate were separated on a Chiracel OD analytical HPLC column. Identification of peaks was made by comparison of reaction products from reaction with a (salen)Co^{III} complex catalyst and NaOH (Schaus *et al.*, 2002). The hydrolytic kinetic resolution reaction gave enhancement of one enantiomer, but not complete resolution of starting material. Peaks were then collected and reanalyzed to show that the *S* enantiomer is $\geq 95\%$ pure and the *R* enantiomer is approximately 80% pure.

2.20 Dansyl-Gly-Phe-Pro-Gly-OEt. Boc-Phe-Pro-OH (870 mg, 2.4 mmol), glycine ethyl ester•HCl (341 mg, 2.4 mmol), DCC (623 mg, 2.4 mmol), HOBT (330 mg, 2.4 mmol), and *N*-ethylmorpholine (309 μ l, 2.4 mmol) were dissolved in THF (10 ml) and stirred at RT overnight. The product was extracted into CH₂Cl₂ (50 ml) from satd aq NaHCO₃ (50 ml). The organic layer was washed with aq citric acid (50 ml, 5% w/v) and brine (50 ml) and concentrated by rotary evaporation. The Boc protecting group was removed by stirring the crude residue in CH₂Cl₂ (20 ml) with TFA (7.2 ml) at 0 °C for 3 h. The intermediate product was purified by silica gel chromatography, eluting with 8% (v/v) MeOH in CH₂Cl₂. Solvent was removed from the fractions containing the desired compound by rotary evaporation, and the residue was dissolved in DMF (20 ml). EDC (631 mg, 3.3 mmol), HOBT (349 mg, 2.6 mmol), *N*-ethyl morpholine (714 μ l, 5.6 mmol), and dansylglycine (802 mg, 2.6 mmol) were added, and the reaction mixture was allowed

to stir for 48 h. H₂O (10 ml) was added to quench the reaction. The product was extracted into EtOAc (50 ml) and washed with aq HCl (50 ml, 5% v/v), satd aq NaHCO₃ (50 ml), and brine (50 ml). The initial aqueous layer was extracted further into CH₂Cl₂ (50 ml), and the CH₂Cl₂ layer was washed with aq HCl (50 ml, 5% v/v), satd aq NaHCO₃ (50 ml), and brine (50 ml). The organic layers were combined and dried over anhydrous MgSO₄, and the solvent was removed by rotary evaporation. The product was purified by silica gel chromatography in 4% (v/v) MeOH in CH₂Cl₂ to yield 328 mg (21.4%) of a bright yellow oil. The NMR spectra show extra peaks due to proline rotamers. ESI MS EMM *m/z*: [M + Na]⁺ 660.2438, calcd. 660.2468. ¹H NMR (CDCl₃, 300 MHz) δ 8.57 (t, *J* = 7 Hz, 1H), 8.30 (d, *J* = 8 Hz, 1H), 8.22 (d, *J* = 6 Hz, 1H), 8.02 (s, 1H), 7.60 (dd, *J* = 8, 8 Hz, 1H), 7.52 (d, *J* = 7, 8 Hz, 1H), 7.21 (t, *J* = 8 Hz, 3H), 7.12 (dd, *J* = 2, 8 Hz, 2H), 6.96 (m, 1H), 6.02 (t, *J* = 6 Hz, 0.25H), 5.76 (t, *J* = 6 Hz, 0.75H), 4.80 (m, 1H), 4.45 (m, 1H), 4.20 (q, *J* = 7 Hz, 1.5H), 4.06 (q, *J* = 7 Hz, 0.5H), 3.94 (d, *J* = 6 Hz, 1.5H), 3.87 (d, *J* = 6 Hz, 0.5H), 3.62 (dd, *J* = 7, 17 Hz, 0.5H), 3.54 (dd, *J* = 8, 16 Hz, 2H), 3.49 (m, 1H), 3.38 (d, *J* = 7 Hz, 0.5H), 3.01 (m, 1H), 2.96 (s, 2H), 2.89 (d, *J* = 2 Hz, 2H), 2.92 (d, *J* = 6 Hz, 1H), 2.86 (s, 6H), 2.77 2.92 (dd, *J* = 6, 13 Hz, 1H), 2.26 (br s, 1H), 2.05 2.92 (d, *J* = 13 Hz, 0.5H), 1.86 (br s, 2H), 1.62, (s, 3H), 1.28 (t, *J* = 7 Hz, 3H), 1.19 (t, *J* = 7 Hz, 1H). ¹³C NMR (CDCl₃, 75 MHz) δ 171.2, 171.1, 170.7, 169.8, 168.8, 168.0, 152.2, 135.9, 135.2, 134.2, 134.1, 131.0, 130.9, 130.1, 129.9, 129.6, 129.5, 129.1, 128.9, 128.7, 127.8, 127.3, 123.4, 123.3, 118.8, 118.7, 115.5, 61.5, 61.3, 61.0, 53.7, 52.4, 47.7, 47.0, 45.8, 45.5, 41.5, 41.4, 38.5, 31.0, 28.1, 25.0, 22.0, 14.3, 14.2, 2.1.

2.21 Dansyl-Gly-Phe-Hyp-Gly-OEt. Dansyl-Gly-Phe-Hyp-Gly-OH was synthesized by using standard Fmoc-protection strategies on an Applied Biosystems Pioneer automated synthesizer with HATU activation. Dansyl-Gly-Phe-Hyp-Gly-OH was cleaved from the solid support with TFA (1 ml) dripped into ice cold ether. The precipitated peptide was collected by centrifugation, and the crude product (341 mg, 0.5 mmol) was dried under vacuum. The dried peptide was heated at refluxed with SOCl_2 (80 μl , 1.1 mmol) in EtOH (20 ml) for 2 h. The solvent was removed by rotary evaporation, and the product was purified by silica gel chromatography, eluting with 6% (v/v) MeOH in CH_2Cl_2 . The NMR spectra show extra peaks due to hydroxyproline rotamers. ESI MS EMM m/z : $[\text{M} + \text{Na}]^+$ 676.2422, calcd. 676.2417. ^1H NMR (CDCl_3 , 300 MHz) δ 8.54 (d, $J = 9$ Hz, 1H) 8.26, (d, $J = 9$ Hz, 1H), 8.18 (dd, $J = 1, 7$ Hz, 1H) 7.51 (m, 2H), 7.36 (t, $J = 6$ Hz, 1H), 7.31 (d, $J = 7$ Hz, 1H), 7.17 (m, 5H), 7.02 (t, $J = 6$ Hz, 1H), 4.7 (m, 2H), 4.34 (br s, 1H), 4.27 (q, $J = 7$ Hz, 0.5H), 4.16 (q, $J = 7$ Hz, 1.5H), 3.94 (d, $J = 6$ Hz, 2H), 3.77 (d, $J = 12$ Hz, 1H), 3.64 (s, 4H), 3.53 (m, 1H), 3.44 (d, $J = 5$ Hz, 0.75H), 3.38 (d, $J = 5$ Hz, 0.25H), 3.11 (dd, $J = 3, 12$ Hz, 1H), 2.94 (dd, $J = 7, 14$ Hz, 2H), 2.86 (s, 6H), 2.75 (dd, $J = 7, 14$ Hz, 2H), 2.66 (m, 1H), 2.18 (m, 2H), 1.26 (t, $J = 7$ Hz, 4H). ^{13}C NMR (CDCl_3 , 75 MHz) δ 171.5, 171.3, 170.5, 169.2, 152.0, 135.8, 131.0, 130.1, 129.9, 128.9, 128.8, 127.3, 123.5, 119.0, 115.7, 70.6, 61.7, 59.0, 56.2, 52.8, 46.0, 45.6, 41.5, 38.1, 37.3, 14.3.

***C. elegans* P4H in vivo assay.** Serial dilutions of inhibitor were made from DMSO stock solutions. Inhibitor (40 or 400 μl) was added to each plate containing 4 ml of solid growth medium (Agar (17 g/l), Bacto-Peptone (2.5 g/l), NaCl (50 mM), cholesterol (5 mg/l), CaCl (1 mM), and MgSO_4 (1 mM), in potassium phosphate buffer (1 mM, pH 6)

(Hope, 1999)). The inhibitor was allowed to diffuse into the agar for 24 h. Four L4 worms were then added to each plate. After sufficient time for the L4 worms to grow to adult stage and lay eggs (24 to 48 h), the adult worms were removed to simplify counting. After allowing sufficient time for all live eggs to hatch into worms (24 h), live worms were counted and compared to the number of dead embryos. An average of 40 to 100 embryos and worms were counted on each plate.

***In vitro* assay for P4H activity.** P4H (0.43 μ M), FeSO₄ (0.1 mM), BSA (1 mg/ml), catalase (0.1 mg/ml), ascorbate (2 mM), DTT (0.1 mM), and α -ketoglutarate (0.5 mM), were added to the reaction mixture in Tris-HCl buffer (50 mM, pH 7.8). Dansyl-Gly-Phe-Pro-Gly-OEt of various concentrations was added to initiate the reaction. Aliquots (30 μ l) were taken at 60, 180, and 300 s, and were quenched by boiling for 30 s. Aliquots were then injected onto a reversed-phase C18 HPLC column (Varian Microsorb-MV, 4.6 x 250 mm, 100 Å pore size) and eluted with 50% (v/v) aq acetonitrile (1 ml/min) and observed at 337.5 nm. All assays were performed in triplicate. Data were fitted to the Michaelis-Menton equation: $v = V_{\max}/((K_m/[Dansyl-Gly-Phe-Pro-Gly-OEt])+1)$

***In vitro* assay for irreversible inhibition of P4H.** P4H (43 μ M) was preincubated for 2.5, 5, 10, or 15 min with FeSO₄ (2 mM) and inhibitor at various concentrations (2 μ l). After preincubation, BSA (1 mg/ml), catalase (0.1 mg/ml), ascorbate (2 mM), DTT (0.1 mM), and α -ketoglutarate (0.5 mM) were added to the reaction mixture in 50 mM Tris-HCl buffer (pH 7.8). Dansyl-Gly-Phe-Pro-Gly-OEt (2.5 mM) was added to initiate the reaction. Aliquots (30 μ l) were taken at 15, 60, 120, 180, 240, and 300 s, and were quenched by boiling for 30 s. Aliquots were then injected onto a reversed-phase C18

HPLC column (Varian Microsorb-MV, 4.6 x 250 mm, 100 Å pore size) and eluted with 50% (v/v) aqueous acetonitrile (1 ml/min) and observed at 337.5 nm. All assays were performed in triplicate. Data are reported as relative activity to control reactions preincubated with buffer in place of inhibitor. Half-times for inactivation at various inhibitor concentrations are determined from linear least squares regression of the log of the relative rates. Half-times for inactivation were plotted against the reciprocal of inhibitor concentration in a Kitz and Wilson plot to determine the binding constant (K_i) and the rate of inactivation (k_{inact}) (Kitz & Wilson, 1962).

***In vitro* assay for reversible P4H inhibition.** P4H (0.43 µM), FeSO₄ (0.1 mM), BSA (1 mg/ml), catalase (0.1 mg/ml), ascorbate (2 mM), DTT (0.1 mM), α-ketoglutarate (0.5 mM), and various concentrations of inhibitor formed a reaction mixture in 50 mM Tris-HCl buffer (pH 7.8). Dansyl-Gly-Phe-Pro-Gly-OEt (2.5 mM) was added to initiate the reaction. Reactions were quenched after 5 min by boiling for 30 s. Aliquots were then injected onto a reversed-phase C18 HPLC column (Varian Microsorb-MV, 4.6 x 250 mm, 100 Å pore size) and eluted with 50% (v/v) aqueous acetonitrile (1 ml/min) and observed at 337.5 nm. All assays were performed in triplicate. Data are reported as relative activity to control reactions without inhibitor. Values of K_i were determined by non-linear least squares regression analysis of data fitted to equation $v_{\text{rel}} = K_i/([I] + K_i)$ where v_{rel} is the relative rate of the reaction.

Trypsin digestion of P4H•inhibitor complex. P4H (20 µg) was preincubated for 30 min with FeSO₄ (2 mM) and epoxy ketone inhibitor **4.23** (222 µM). The reaction mixture was diluted 10-fold with Tris-HCl buffer (50 mM, pH 7.8) and trypsin (2 µg) was added. The

digestion reaction was incubated at 37 °C overnight. An aliquot (10 µl) and desalted by Zip-Tip™ purification for analysis by MALDI-TOF mass spectrometry.

Immobilization of P4H. P4H (50 µg) was incubated for 30 min at 37 °C with FeSO₄ (0.1 mM), ascorbate (5 mM) and epoxy ketone inhibitor **4.23** (13 mM) in PBS. Biocytin hydrazide (11 mM) was added, and the reaction mixture was incubated for an additional 30 min at 37 °C. NaBH₄ (30 mg/ml in 10 mM NaOH) was added to the reaction mixture to reduce the acylhydrazone to an amine. The P4H complex was desalted using a NICK™ column (Amersham Pharmacia, Uppsala, Sweden) and incubated on Reacti-Bind™ streptavidin coated microtiter plates (Pierce, Rockford, IL) for 1 h at 37 °C. The plates were washed with blocking buffer (0.1% BSA, 0.05% Tween, in PBS) 4 times. A mouse monoclonal antibody specific to the α-subunit of P4H (ICN Biomedicals, Costa Mesa, CA) was added to the plates and incubated for 1 h at 37 °C. The plates were again washed with blocking buffer 4 times. Anti-mouse IgG peroxidase (Sigma, St. Louis, MO) was added to the plates, which were then incubated for 1 h at 37 °C. The plates were again washed with blocking buffer 4 times. *O*-Phenylenediamine solution (0.05 M citric acid, 0.05 M sodium phosphate (pH 5), 1 mg/ml *O*-phenylenediamine, 0.003% v/v H₂O₂) was added to the plates and the horseradish peroxidase reaction was monitored at 490 nm after the reaction was quenched with H₂SO₄ (2.5 M).

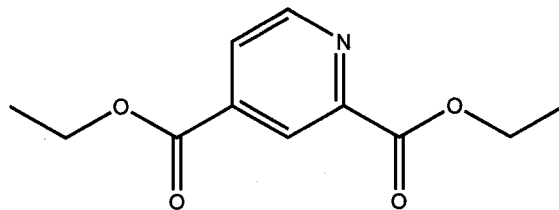
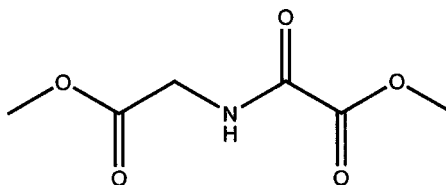
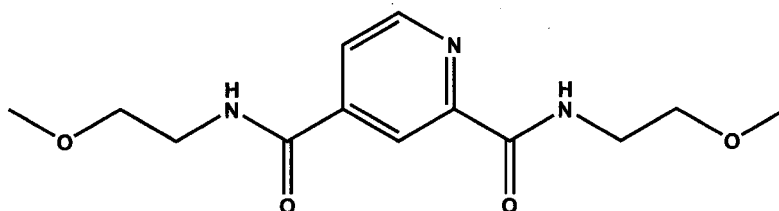
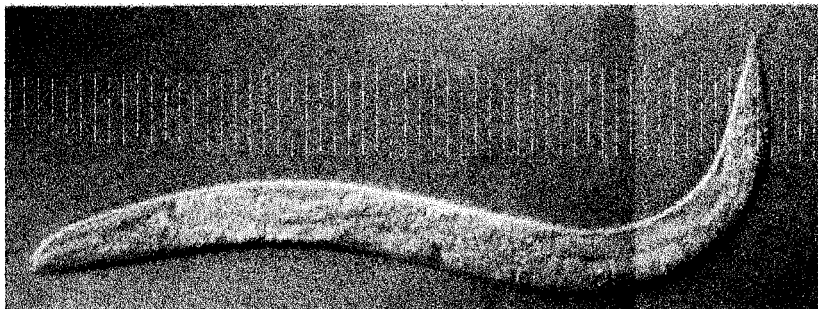
**2.1****2.2****2.3**

Figure 2.1 Example of prodrugs of P4H with *in vivo* activity.



Wild type worm

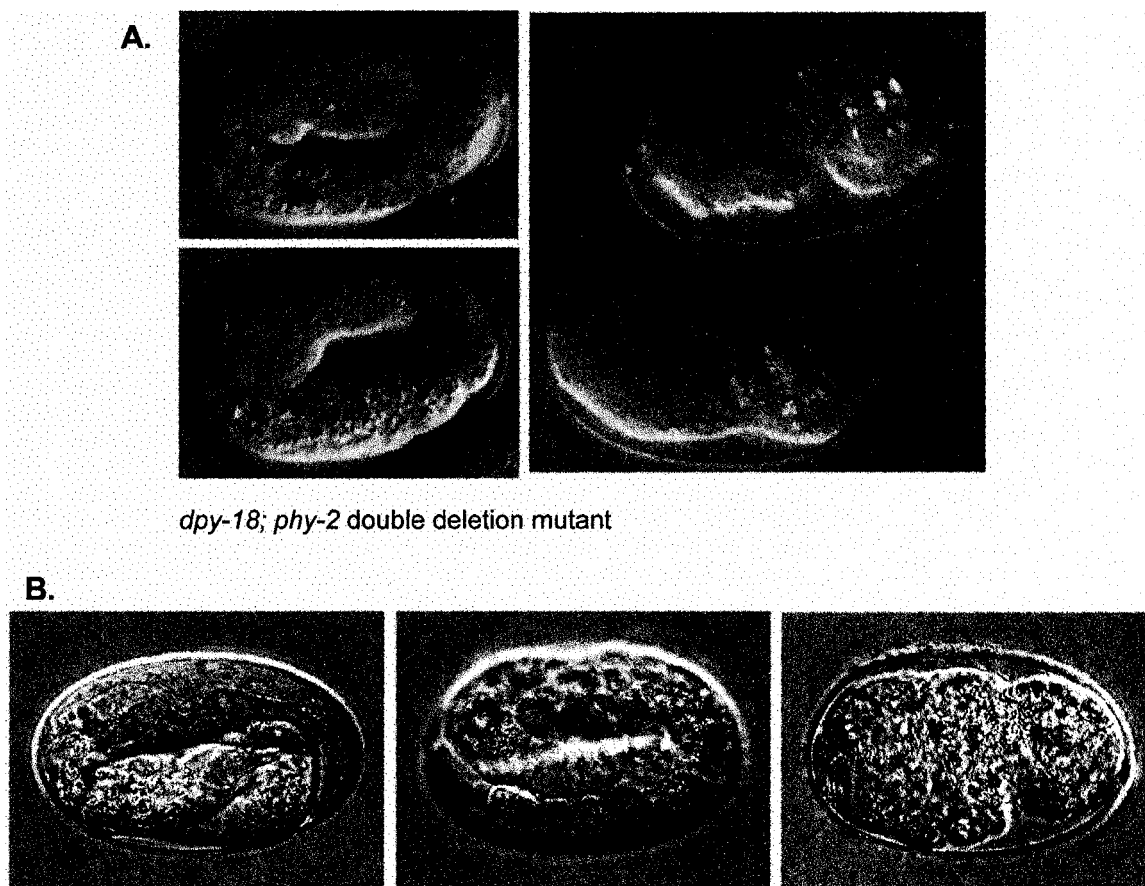


dpy-18 worm



phy-2 worm

Figure 2.2 The *dpy-18* and *phy-2* *C. elegans* phenotypes. Nomarski differential interference contrast images, lateral view; young adult hermaphrodites that have not begun to lay embryos. All three animals are shown at the same magnification. (A) wild type; (B) *dpy-18(ok162)* homozygote; and (C) *phy-2(ok177)* homozygote.



dpy-18; phy-2 double deletion mutant

Eggs from *dpy-18* worm exposed to dimethyl oxalyglycine

Figure 2.3 Nomarski differential interference contrast image of dead embryos. (A) Double deletion embryos from *dpy-18(ok162)/+; phy-2(ok177)/unc-22(e66)* parent. Counterclockwise from top left: twofold embryo, embryo starting to explode, and embryo after explosion. (B) Embryo from homozygote *dpy-18(ok162)* exposed to dimethyl oxalyglycine (2.2). From left to right: twofold embryo, embryo starting to explode, and embryo after explosion.

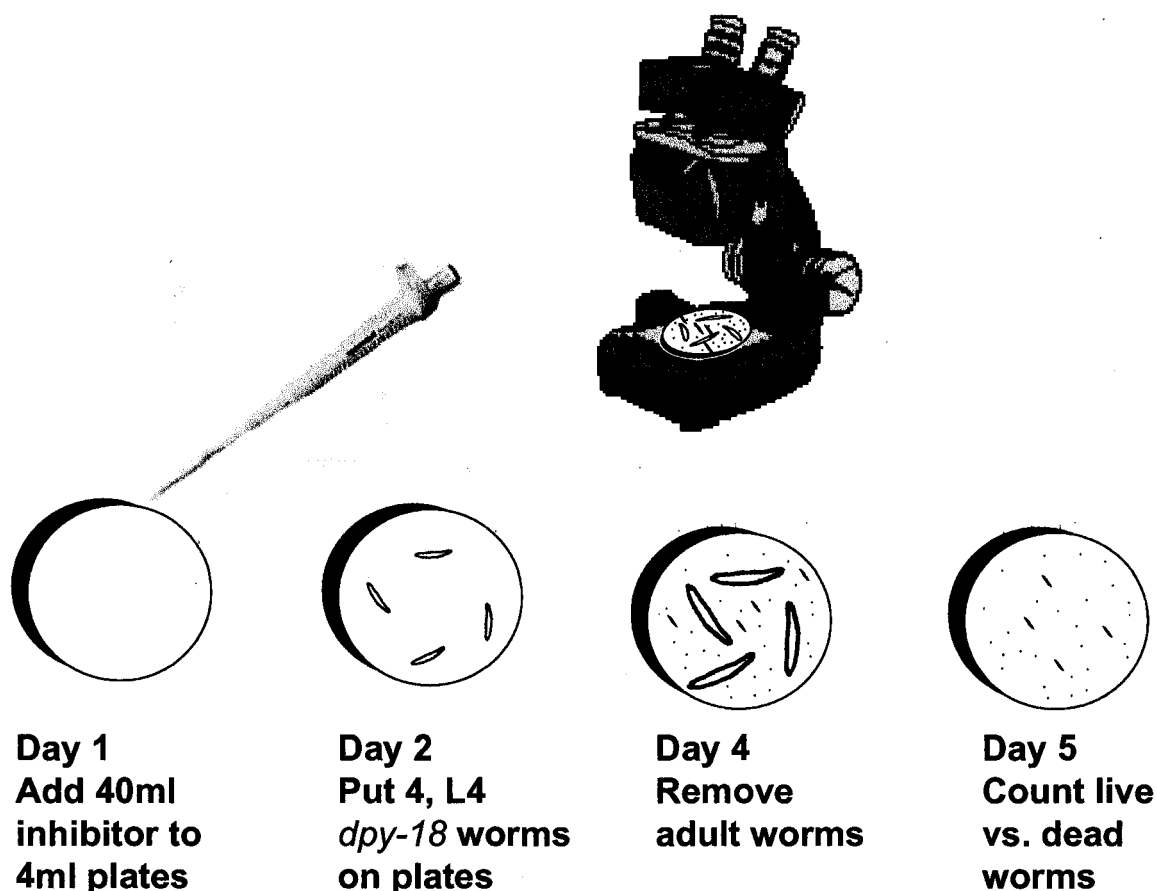


Figure 2.4 *C. elegans* P4H *in vivo* assay. Serial dilutions of inhibitor made from stock solutions (40 or 400 μ l) were added to each plate containing 4 ml of solid growth medium. Inhibitor were allowed to diffuse into the agar for 24 h. Four L4 worms were then added to each plate. After sufficient time for the L4 worms to grow to adult stage and lay eggs (24 to 48 h), the adult worms were removed to simplify counting. After allowing sufficient time for all live eggs to hatch into worms (24 h), live worms were counted and compared to the number of dead embryos. An average of 40 to 100 embryos and worms were counted on each plate.

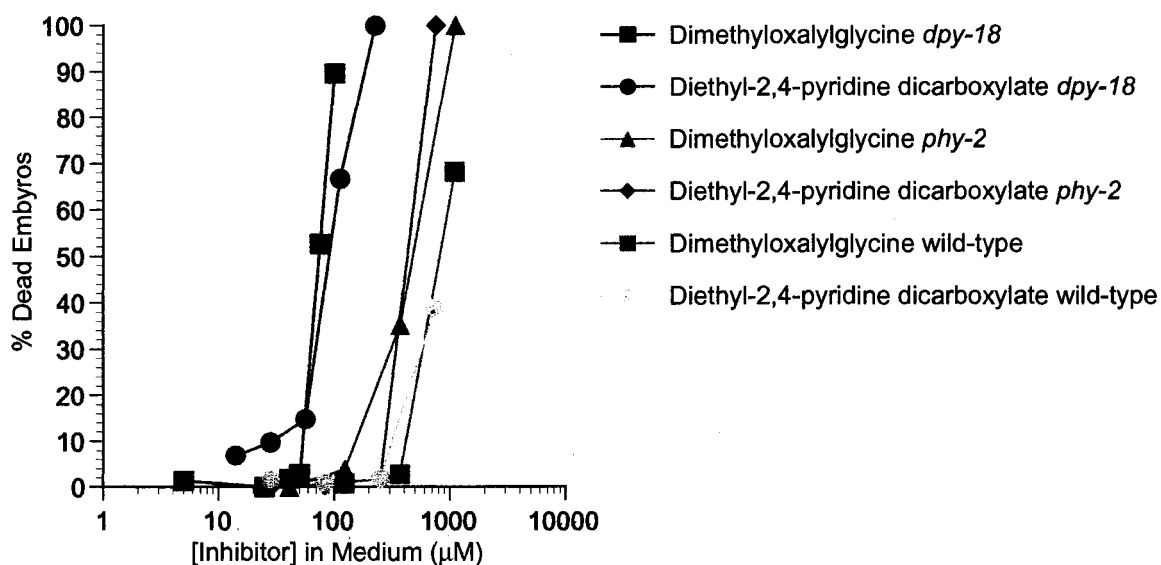
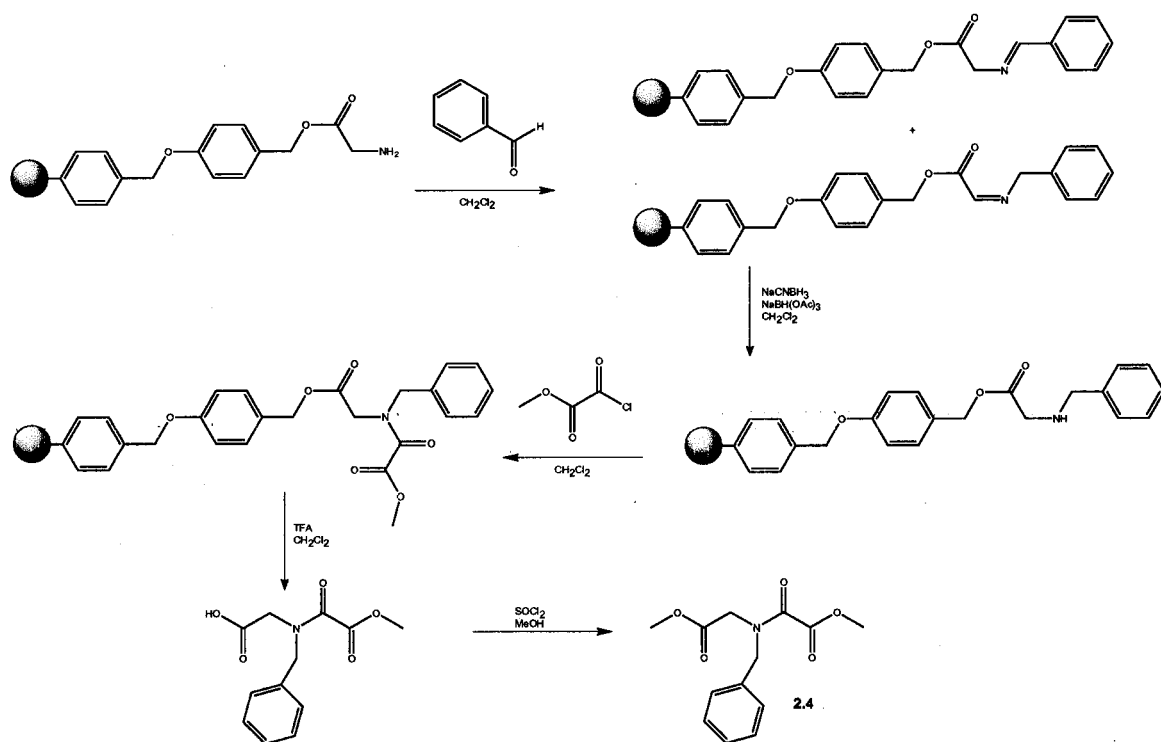


Figure 2.5 Dose response of wild-type, *dpy-18*, and *phy-2* *C. elegans* to diethyl-2,4-pyridine dicarboxylate (2.1) and dimethyloxalyglycine (2.2). Serial dilutions of inhibitor were prepared from DMSO stock solutions. Inhibitor was added to 4 ml plates of Nematode Growth Medium agar, and allowed to diffuse through the agar. Four L4 animals were then added to each plate. Animals were then allowed to grow to adult stage and lay eggs. After sufficient time for eggs to hatch, live worms were counted and compared to the number of dead embryos. Percent dead embryos are presented as a function of the inhibitor concentration on the growth plates.



Scheme 2.1 Synthetic scheme for the library of *N*-branched oxalyglycine compounds.

Reproduced with permission of the copyright owner. Further reproduction prohibited without permission.

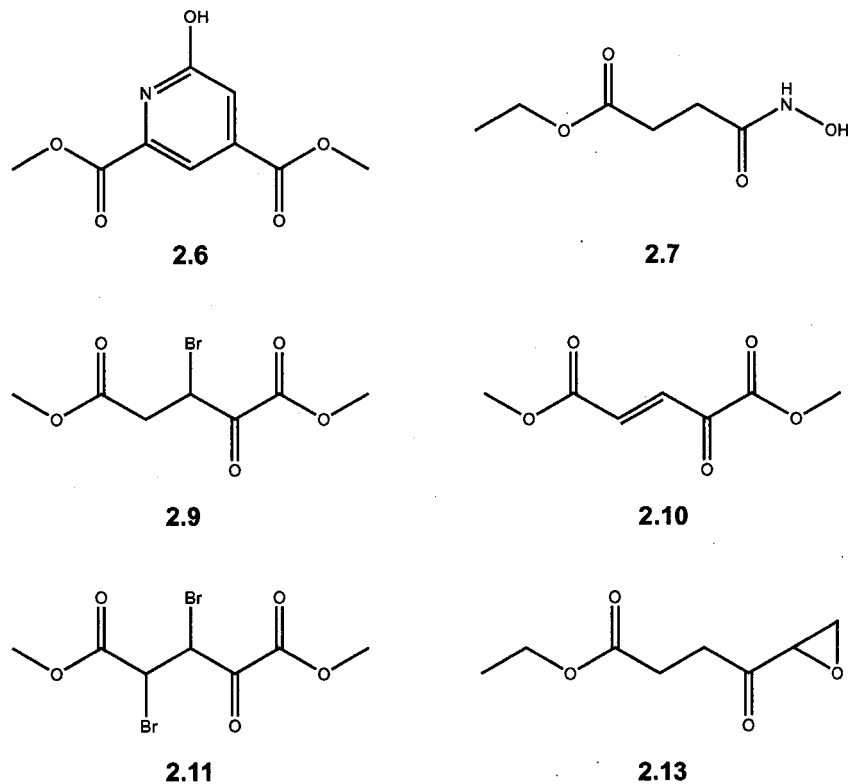
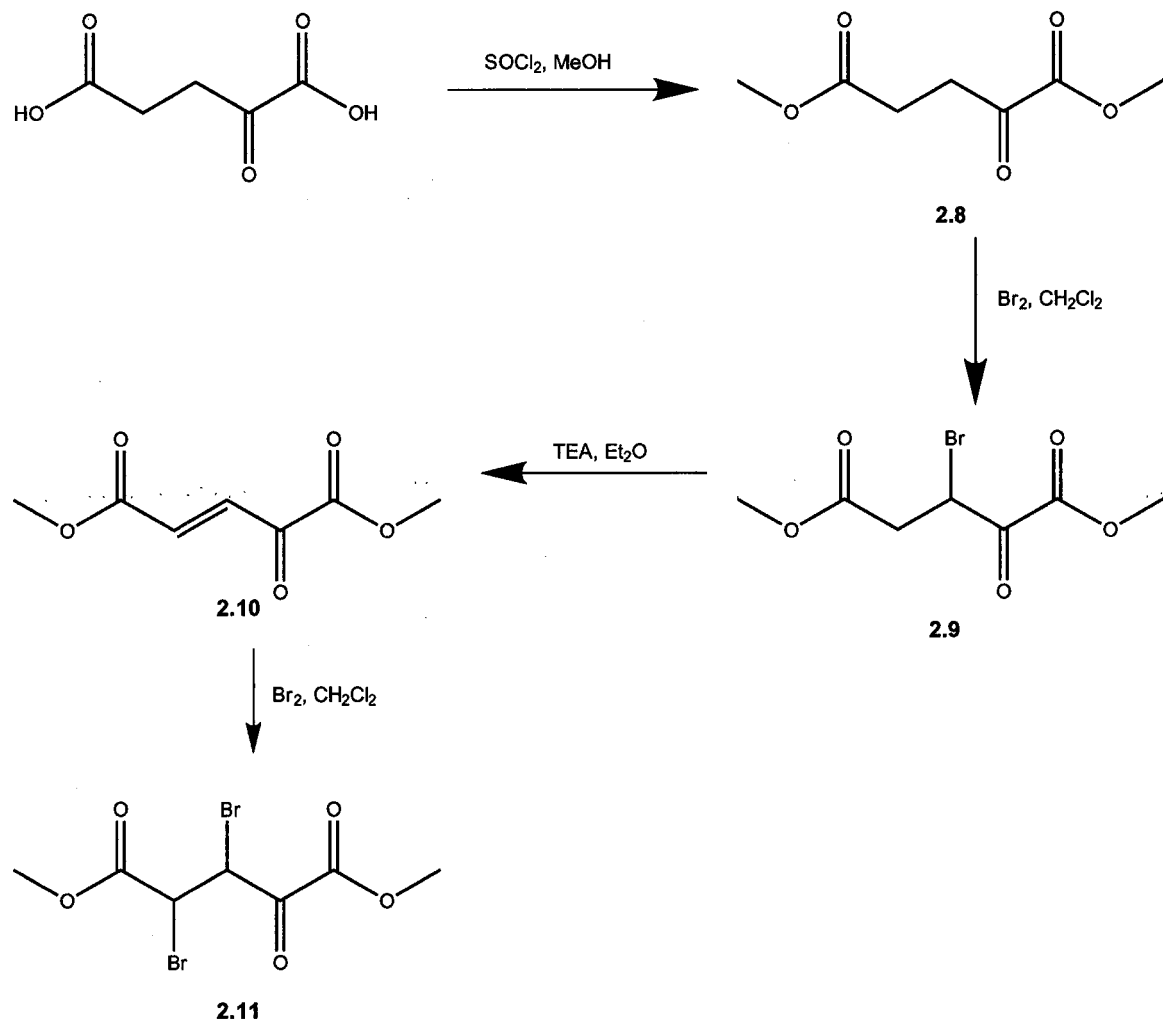
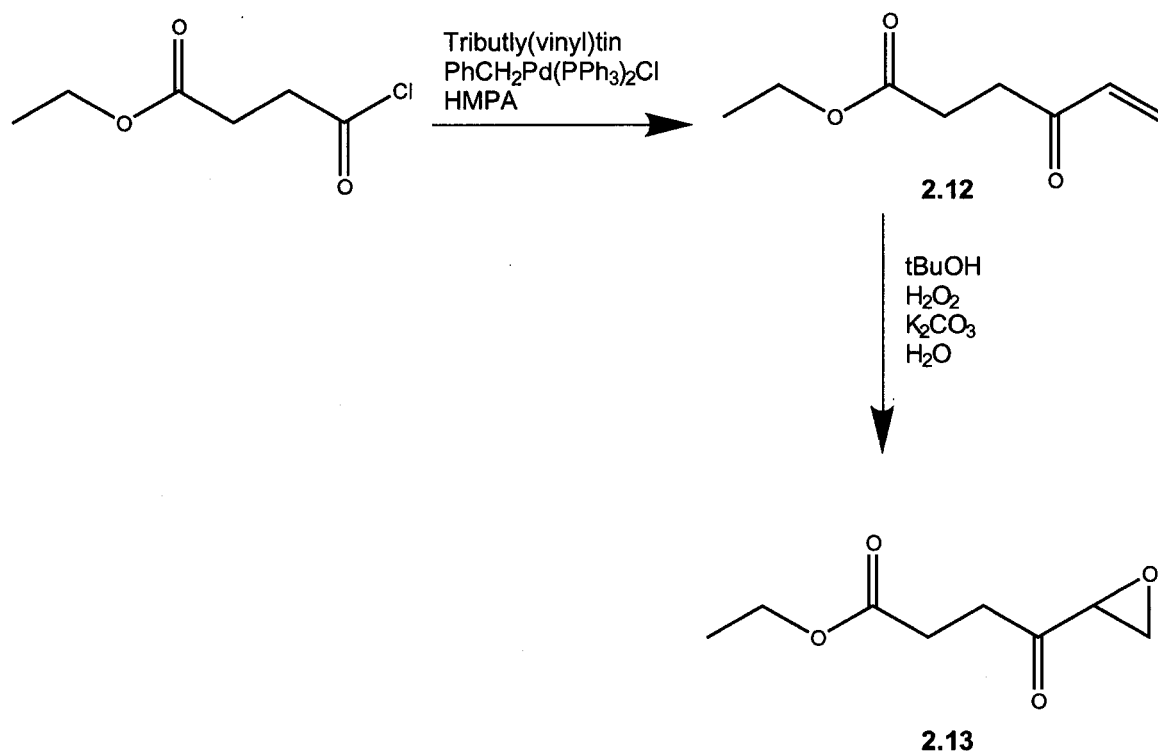


Figure 2.7 Rationally designed inhibitors of P4H based on α -KG.



Scheme 2.2 Synthetic scheme for C3-C4 electrophilic α -KG analogs.



Scheme 2.3 Synthetic scheme for bioavailable epoxy ketone **2.13**.

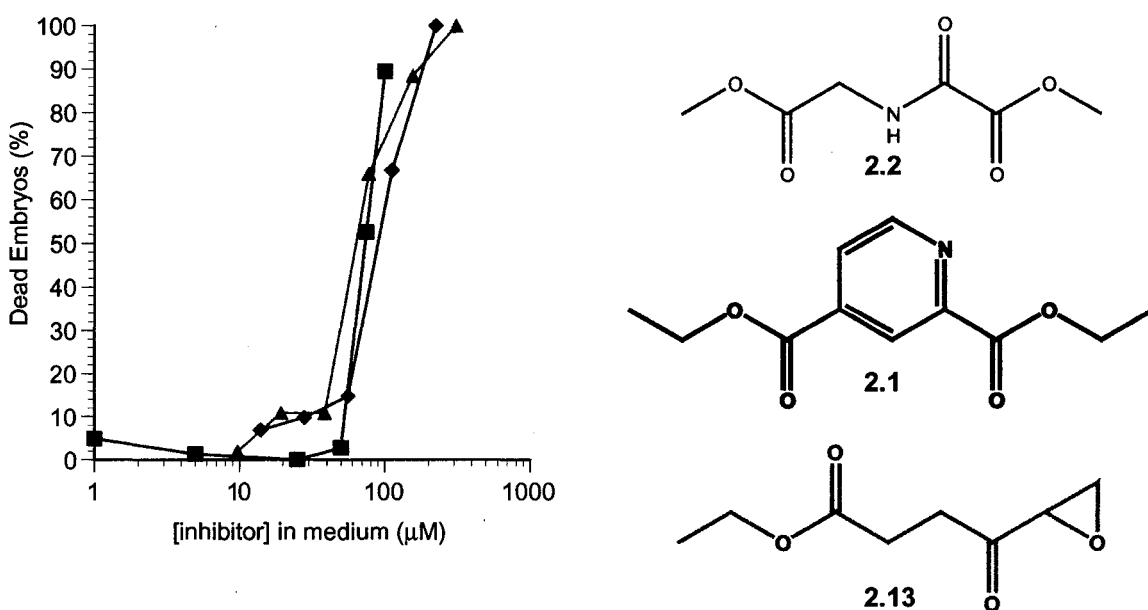
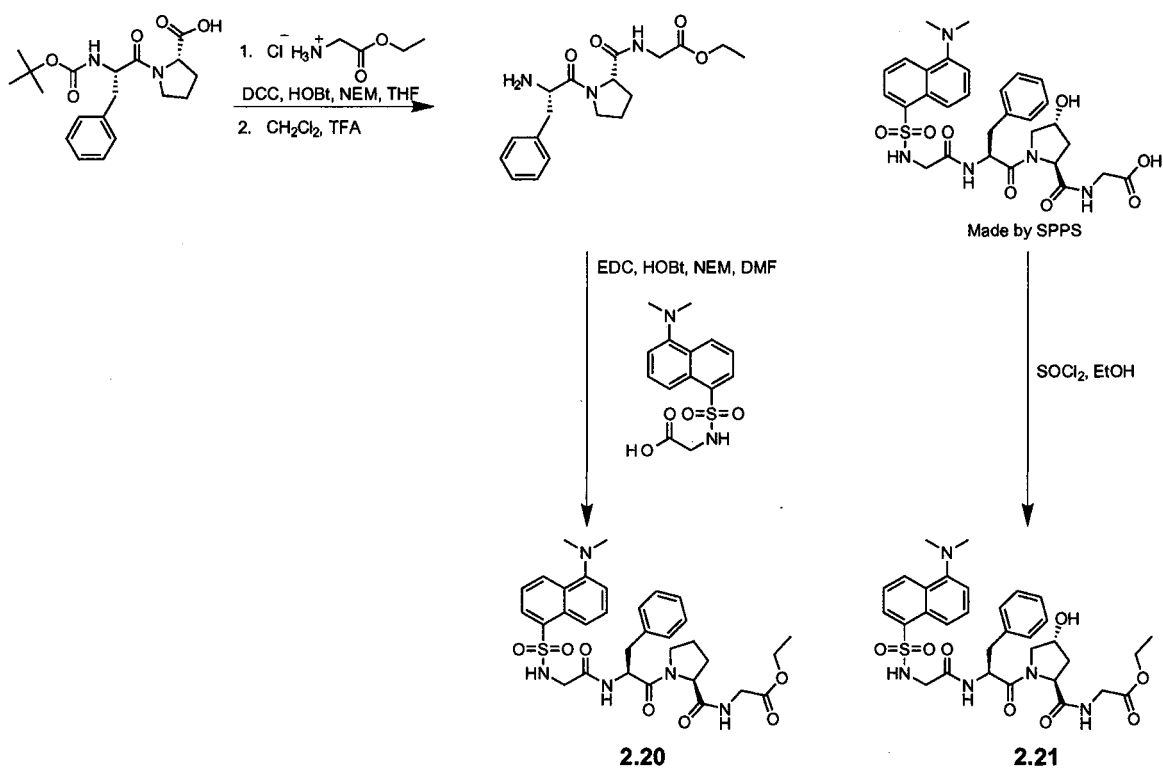


Figure 2.8 Comparison of bioavailable inhibitors in the *dpy-18 C. elegans* assay. Compounds **2.13**, **2.2**, and **2.1** have apparent LC_{50} values of 65 μM , 74 μM , and 90 μM respectively. Serial dilutions of inhibitors were prepared from DMSO stock solutions. Inhibitors were added to 4 ml plates of solid Nematode growth medium, and allowed to diffuse through the agar. Four L4 animals were then added to each plate. After the L4 worms were allowed to grow to adult stage and lay eggs, and after sufficient time for all eggs to hatch, live worms were counted and compared to the number of dead embryos. Percent dead embryos are presented as a function of inhibitor concentration on the growth medium.



Scheme 2.4 Synthetic scheme for the dansylated peptide substrate and product for the *in vitro* P4H activity assay.

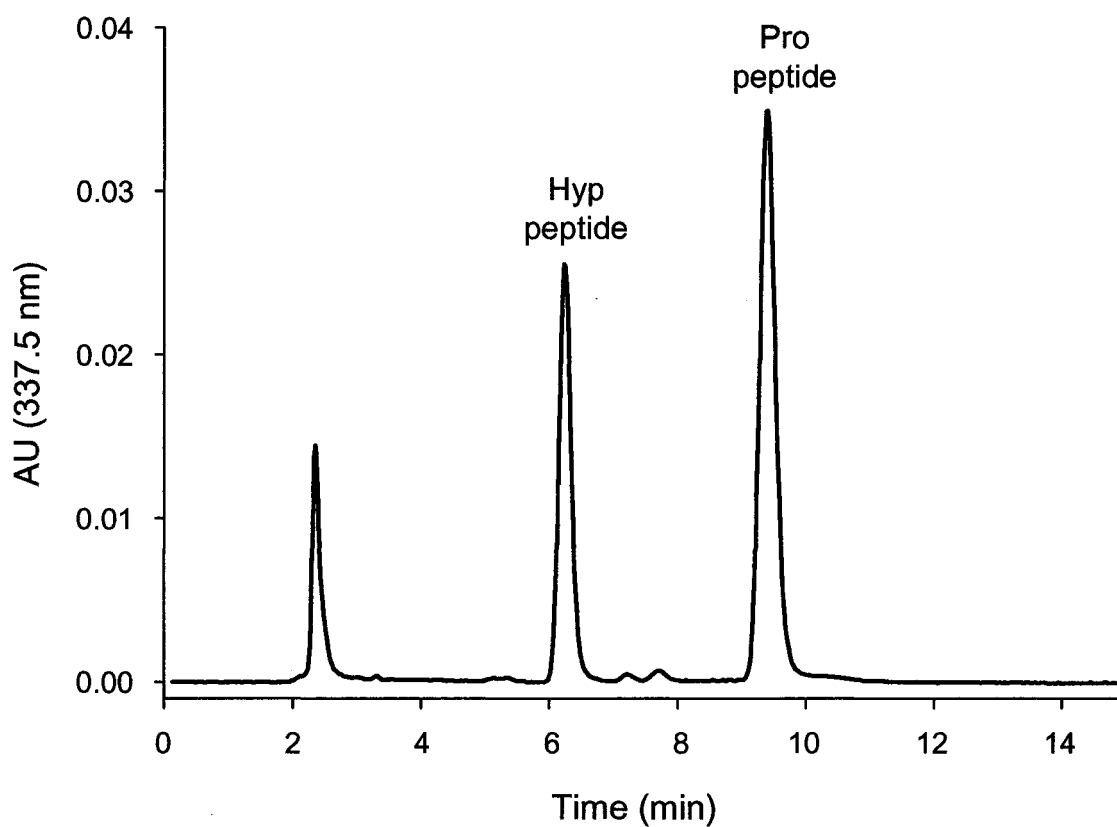


Figure 2.9 Representative HPLC trace of the *in vitro* P4H activity assay. Hydroxylation reactions were injected onto a reversed-phase C18 HPLC column (Varian Microsorb-MV, 4.6 x 250 mm, 100 Å pore size) (50% v/v, aq acetonitrile, 1 ml/min) and observed at 337.5 nm.

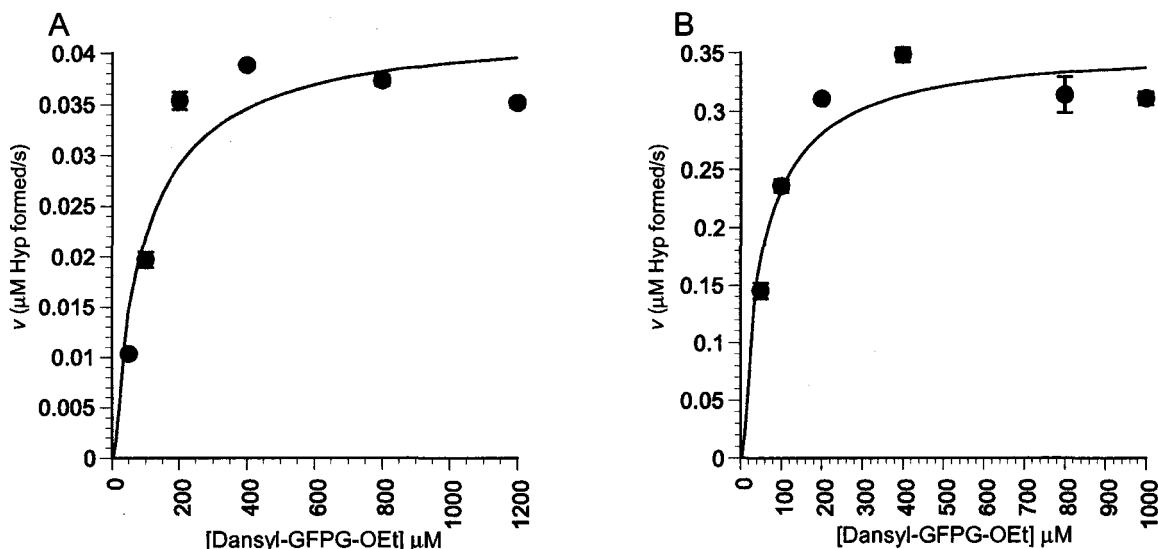
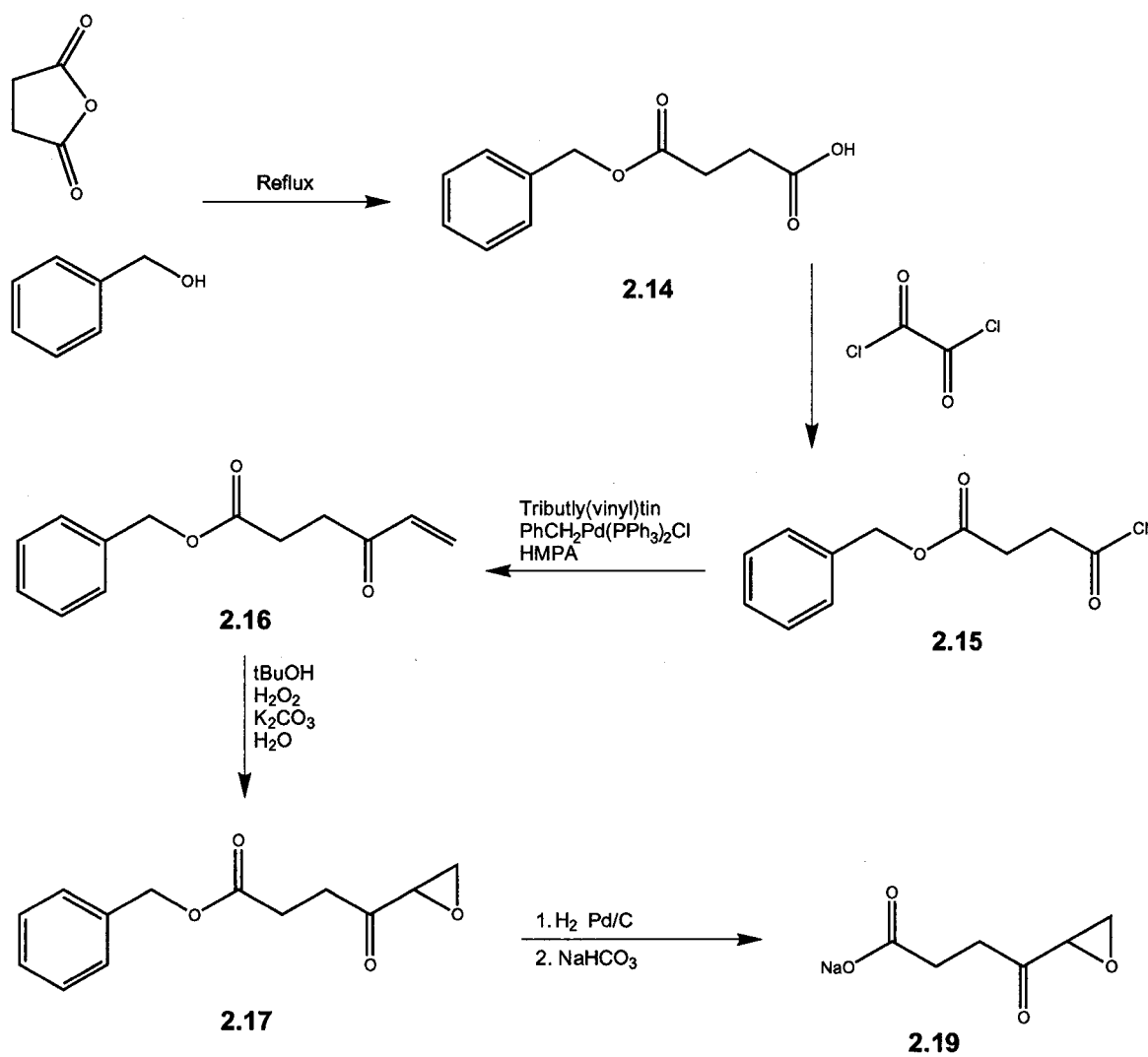


Figure 2.10 Comparison of catalysis by human P4H produced in a baculovirus system and human P4H produced in *E. coli*. The reactions contained P4H (0.43 μM), FeSO_4 (0.1 mM), BSA (1 mg/ml), catalase (0.1 mg/ml), ascorbate (2 mM), DTT (0.1 mM), α -KG (0.5 mM), and dansyl-Gly-Phe-Pro-Gly-OEt in Tris-HCl buffer (50 mM, pH 7.8) at 25 °C. The reactions were quenched at 5 min by boiling for 30 s. The aliquots were injected onto a reversed-phase C18 HPLC column (50% (v/v), aqueous acetonitrile, 1 ml/min) and observed at 337.5 nm. A: Human P4H produced in a baculovirus system hydroxylates dansyl-Gly-Phe-Pro-Gly-OEt to dansyl-Gly-Phe-Hyp-Gly-OEt with kinetic constants of $V_{\text{max}} = 0.04 \mu\text{M Hyp/sec}$, $K_m = 90 \mu\text{M}$, and $k_{\text{cat}} = 0.09 \text{ s}^{-1}$. B: Human P4H produced in *E. coli* hydroxylates dansyl-Gly-Phe-Pro-Gly-OEt to dansyl-Gly-Phe-Hyp-Gly-OEt with kinetic constants of $V_{\text{max}} = 0.4 \mu\text{M Hyp/sec}$, $K_m = 50 \mu\text{M}$, and $k_{\text{cat}} = 0.7 \text{ s}^{-1}$. Constants were derived from the Michaelis-Menton equation $v = V_{\text{max}} / ((K_m / [\text{substrate}]) + 1)$.



Scheme 2.5 Synthetic scheme for the epoxy ketone **2.19** for *in vitro* analysis.

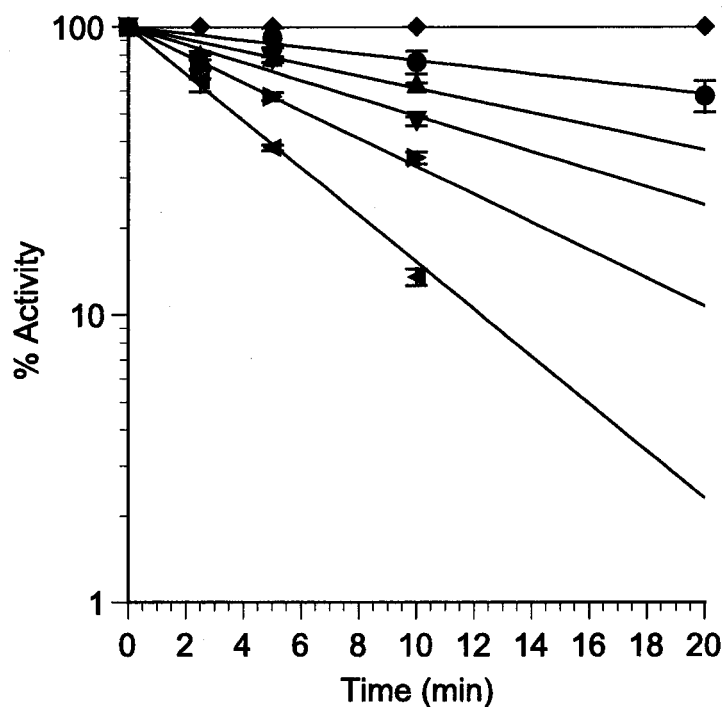


Figure 2.11 Epoxy ketone inhibitor **2.19** shows first-order time- and concentration-dependent inactivation vs activity on a log scale. Epoxy ketone (● = 33, ▲ = 67, ▼ = 111, ▴ = 178 and ◆ = 356 mM) **2.19**, P4H (43 μ M), FeSO₄ (2 mM) were preincubated at 25 °C for various times. BSA (1 mg/ml), catalase (0.1 mg/ml), ascorbate (2 mM), DTT (0.1 mM), α -KG (0.5 mM), and dansyl-Gly-Phe-Pro-Gly-OEt (2.5 mM) in 50 mM Tris-HCl buffer (pH 7.8) were added to initiate the reaction. Aliquots were taken at 15, 60, 120, 180, 240, and 300 s., and were quenched by boiling for 30 s. The aliquots were injected onto a reversed phase C18 HPLC column (50% (v/v), aqueous acetonitrile, 1 ml/min) and observed at 337.5 nm. Rates were compared to reaction without inhibitor (control = ◆).

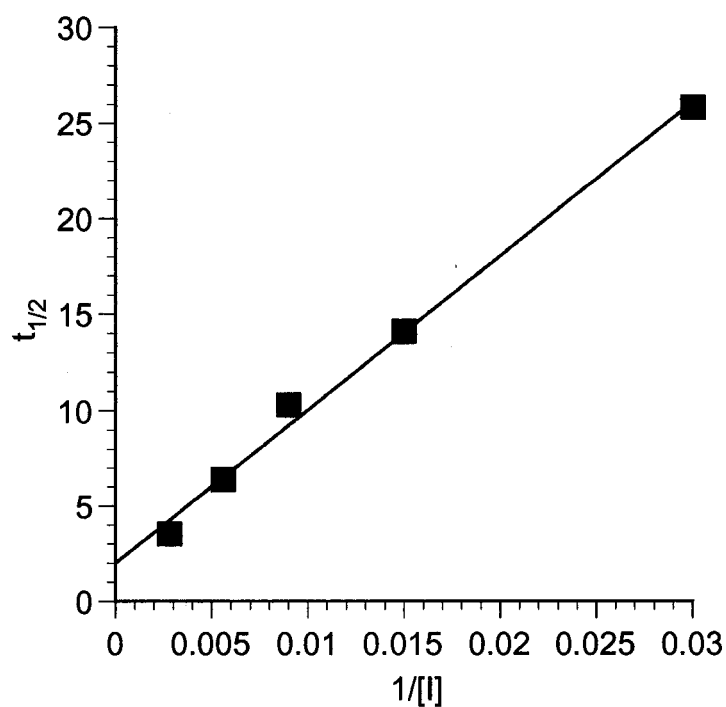


Figure 2.12 Kitz and Wilson plot of half-times for inactivation of human P4H with epoxy ketone **2.19**. Data are from Figure 2.11. The rate of inactivation (k_{inact}) for epoxy ketone **2.19** is 2 min^{-1} and the binding constant (K_I) value is 400 mM. K_I is extrapolated from the negative reciprocal of the y -intercept and k_{inact} is equal to the x -intercept.

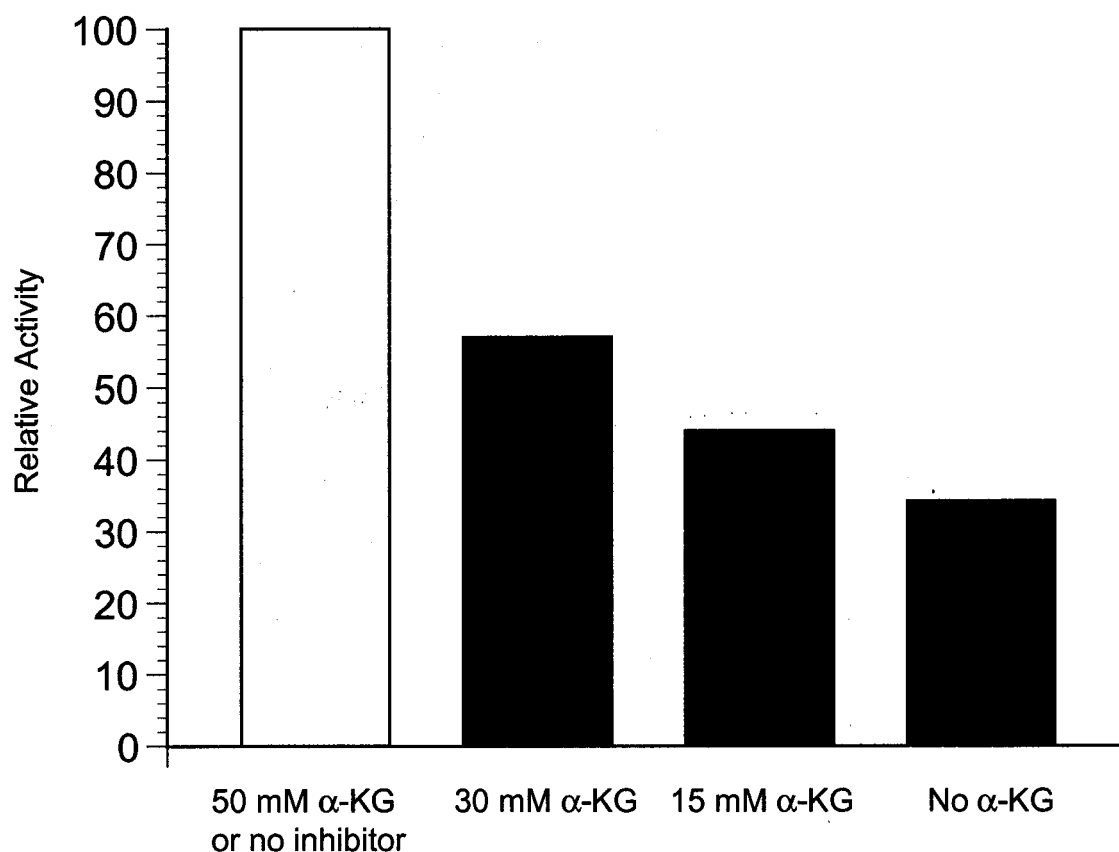


Figure 2.13 α -KG protects human P4H from inactivation by epoxy ketone **2.19**, suggesting irreversible binding in the α -KG binding site of P4H. Epoxy ketone (356 mM) **2.19**, P4H (43 μ M), and FeSO_4 (2 mM) were preincubated for 5 min with α -KG (0, 15, 30, 50 mM). BSA (1 mg/ml), catalase (0.1 mg/ml), ascorbate (2 mM), DTT (0.1 mM), and dansyl-Gly-Phe-Pro-Gly-OEt (2.5 mM) in Tris-HCl buffer (50 mM, pH 7.8) at 25 °C were added to initiate the reaction. Aliquots were taken at 15, 60, 120, 180, 240, and 300 s, and were quenched by boiling for 30 s. The aliquots were injected onto a reversed-phase C18 HPLC column (50% v/v, aq acetonitrile, 1 ml/min) and observed at 337.5 nm. Rates were compared to the reaction without inhibitor.

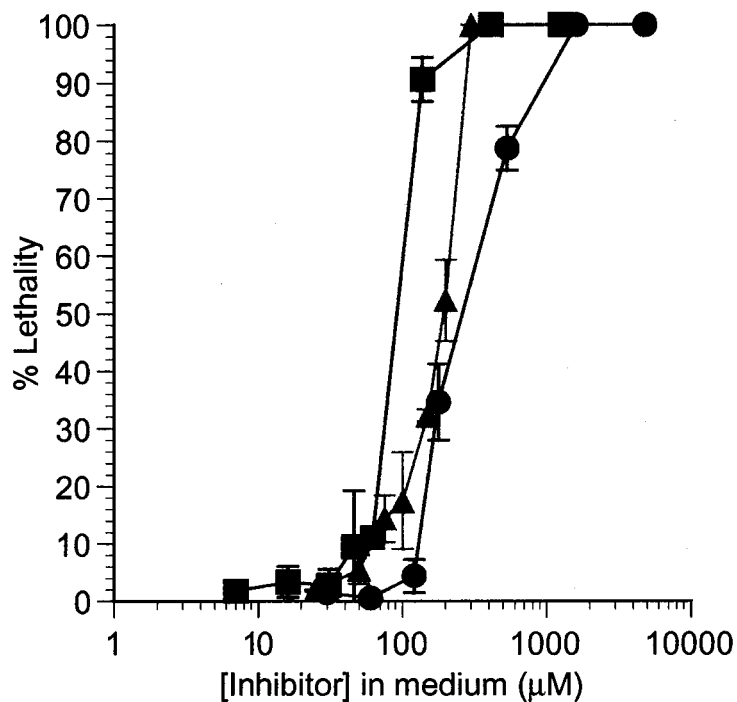
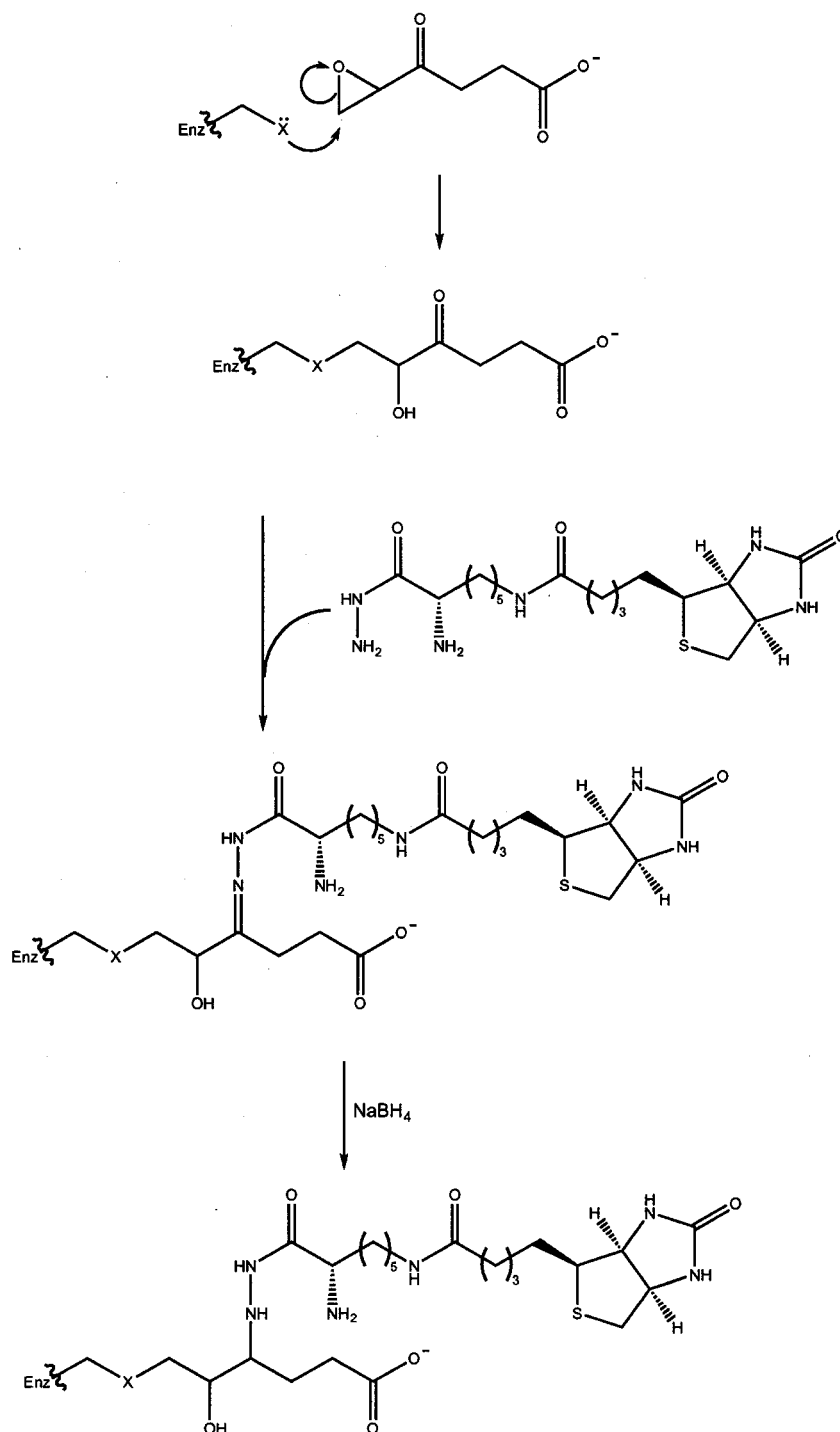


Figure 2.14 Comparison of enantiomers of epoxy ketone **2.13** vs racemic **2.13** in the *dpy-18 C. elegans* assay. ■ = (*S*)-**2.13**, ▲ = racemic **2.13**, and ● = (*R*)-**2.13** have apparent LC₅₀ values of 90 μM, 110 μM, and 115 μM respectively. Serial dilutions of inhibitors were prepared from DMSO stock solutions. Inhibitors were added to 4-ml plates of solid nematode growth medium, and allowed to diffuse through the agar. Four L4 animals were then added to each plate. After the L4 worms were allowed to grow to adult stage and lay eggs, and after sufficient time for all eggs to hatch, live worms were counted and compared to the number of dead embryos. Percent dead embryos are presented as a function of inhibitor concentration on the growth plate.



Scheme 2.6 Proposed mechanism for specific biocytin hydrazide conjugation to irreversibly bound P4H inhibitor **2.19**. Attack at the terminal carbon of the epoxyketone is shown for simplicity, though attack at either epoxide carbon is likely.

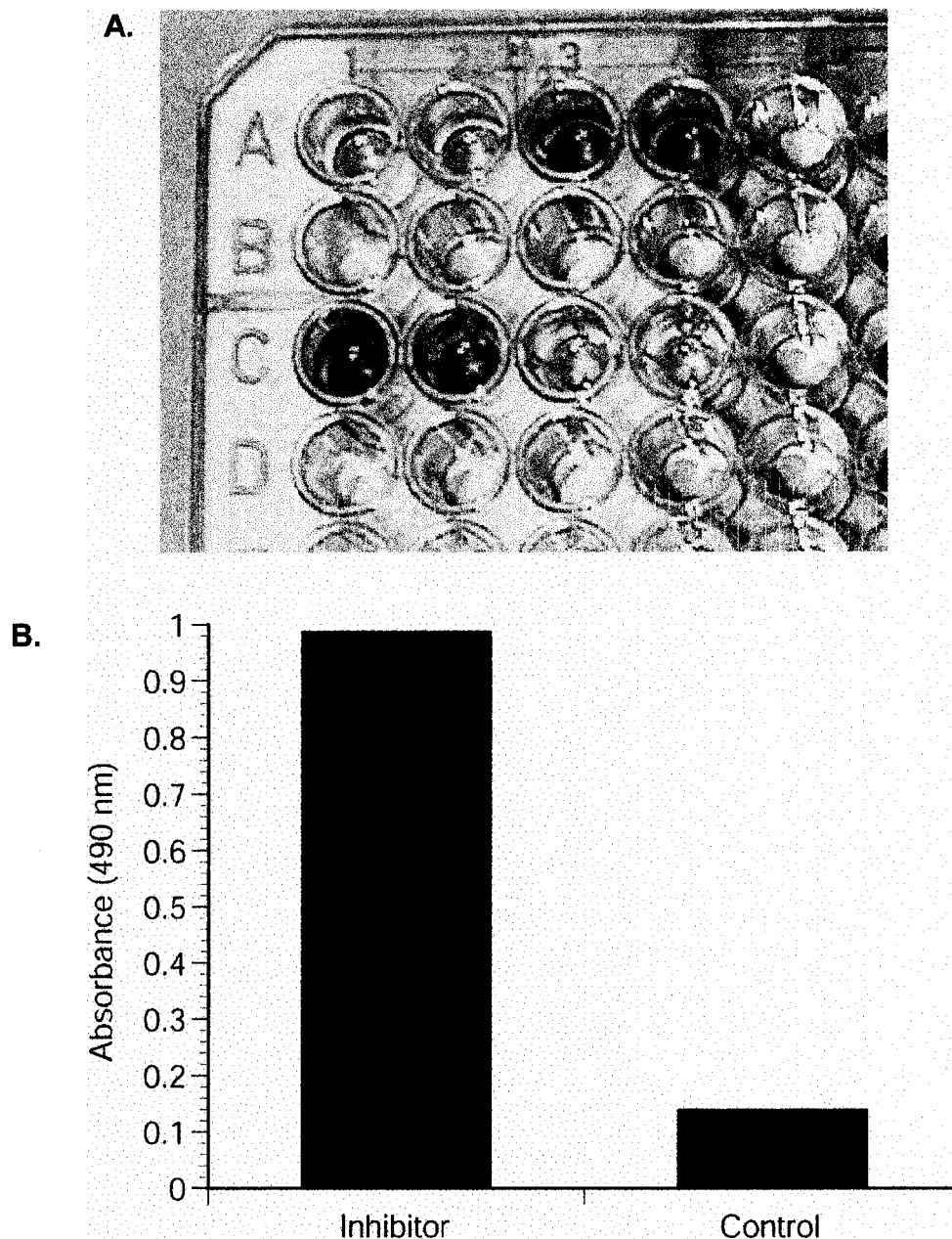
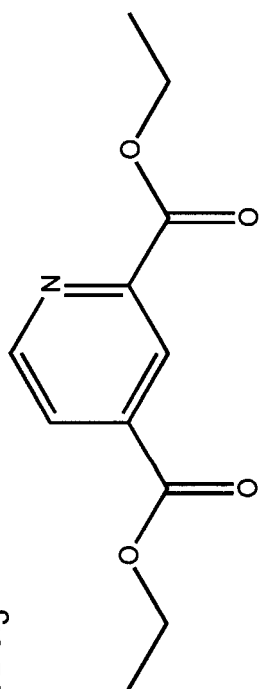
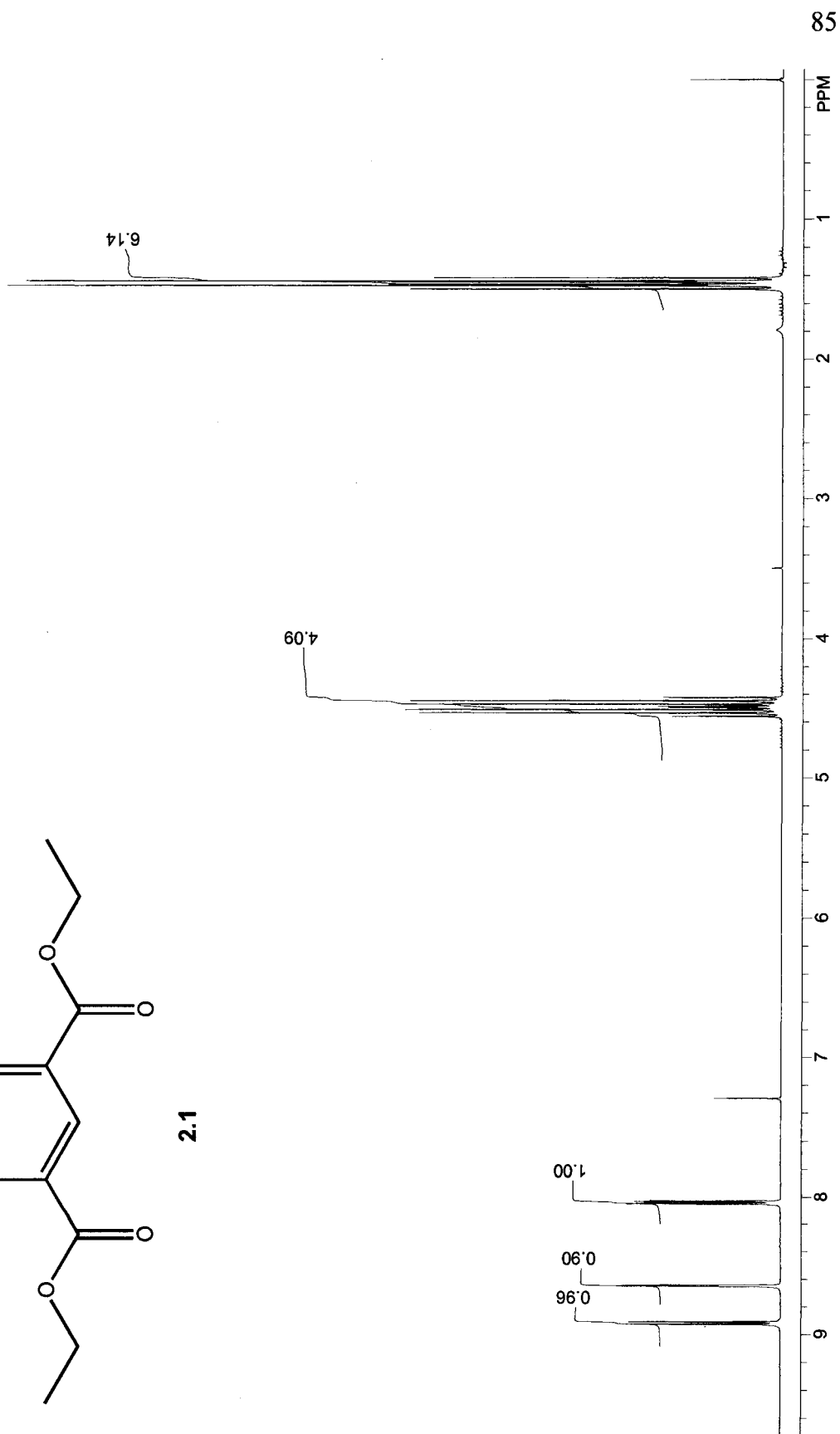


Figure 2.15 P4H immobilization assay. A. Biocytin•inhibitor•P4H complex binds specifically to streptavidin plates. A1: P4H control without inhibitor **2.19**, A2: P4H control without inhibitor **2.19**, A3: P4H with inhibitor **2.19**, A4: P4H with inhibitor **2.19**, C1: 1000 nM peroxidase antibody, C2: 100 nM peroxidase antibody, C3: 10 nM peroxidase antibody, C4: 1 nM peroxidase antibody. B. Quantitation of immobilized P4H. Wells with inhibitor showed peroxidase activity indicating that P4H can be immobilized using the epoxy ketone inhibitor **2.19**.

¹H NMR 300 MHz
CDCl₃



2.1



85

PPM

1

2

3

4

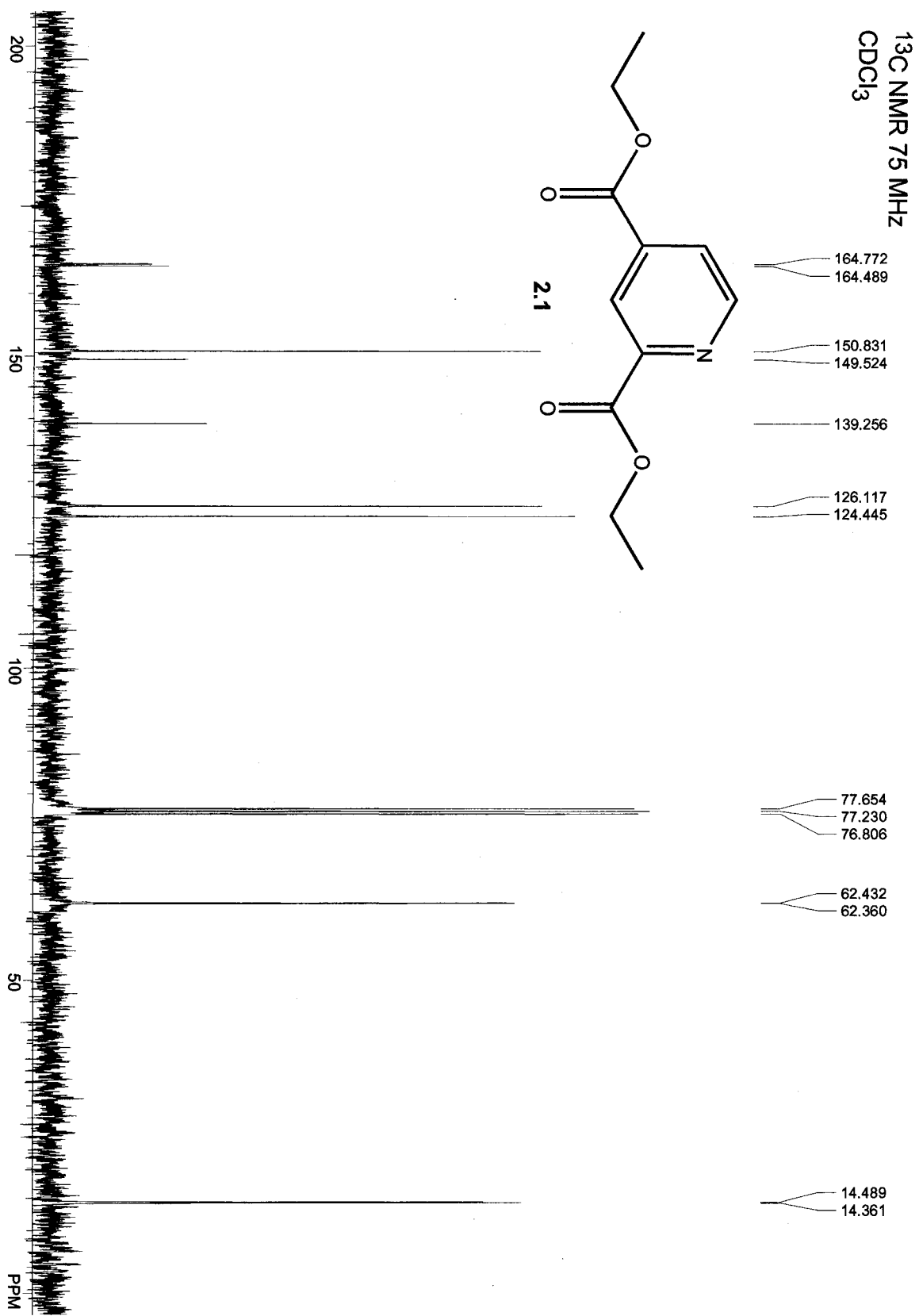
5

6

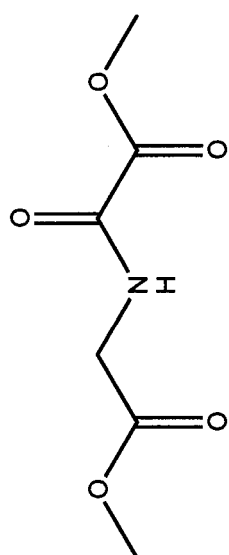
7

8

9



¹H NMR 300 MHz
CDCl₃



2.2

3.00
2.95

2.05

0.56

0.69

87

PPM

1

2

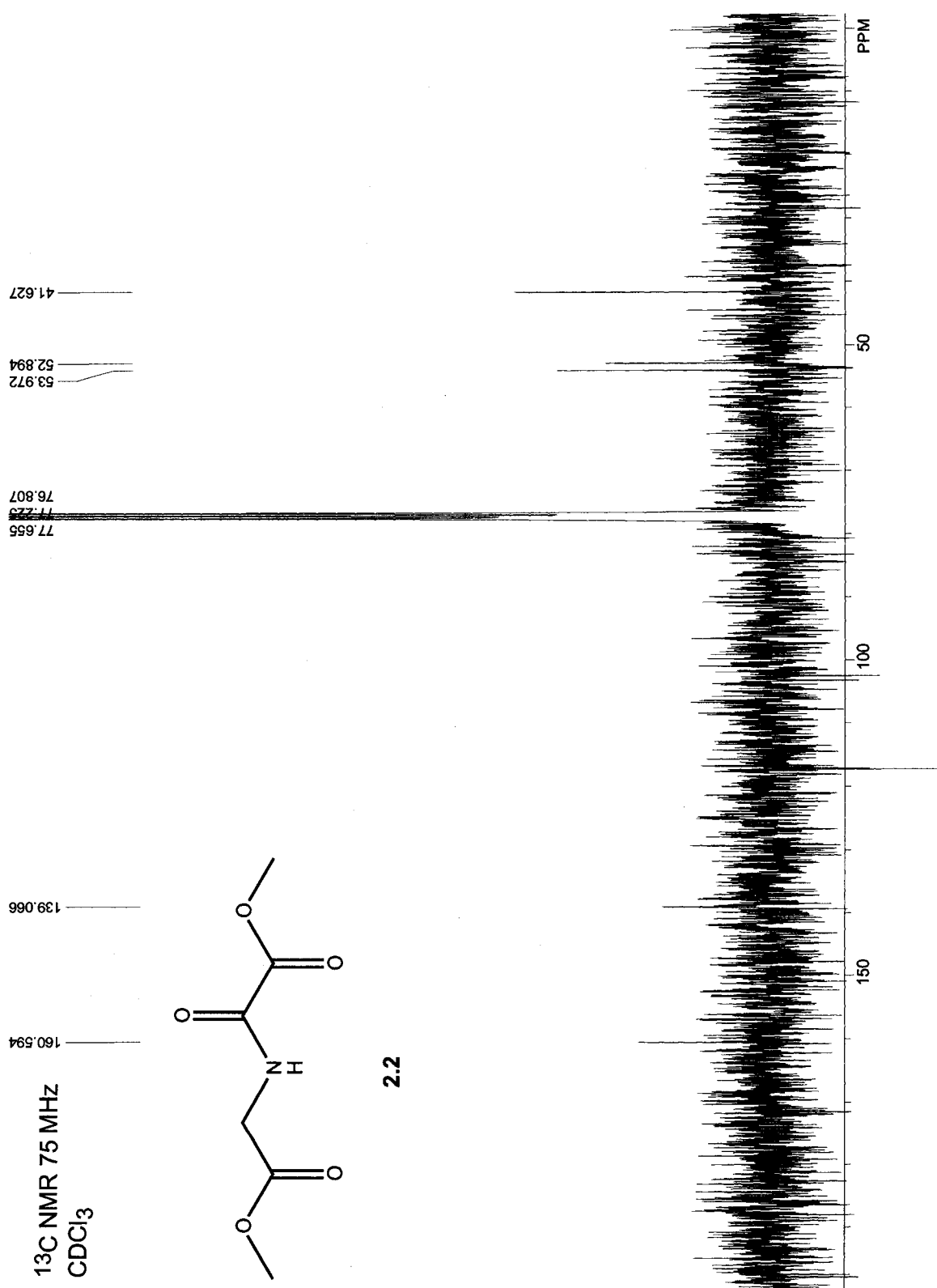
3

4

5

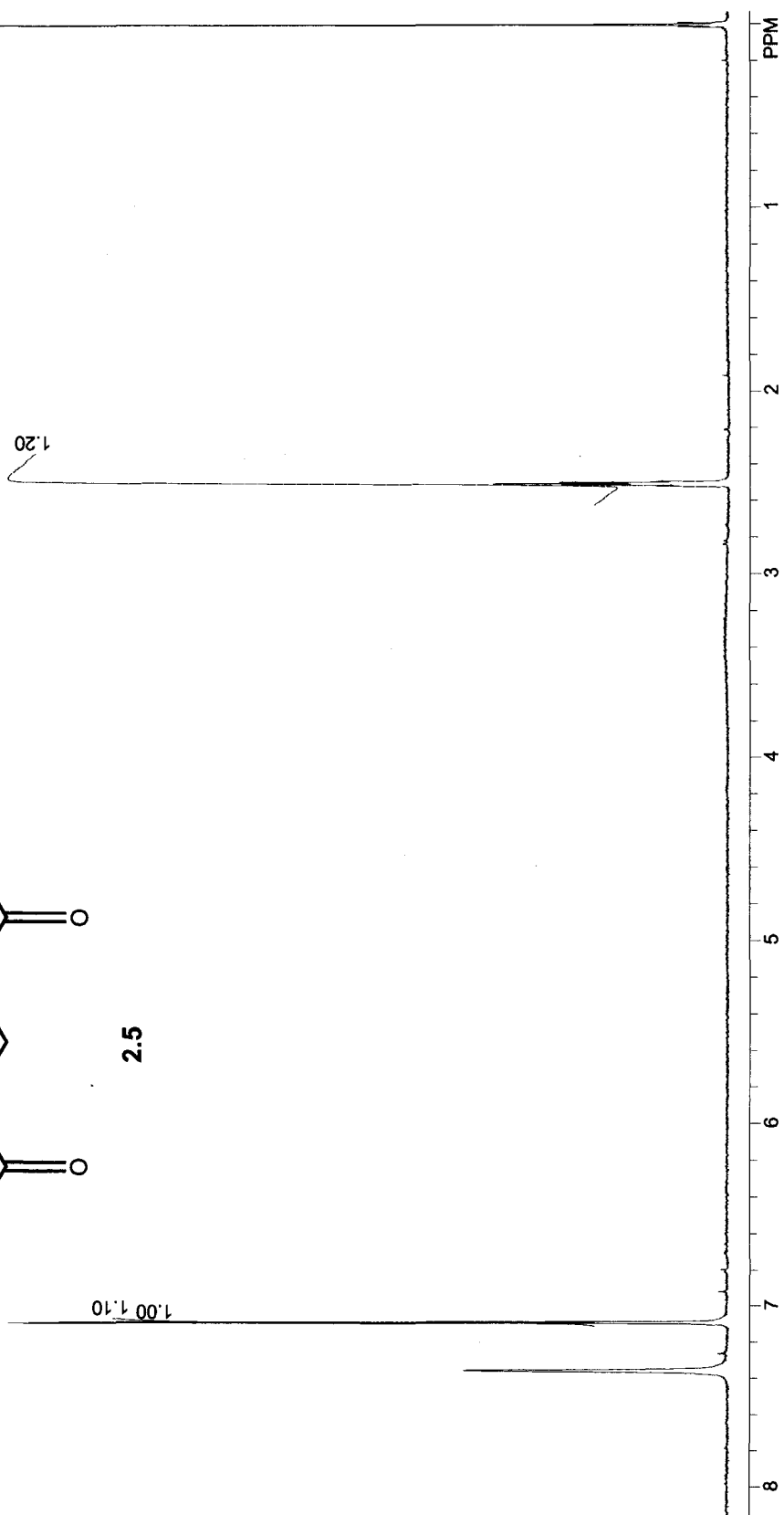
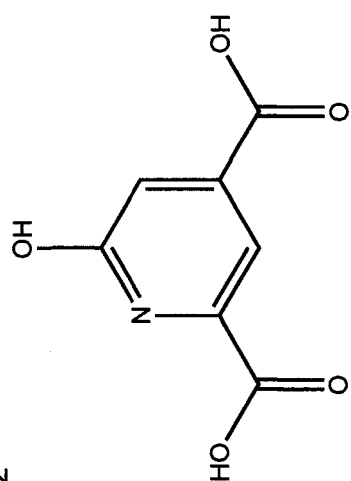
6

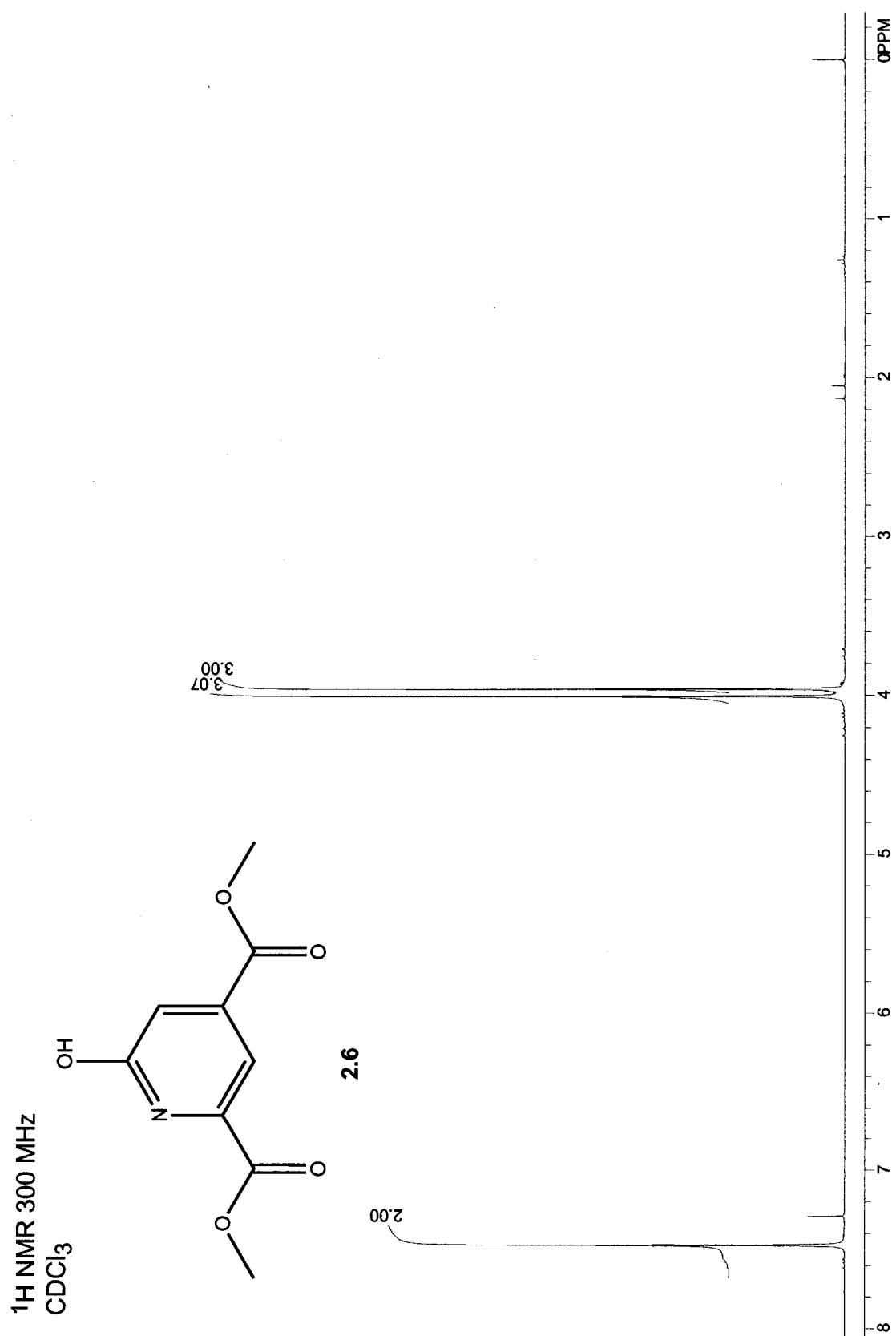
7

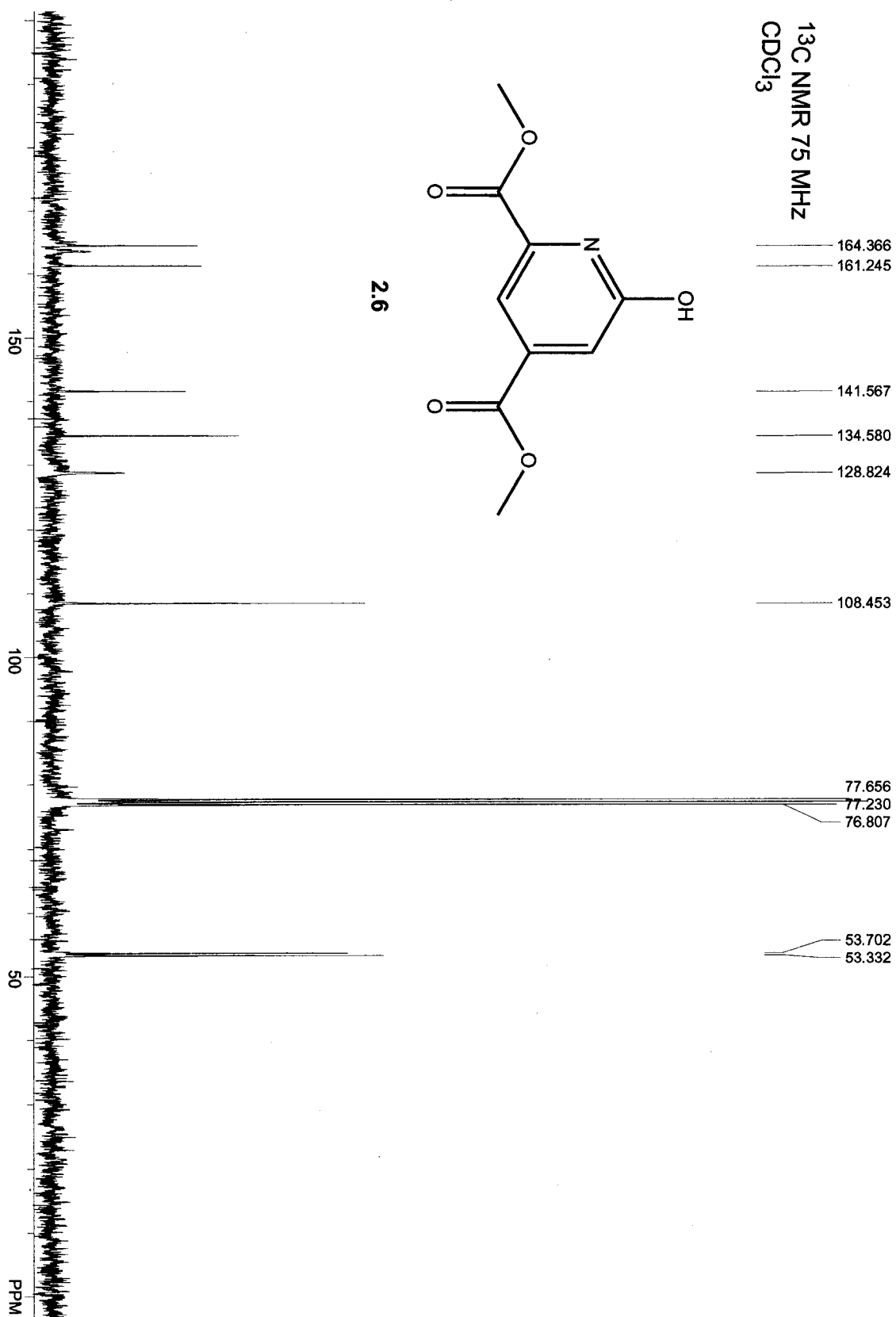


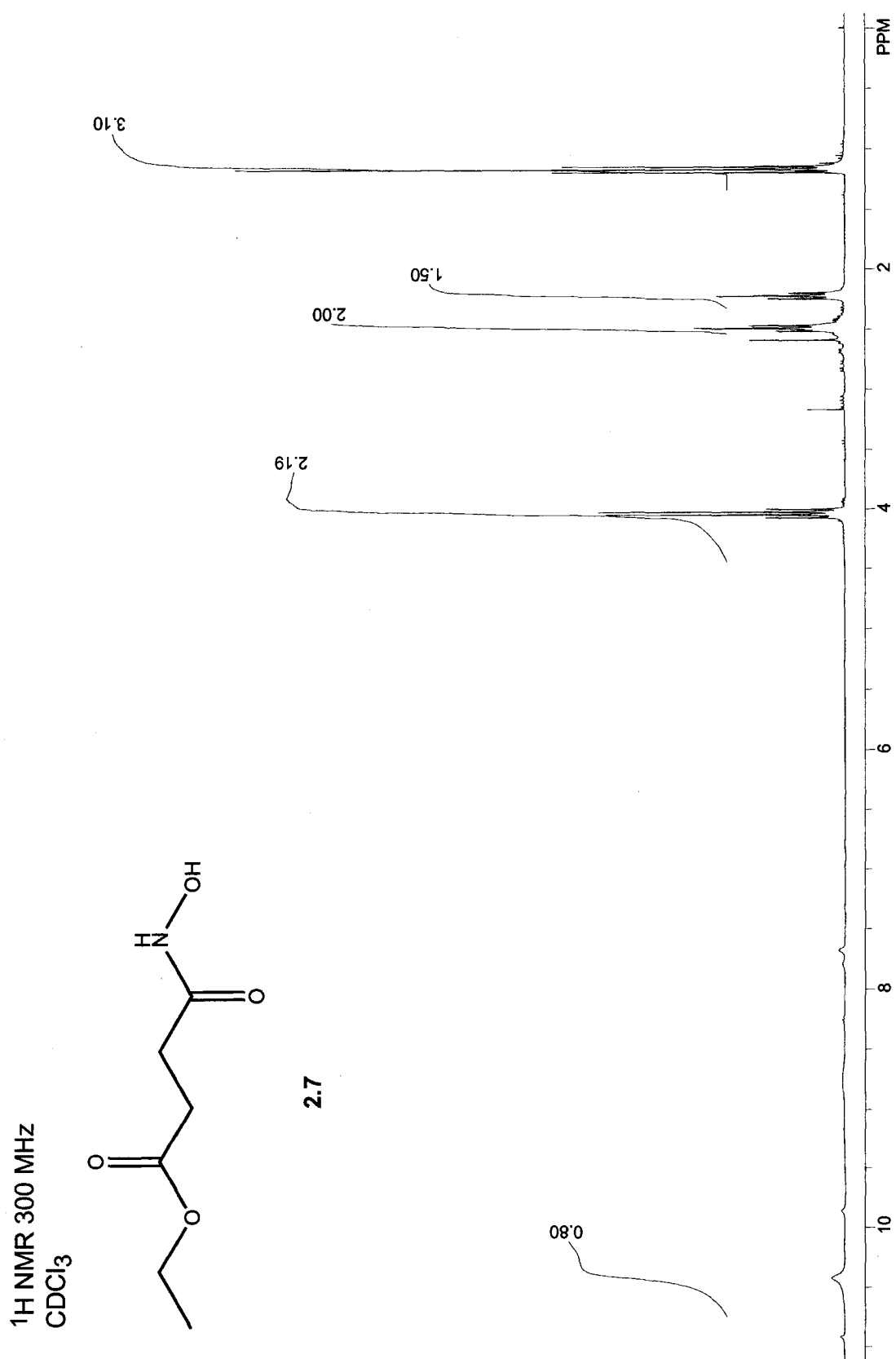


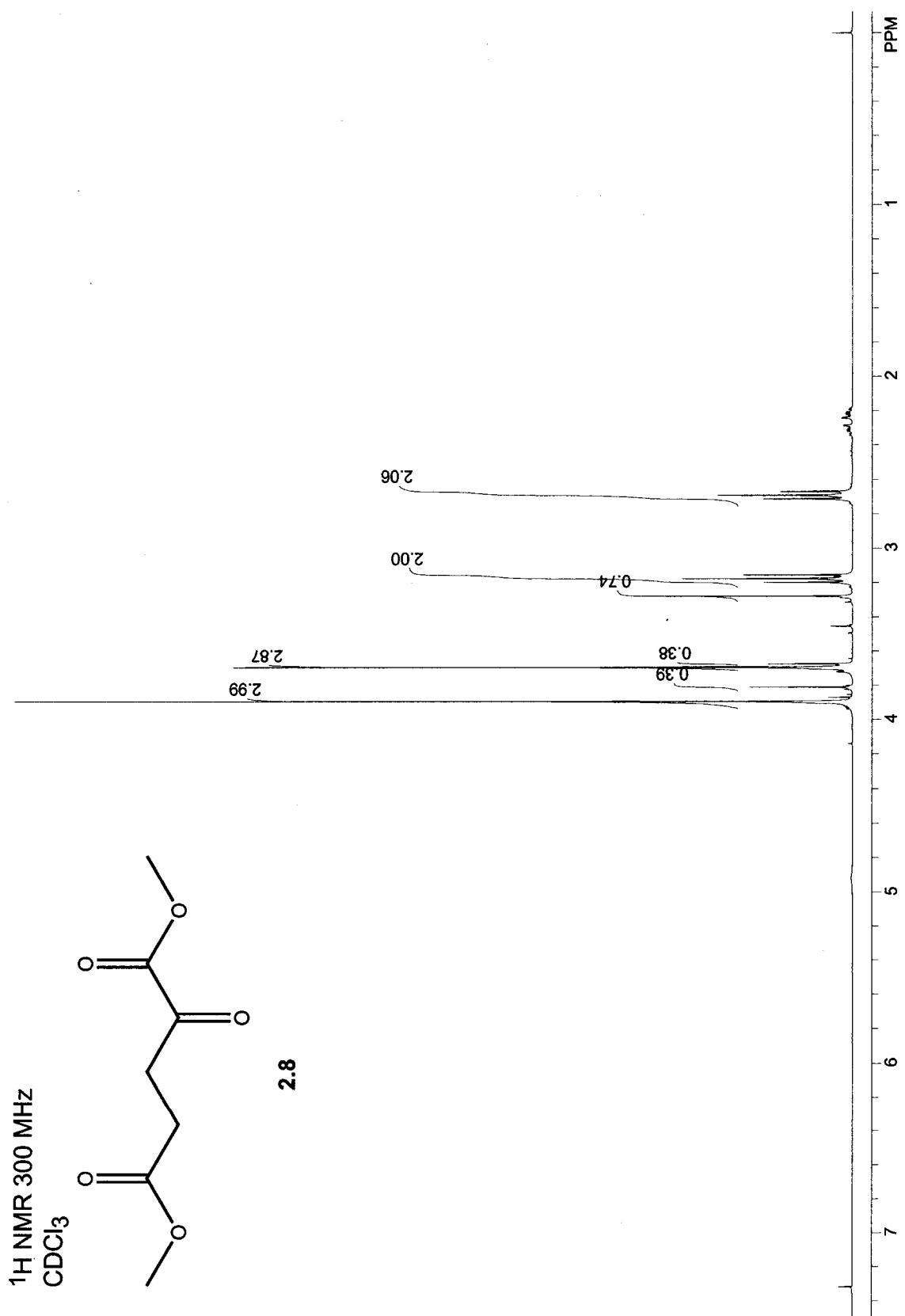
¹H NMR 300 MHz
CDCl₃

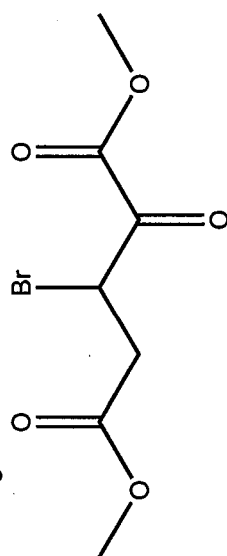




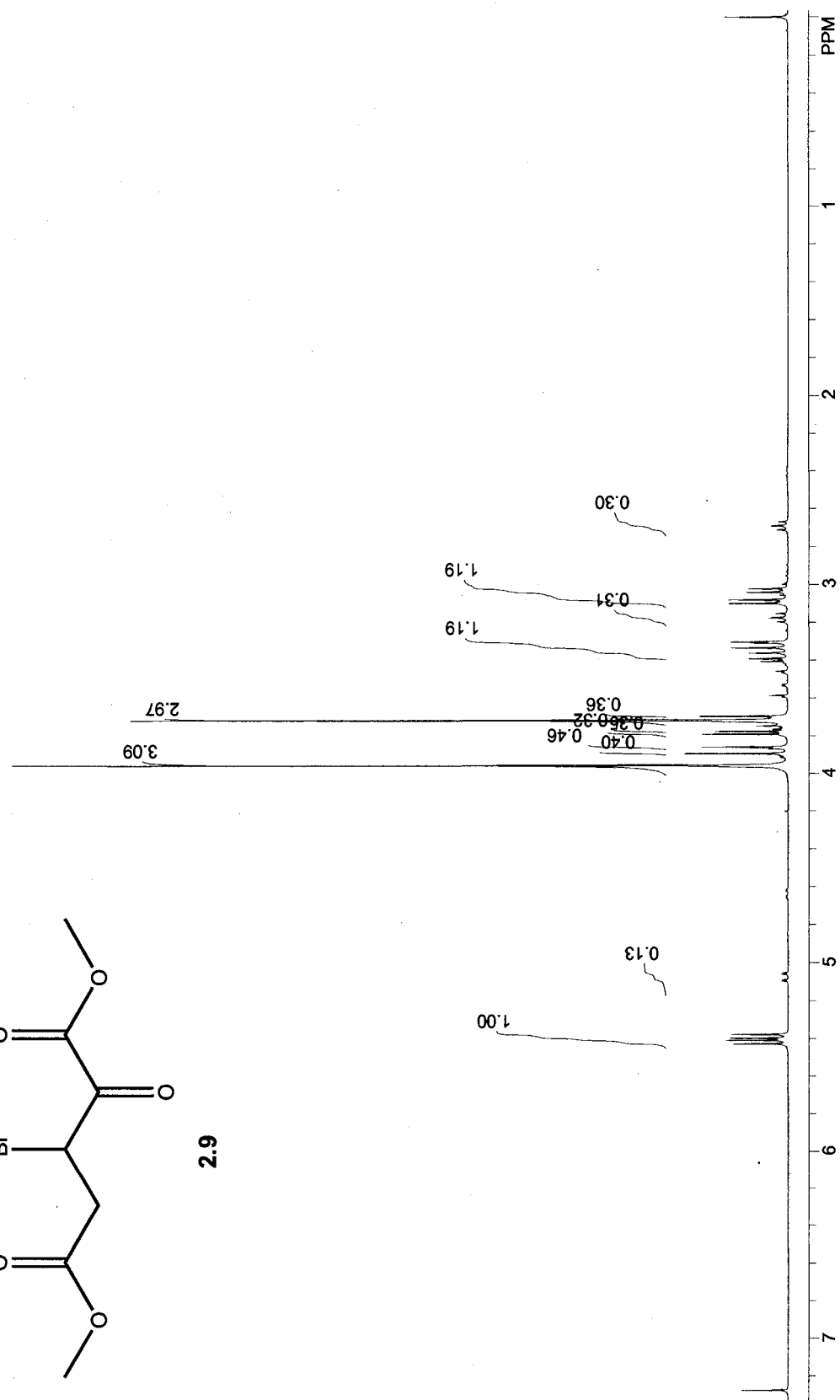


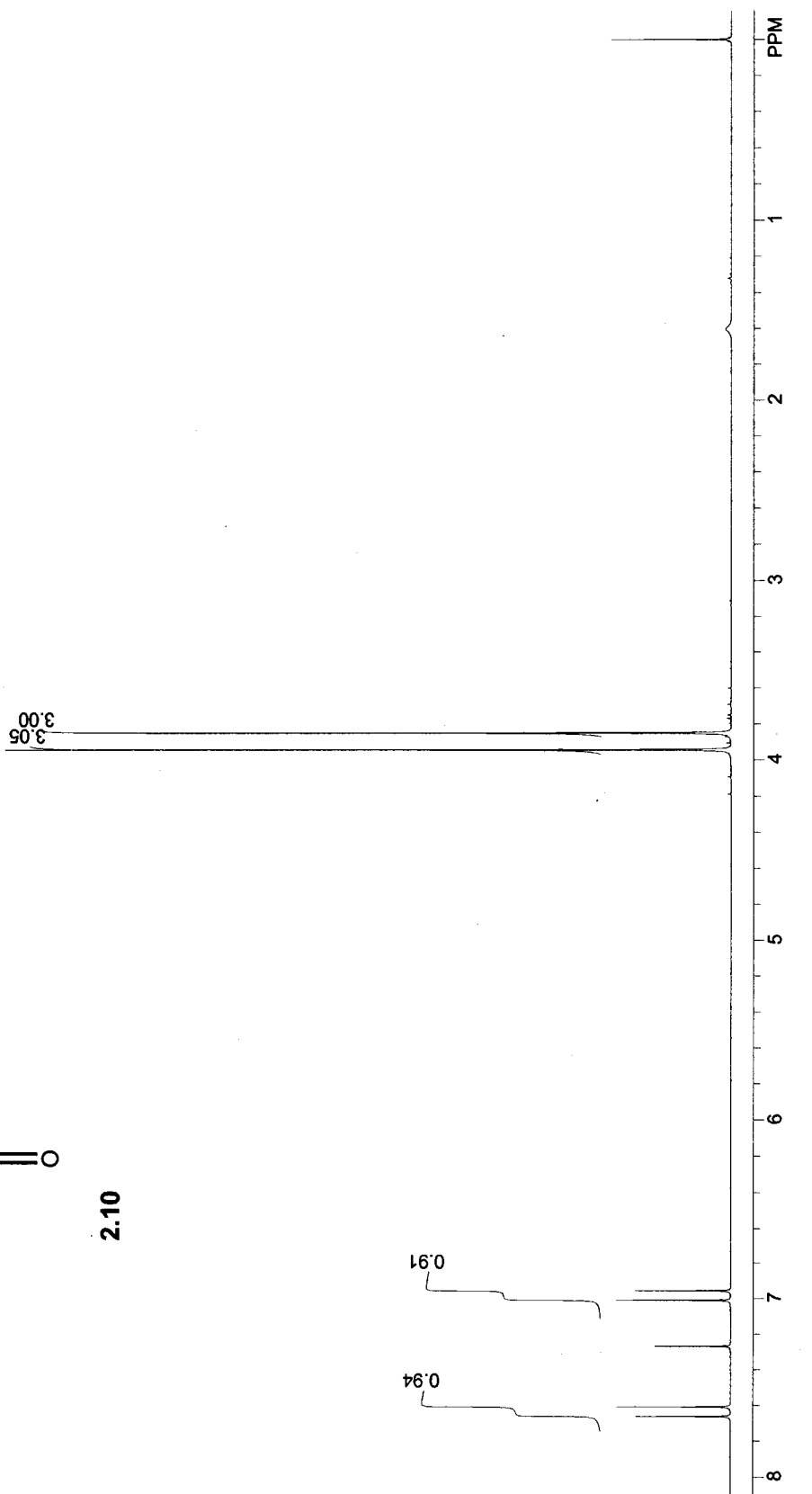
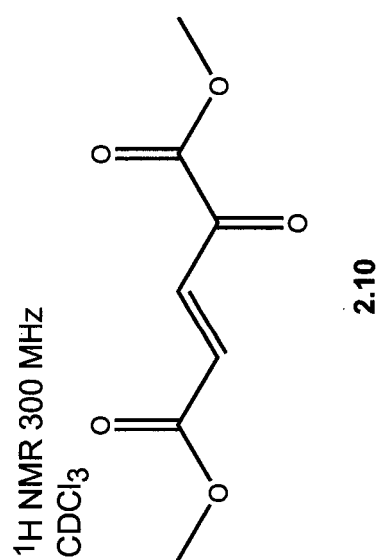


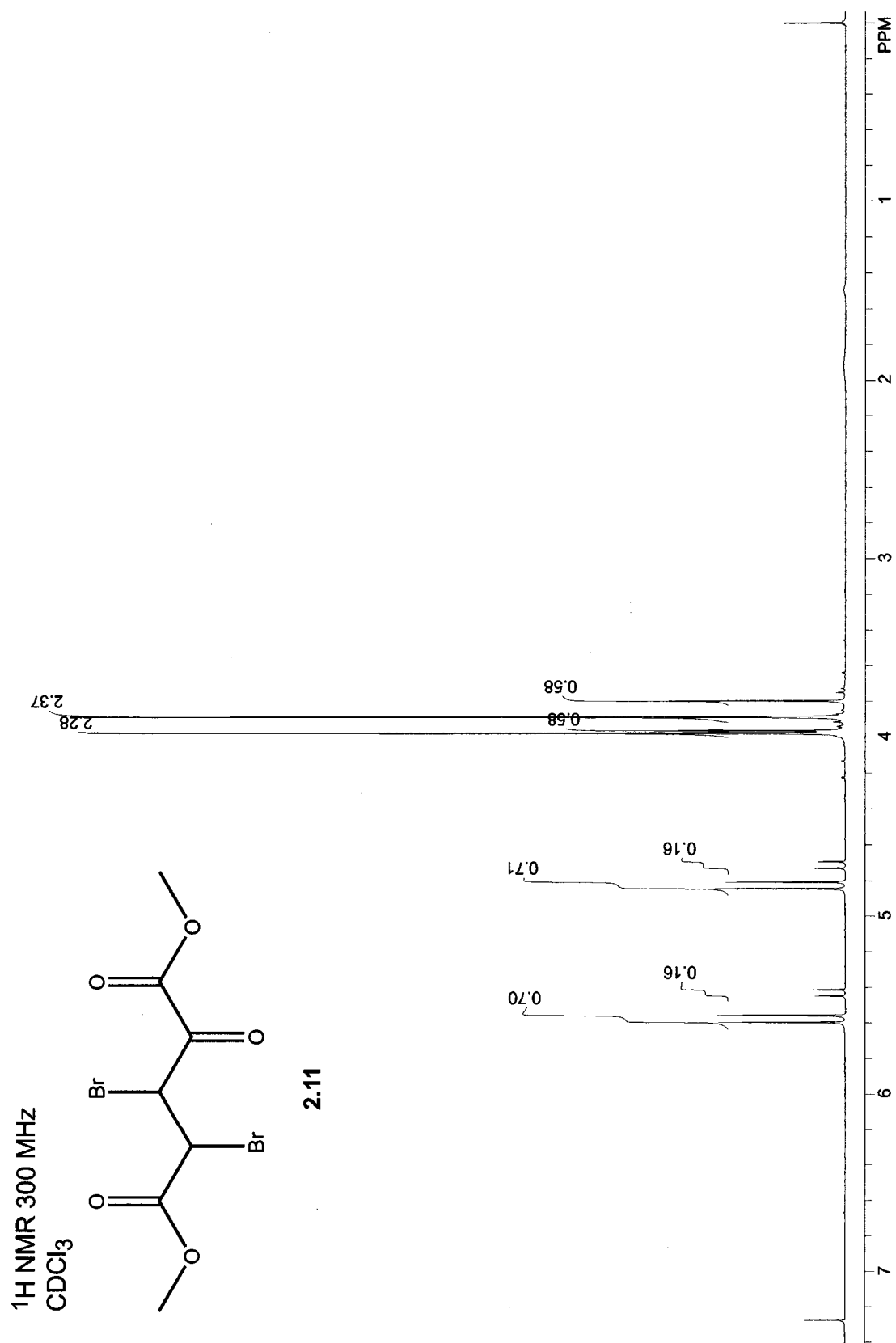


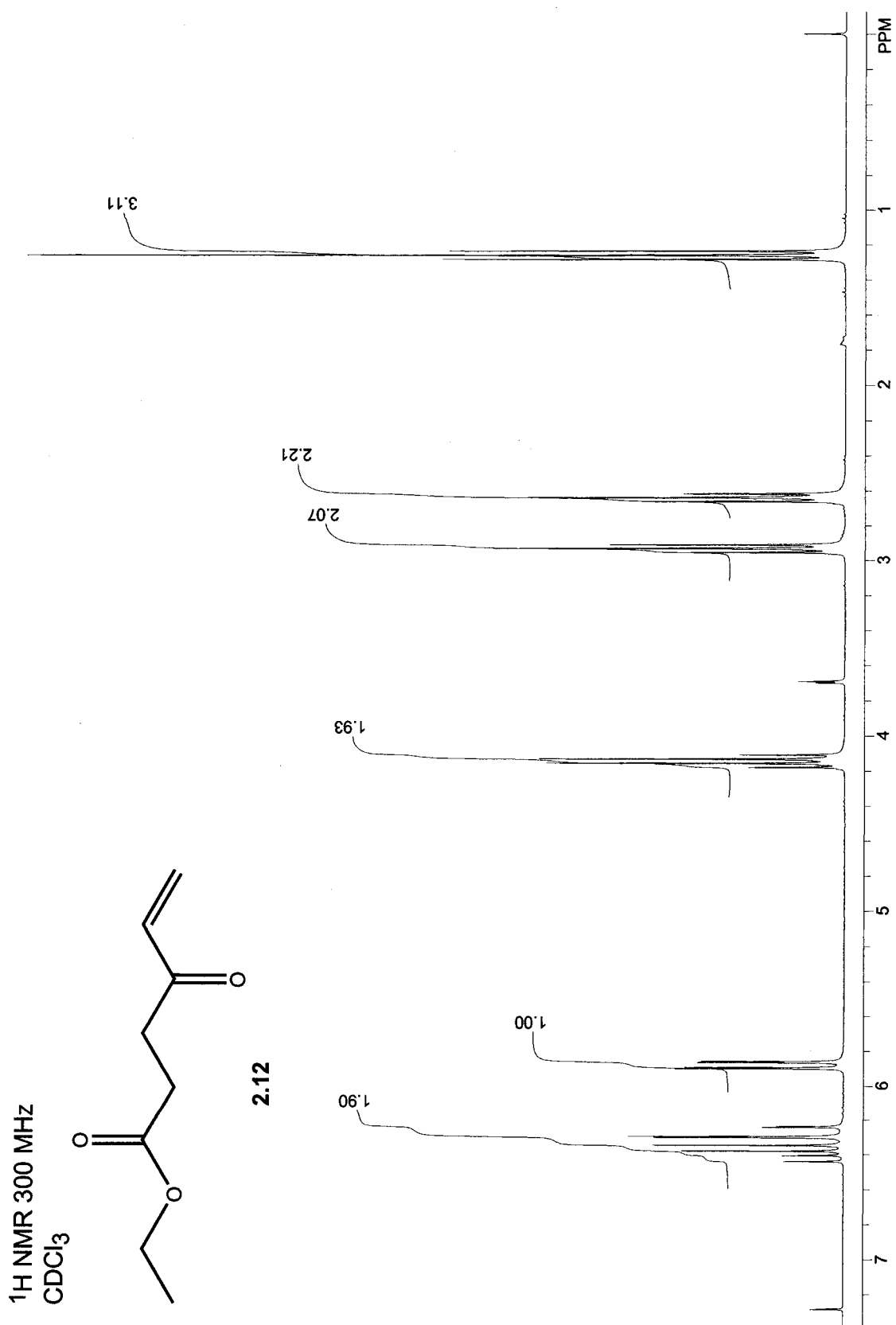


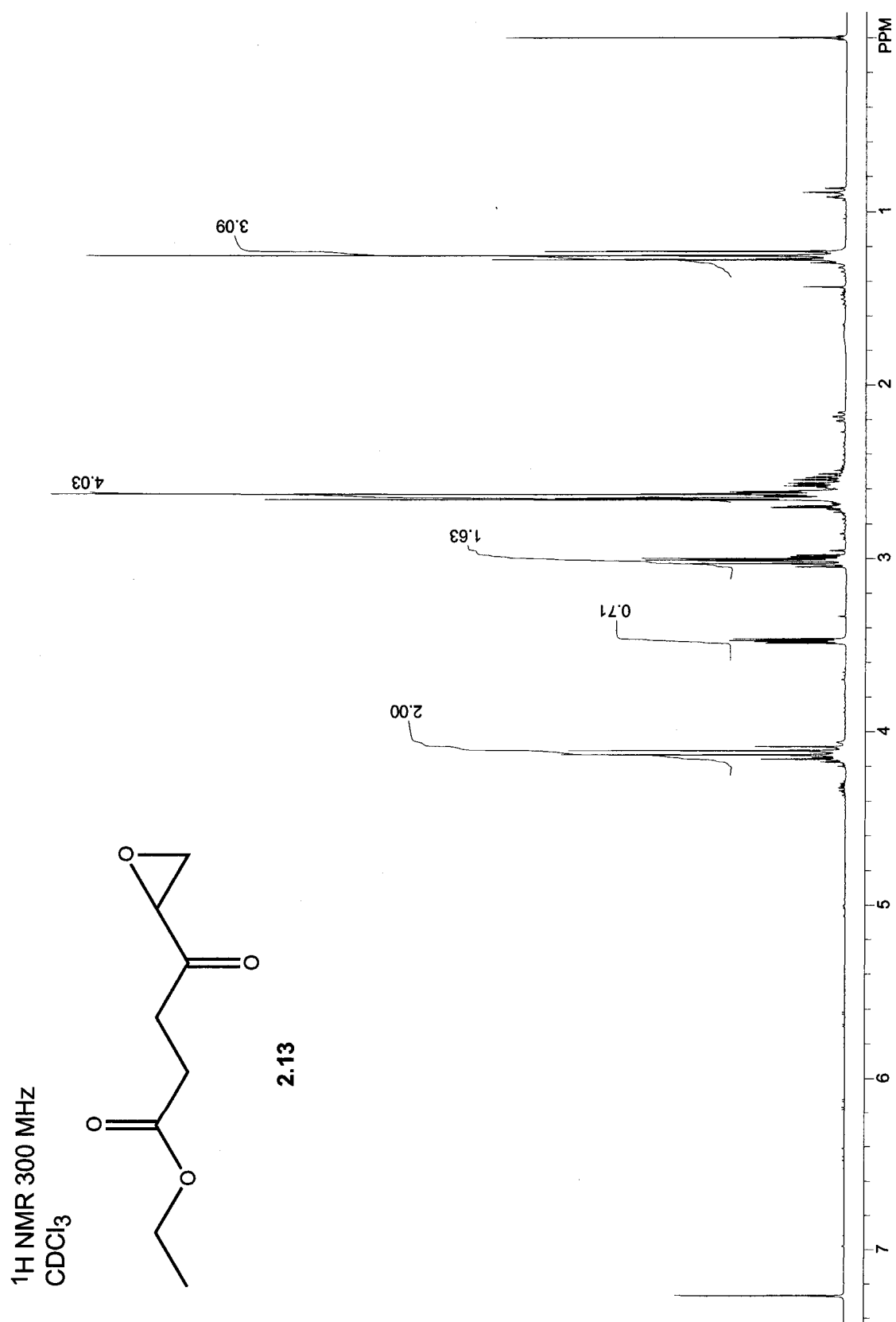
2.9

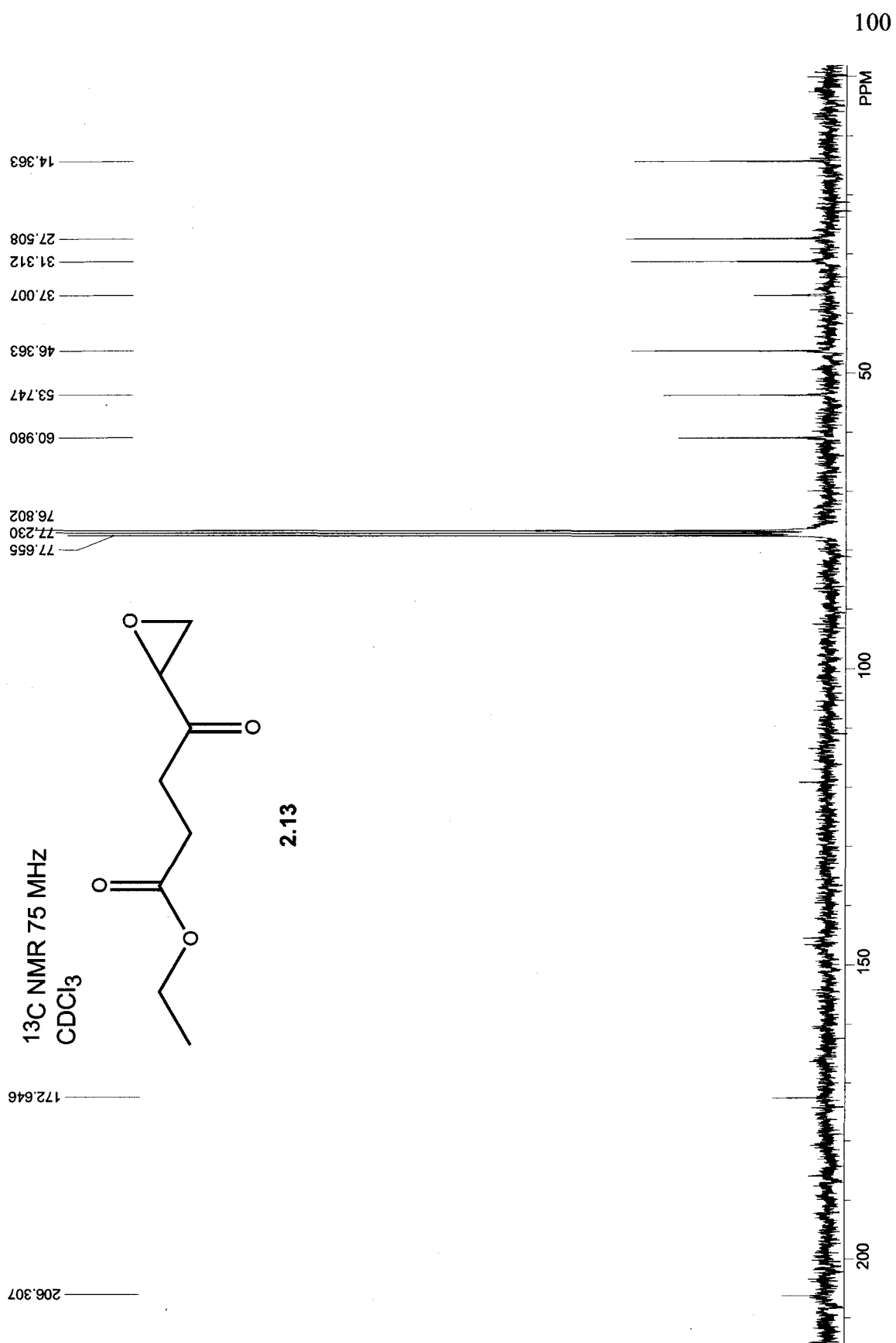


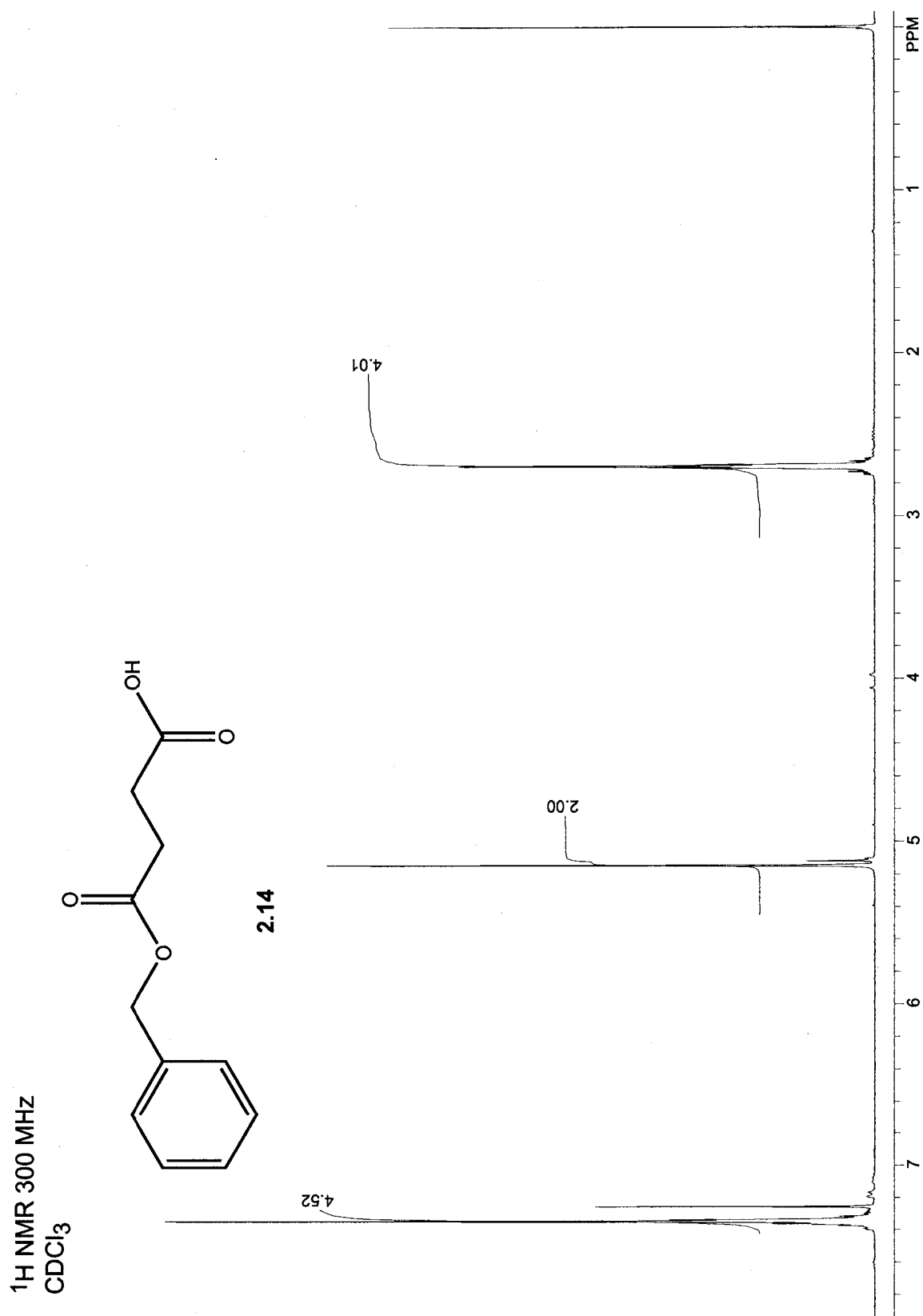


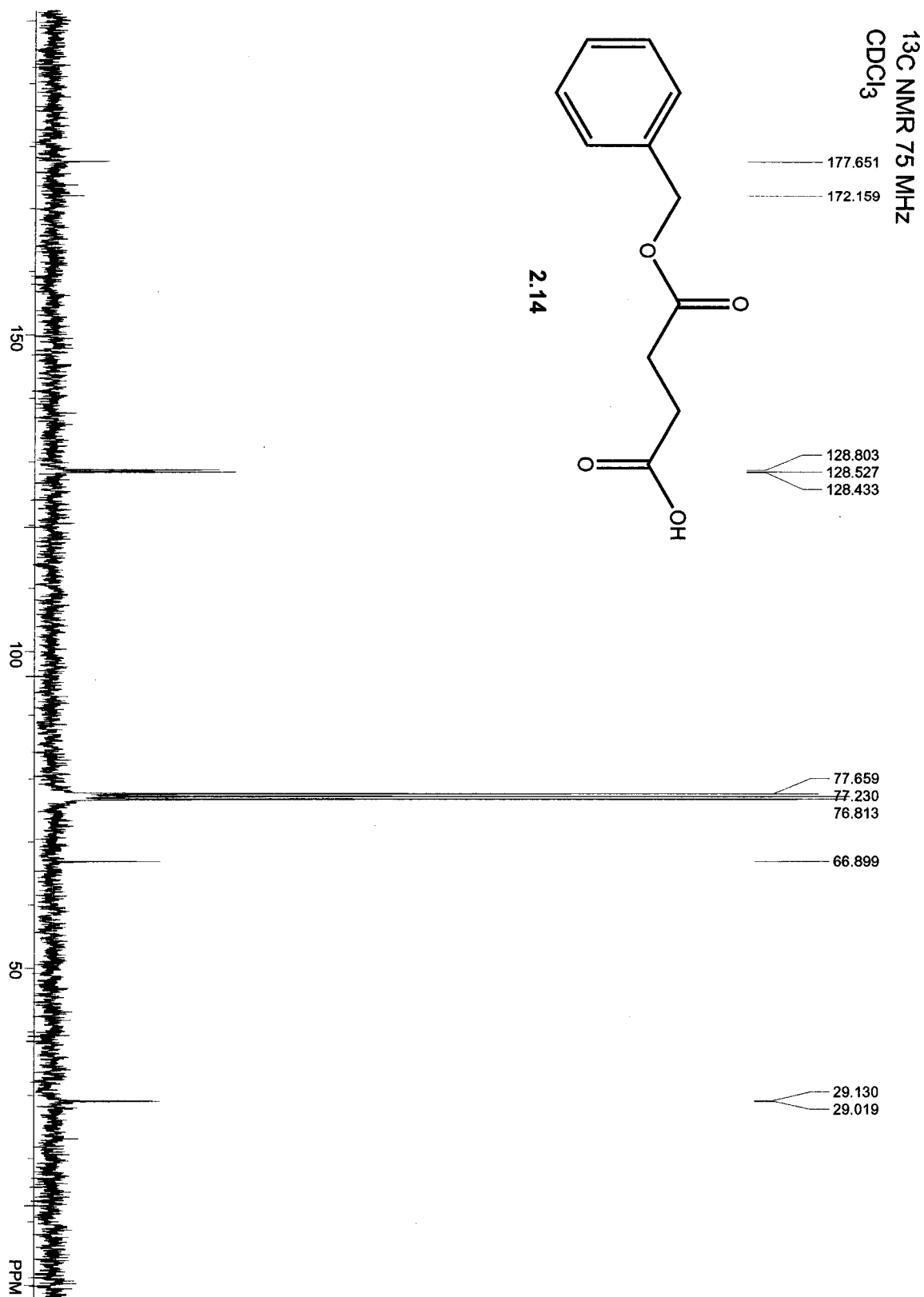


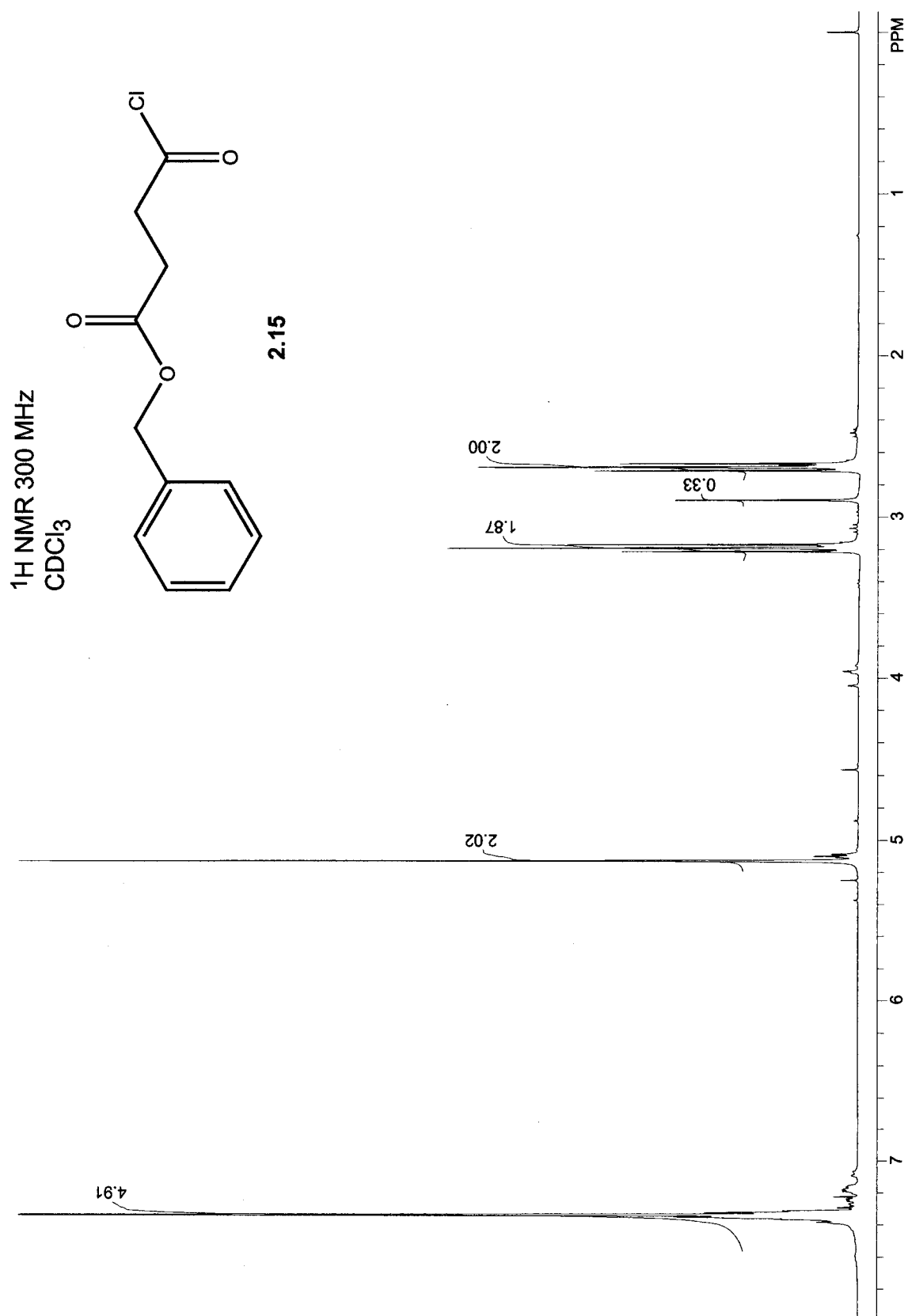




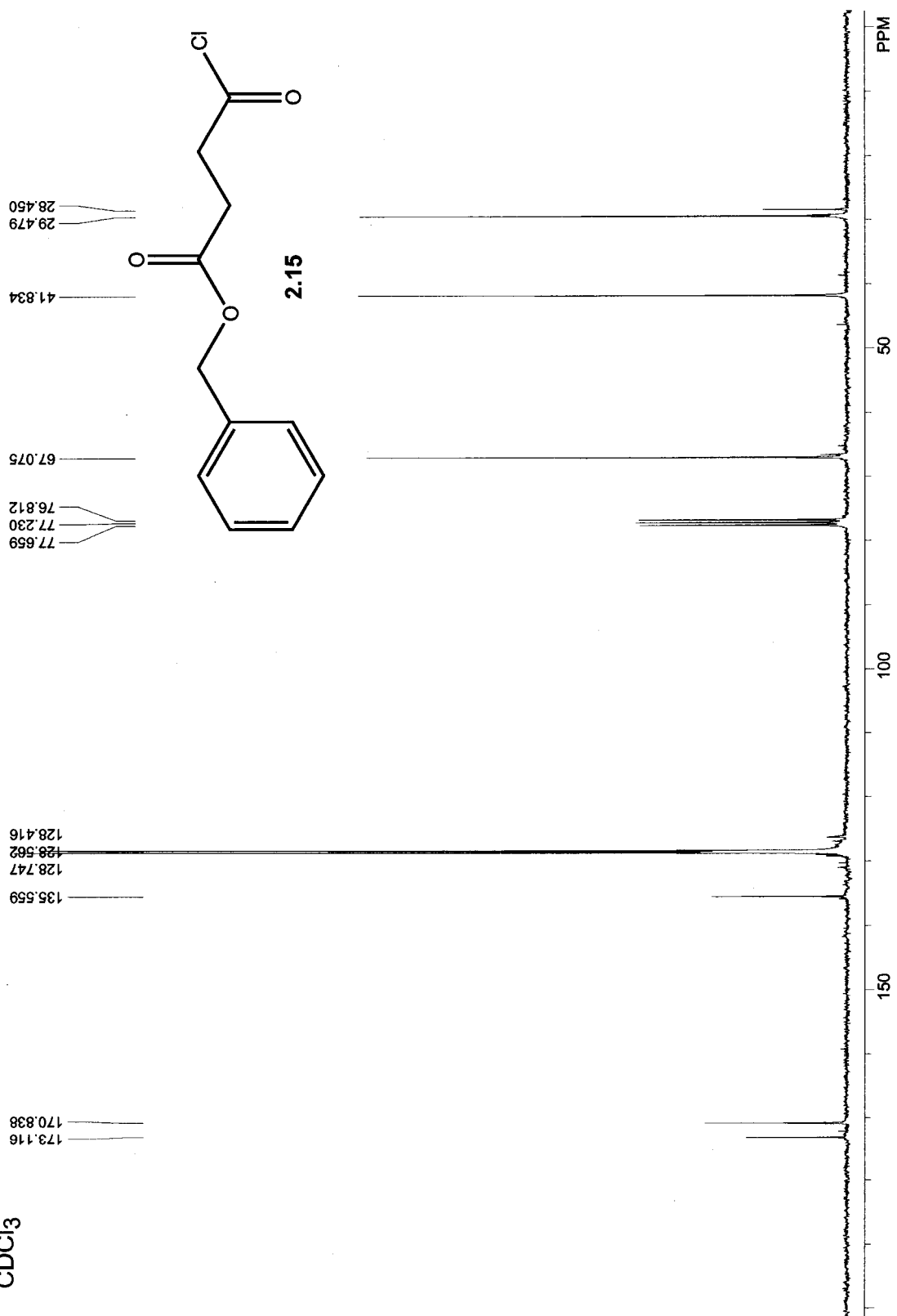


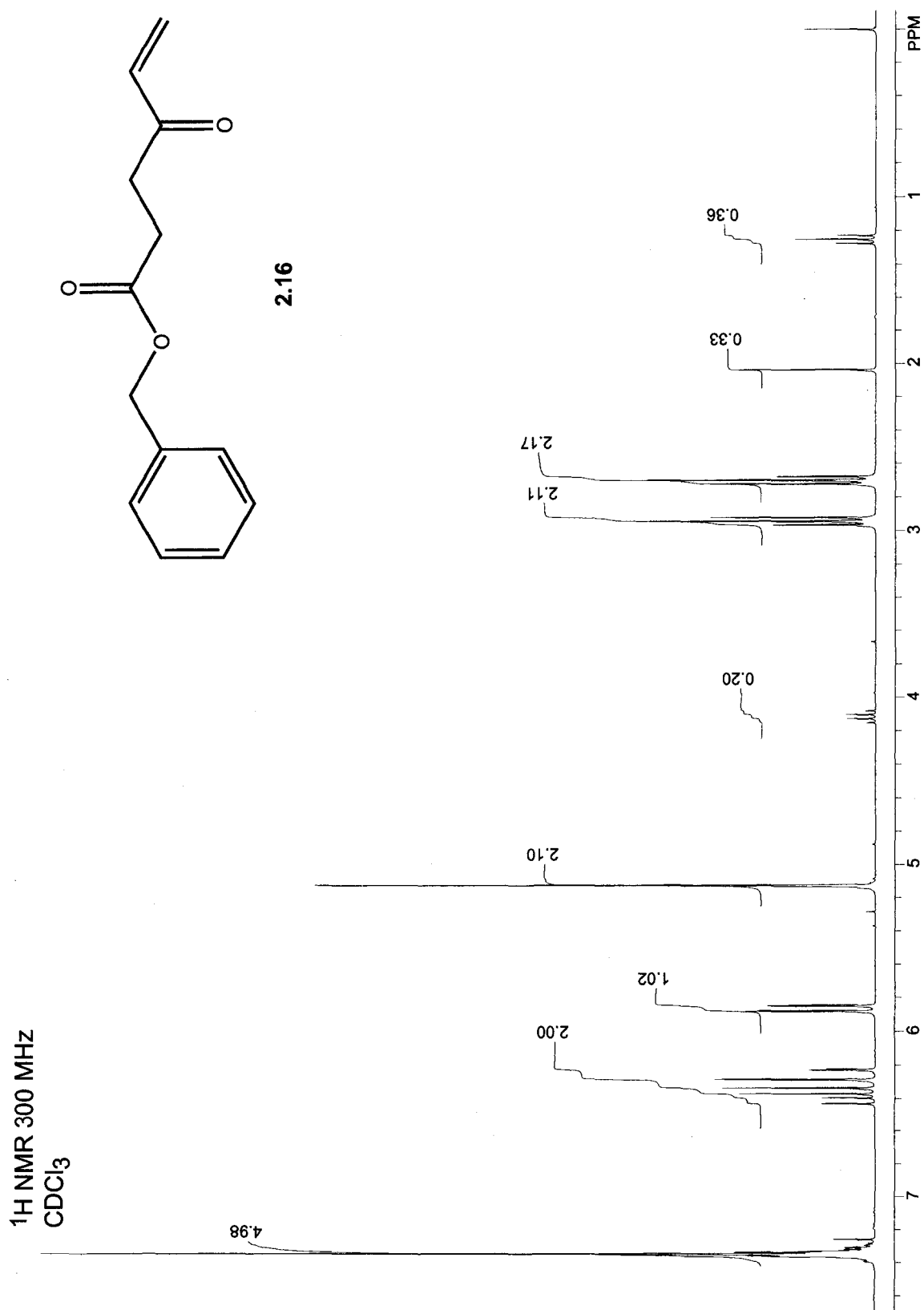


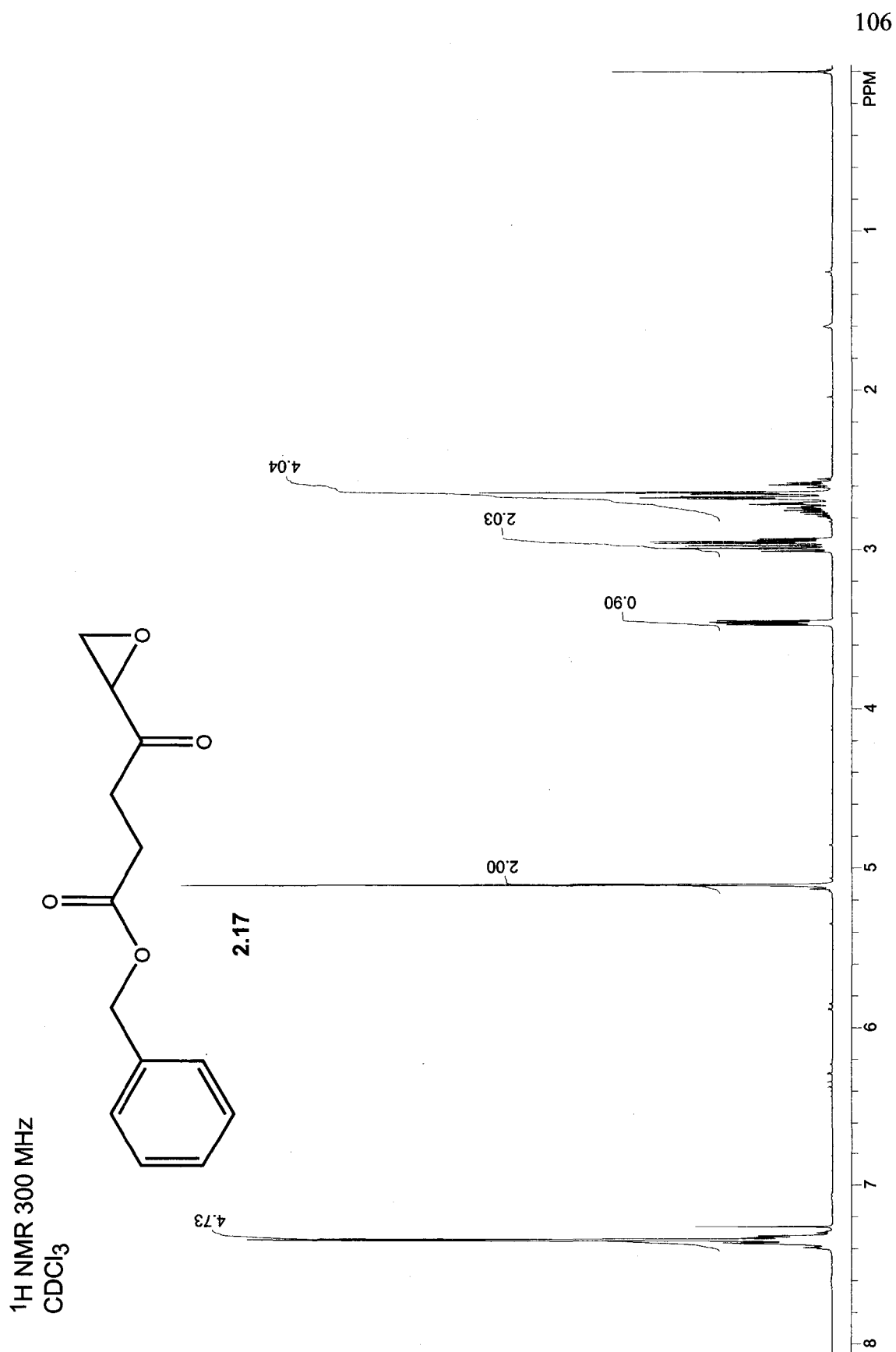


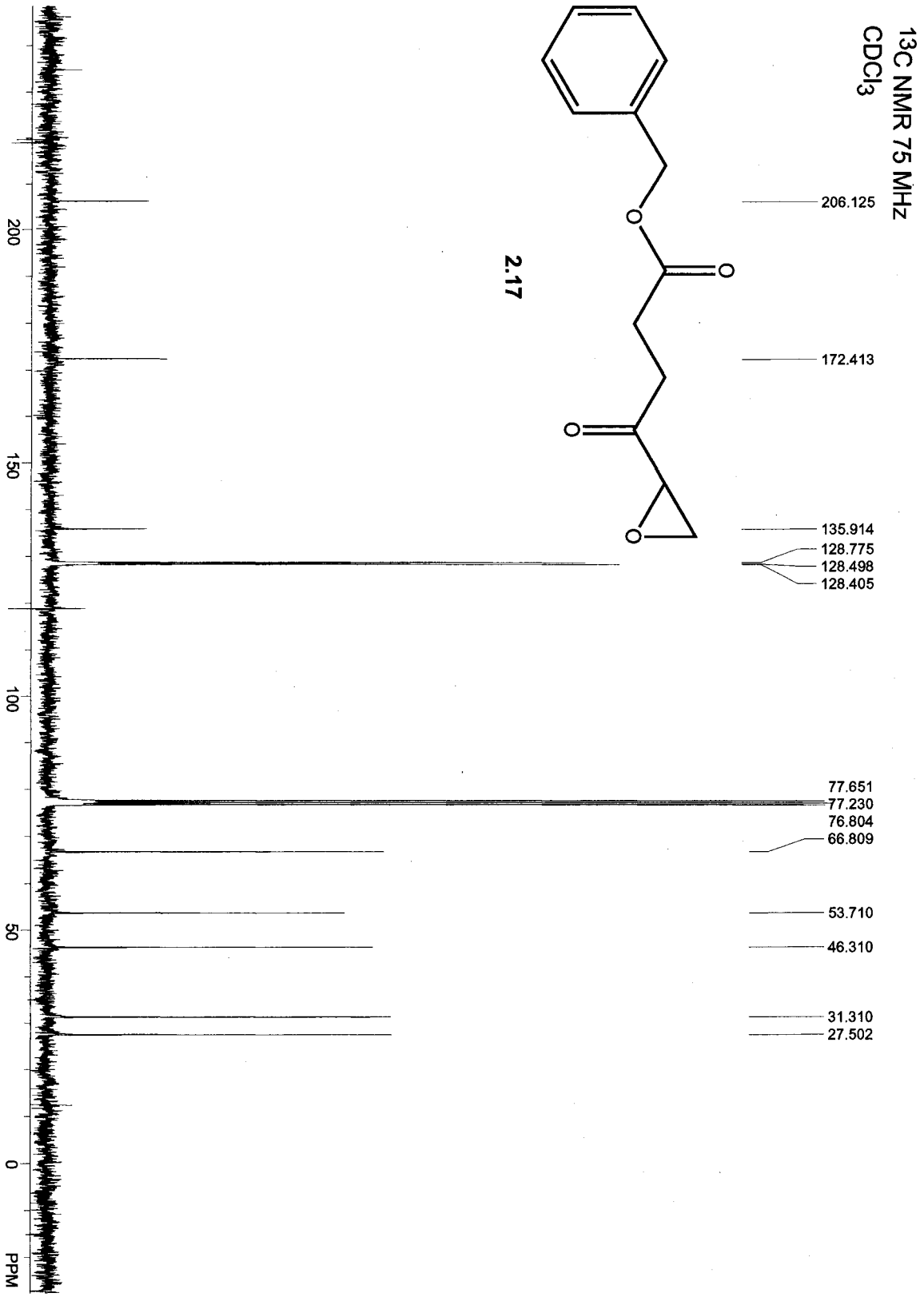


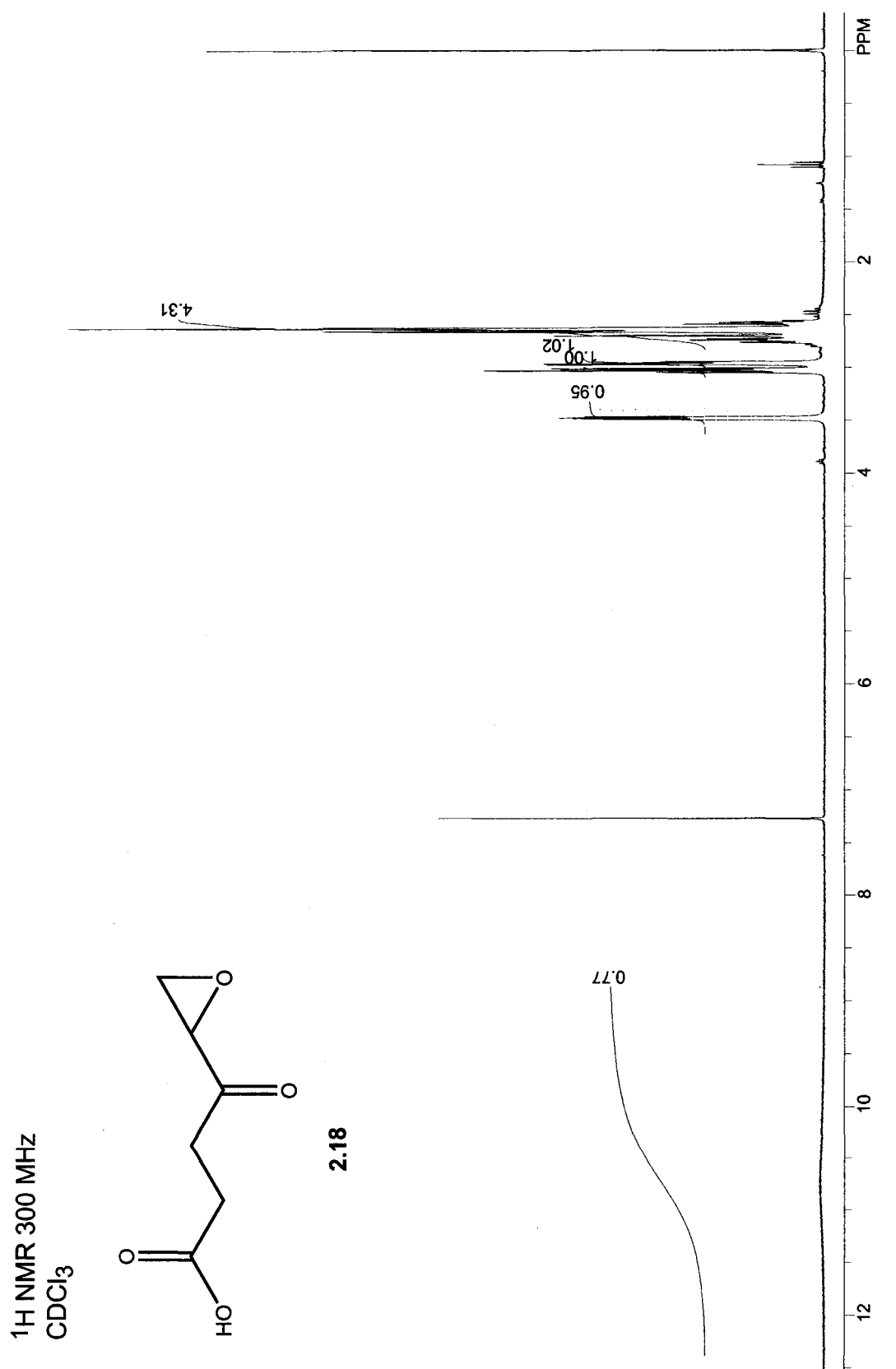
¹³C NMR 75 MHz
CDCl₃

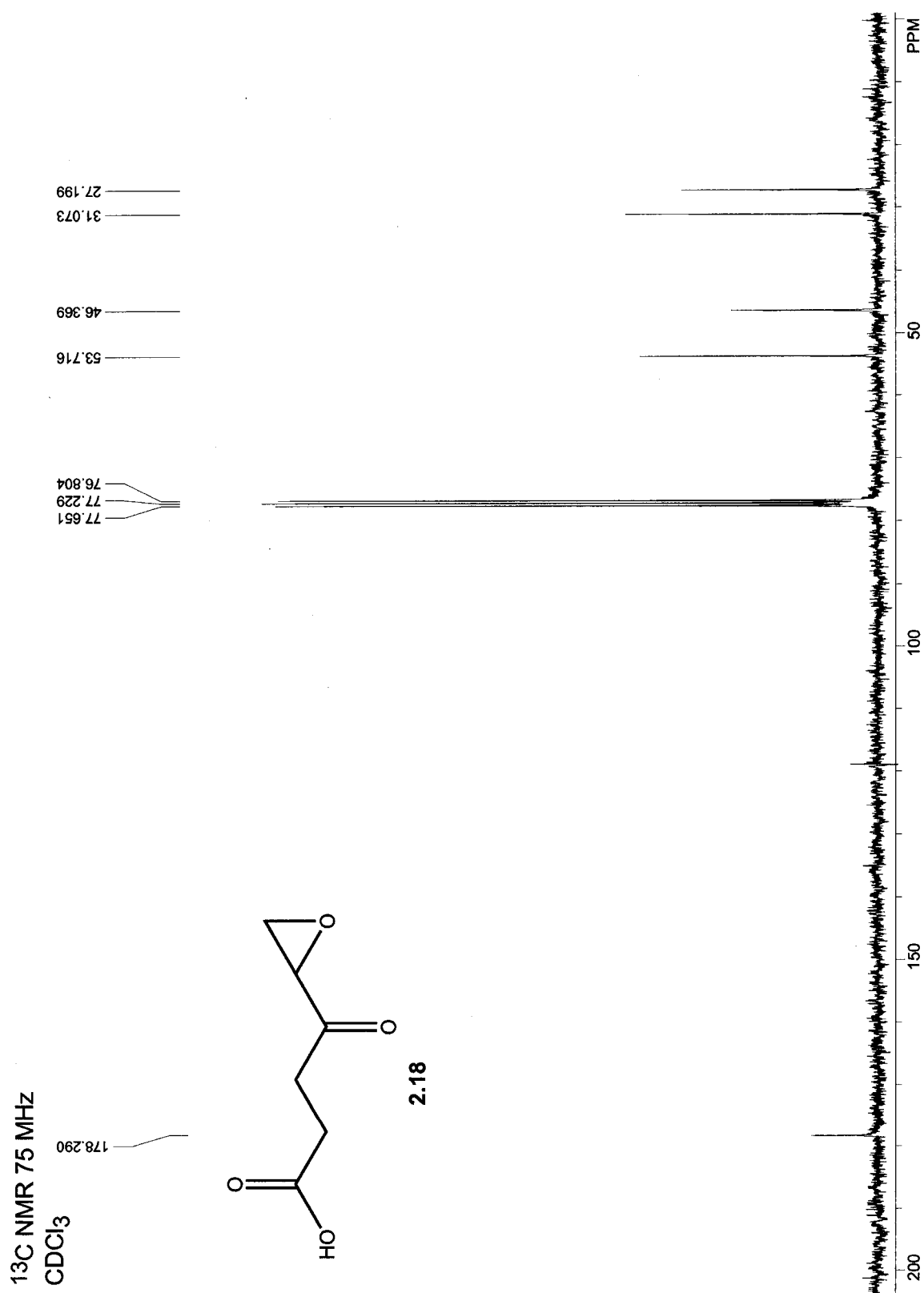


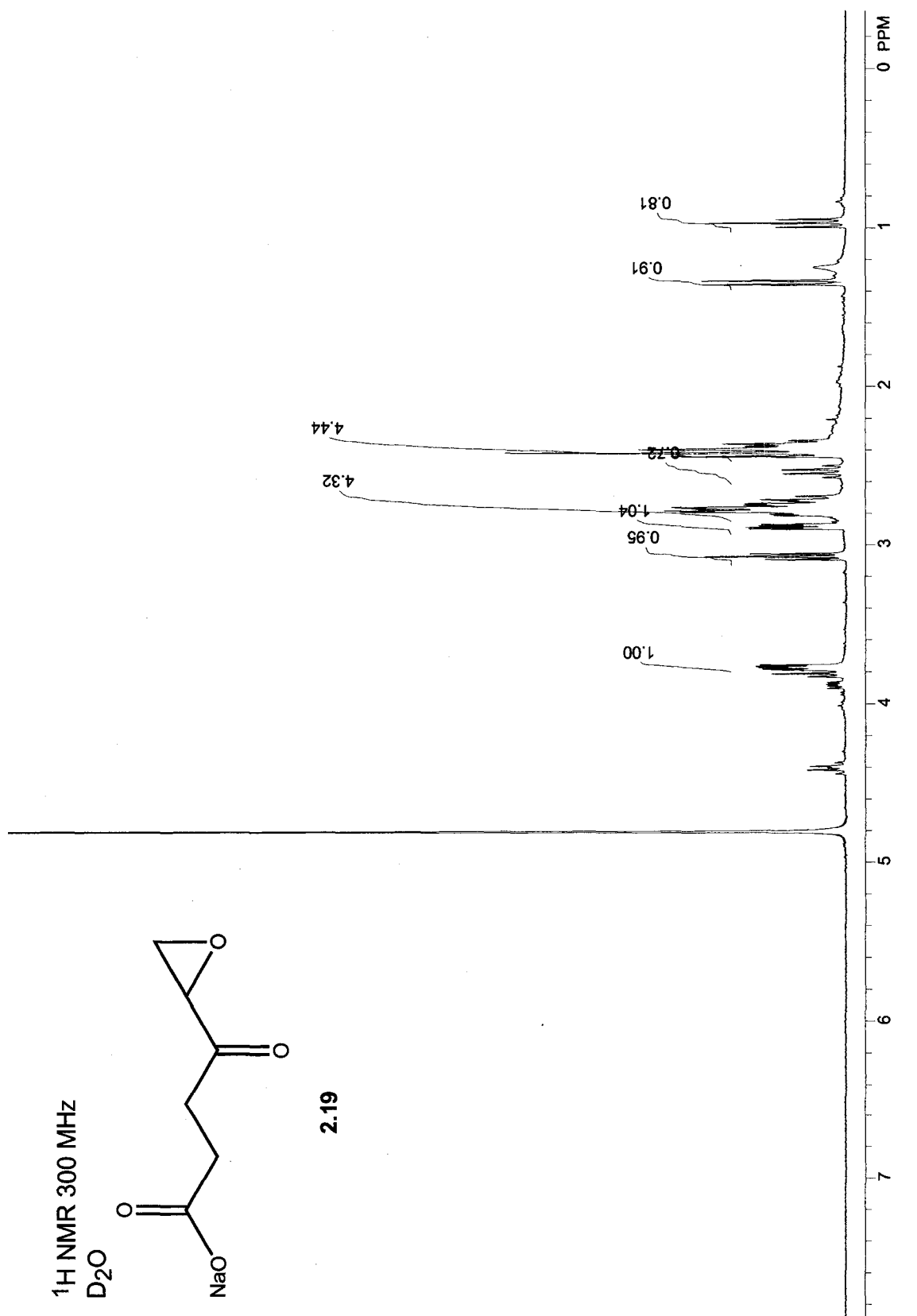


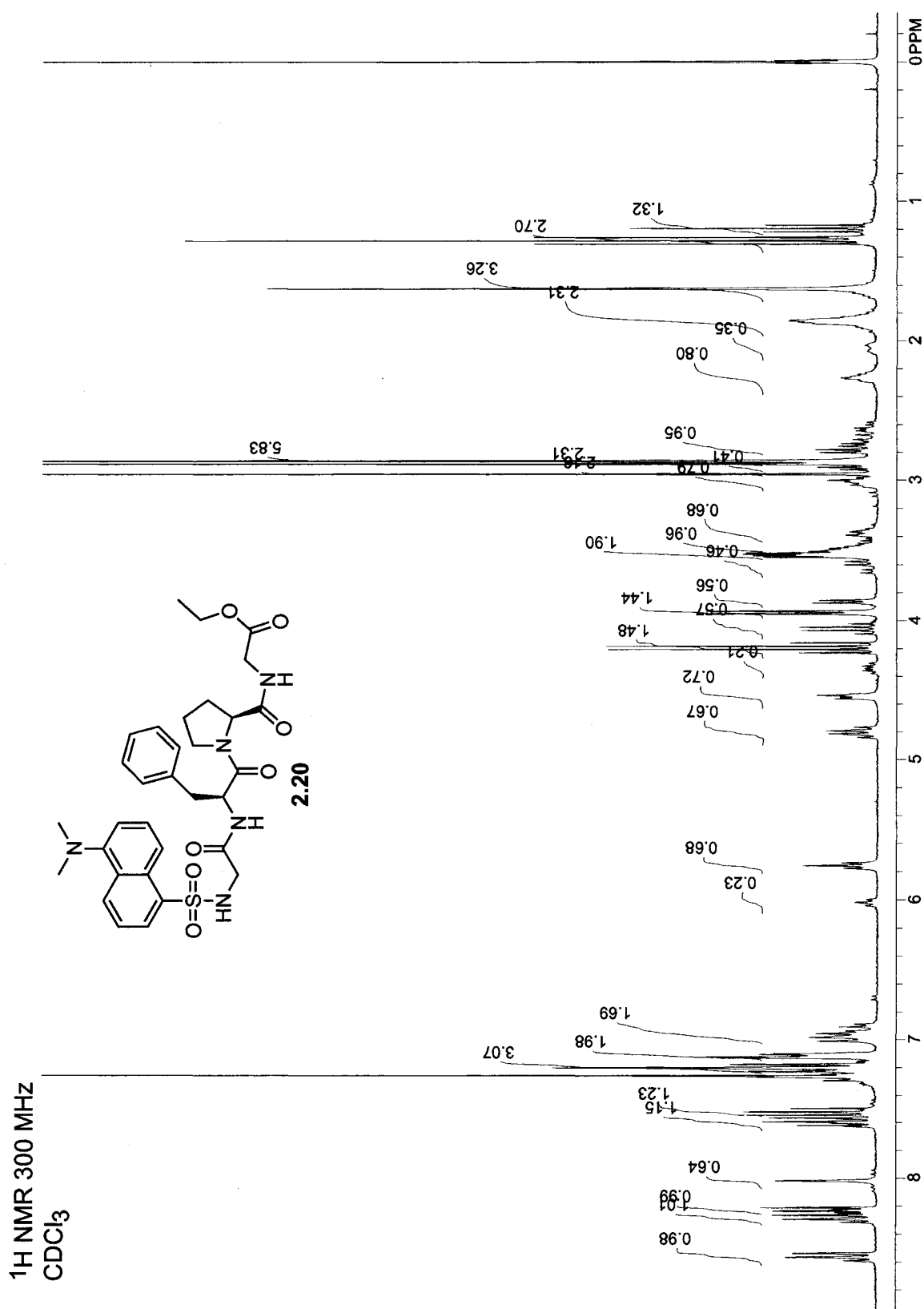




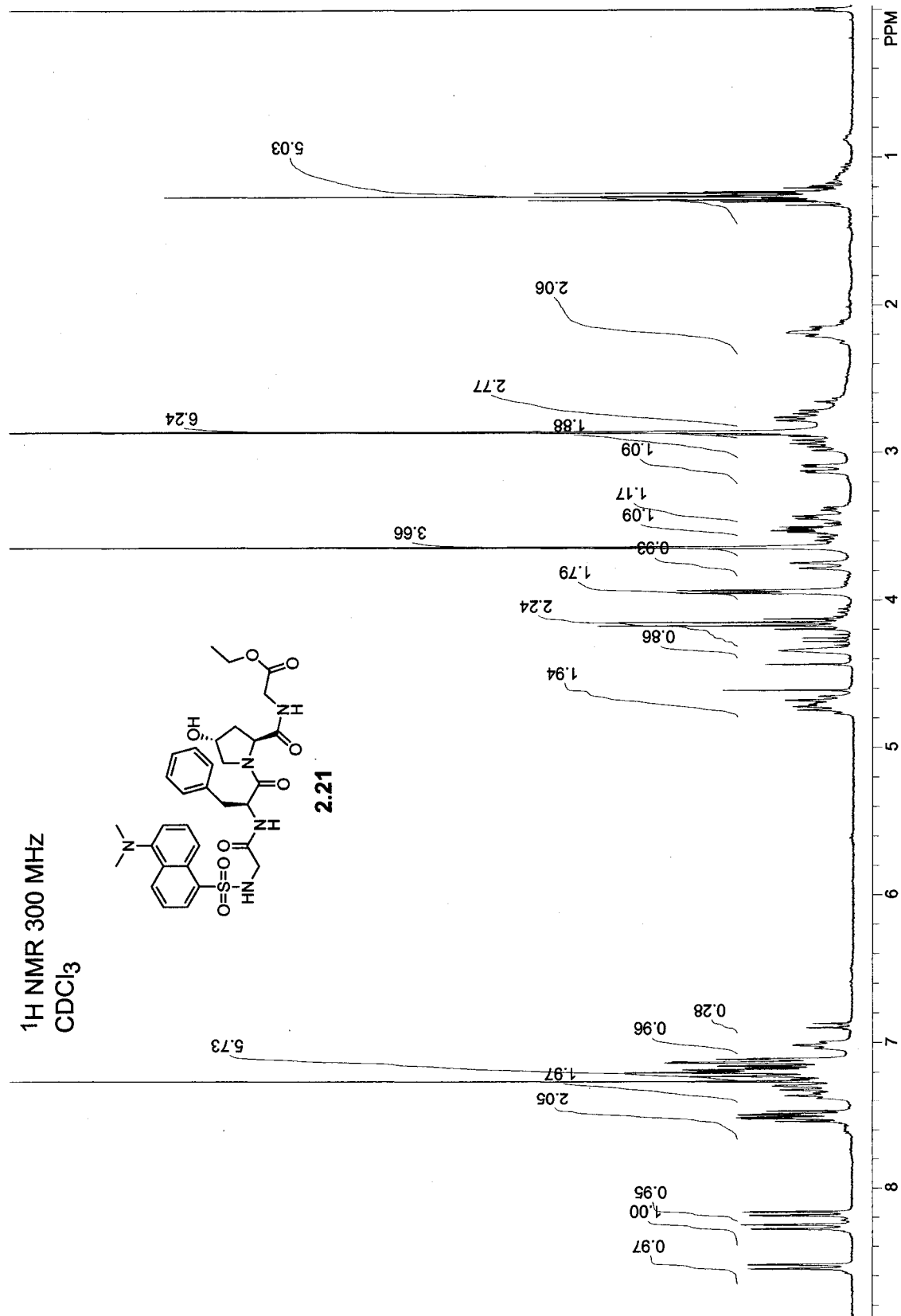


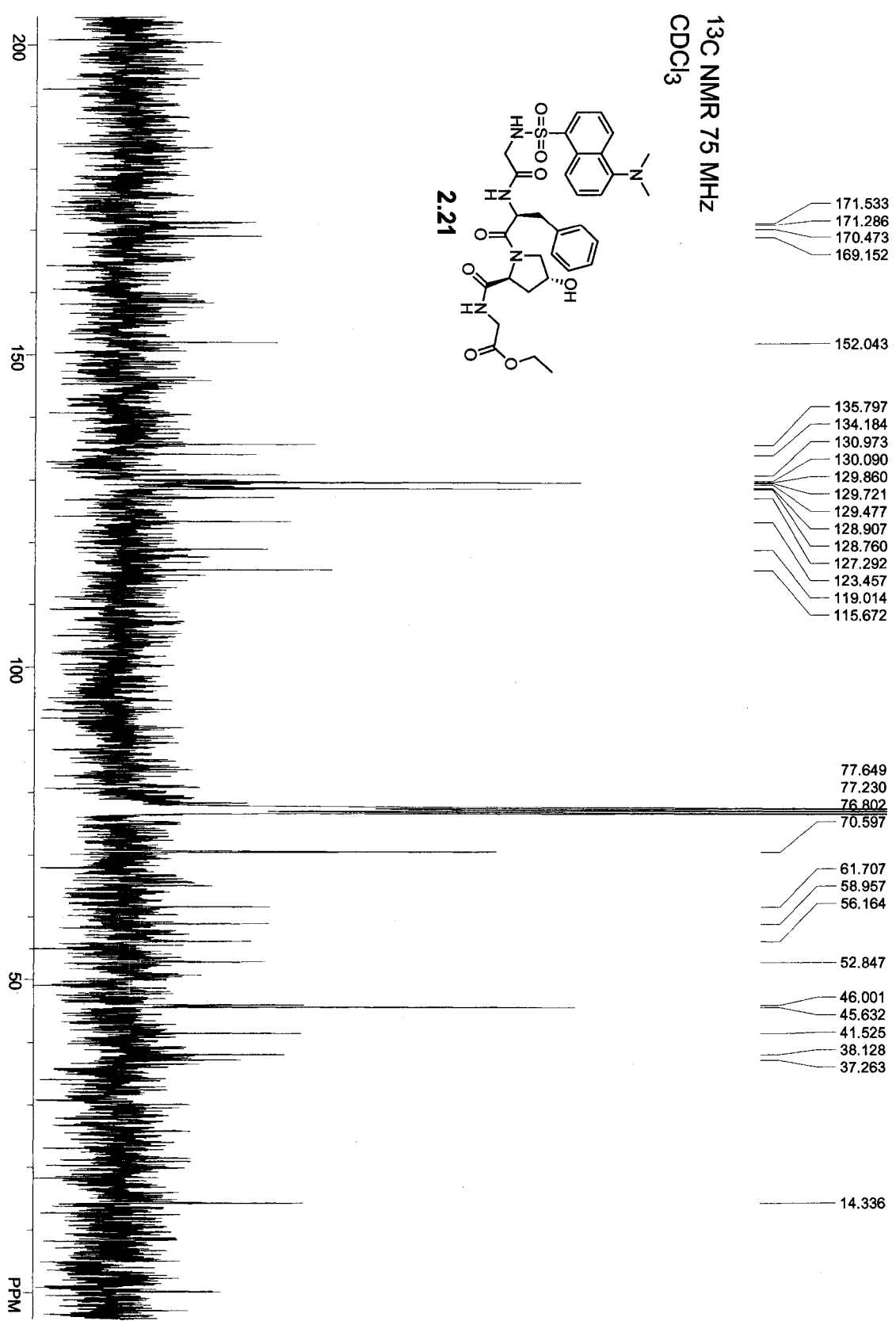












Chapter Three

Zinc(II)-Mediated Inhibition of a Ribonuclease by an *N*-Hydroxyurea Nucleotide

This chapter was published as:

Joshua J. Higgin, Gennady I. Yakovlev, Vladimir A. Mitkevich, Alexander A. Makarov and Ronald T. Raines. (2003) Zinc(II)-mediated inhibition of a ribonuclease by an *N*-hydroxyurea nucleotide, *Bioorganic and Medicinal Chemistry Letters*. **13** 409-412.

3.1 Abstract

The inhibition of ribonuclease Bi by 3'-*N*-hydroxyurea-3'-deoxythymidine 5'-phosphate is enhanced by 30-fold in the presence of Zn^{2+} . Thus, an *N*-hydroxyurea nucleotide can recruit Zn^{2+} to inhibit the enzymatic activity of a ribonuclease. This result engenders a general strategy for the inhibition of non-metalloenzymes by metal complexes.

3.2 Introduction

Like proteases, ribonucleases are prevalent enzymes that are worthwhile targets for inhibitor development (D'Alessio & Riordan, 1997; Raines, 1998). In many laboratory procedures, RNA must be protected from degradation. Moreover, the neovascularization promoted by angiogenin relies on the ribonucleolytic activity of that enzyme (Shapiro & Vallee, 1989). Indeed, variants of angiogenin with greater ribonucleolytic activity are more effective at promoting neovascularization, (Harper & Vallee, 1988) and inhibiting the ribonucleolytic activity of angiogenin could be an effective anti-angiogenesis strategy (Folkman, 1995).

The development of ribonuclease inhibitors lags far behind that of protease inhibitors. The most potent known small-molecule inhibitor of a ribonuclease is pdUppAp, which has $K_i = 0.22 \mu\text{M}$ for the inhibition of ribonuclease A in 0.2 M Hepes buffer, pH 7.0, with no added salt (Russo & Shapiro, 1999). This inhibitor emerged from multiple iterations of inhibitors that closely resemble substrates (Leonidas *et al.*, 1997; Russo *et al.*, 1997). It is unlikely that this iterative strategy will yield substantially better ribonuclease inhibitors. UpOC₆H₄-*p*-CH₂F is a mechanism-based inactivator of ribonuclease A (Stowell *et al.*, 1995). Unfortunately, inactivation by UpOC₆H₄-*p*-CH₂F is not complete. Hence, new strategies for inhibiting or inactivating ribonucleases are desirable.

Zinc(II) is the second most abundant transition metal in biology and is essential for life (Vallee, 1988). In cells, almost all zinc is bound to proteins as zinc(II) (Outten &

O'Halloran, 2001). The ability of proteins to bind Zn^{2+} ions with high affinity portends a new strategy for ribonuclease inhibition. The efficacy of this strategy has been demonstrated with serine proteases. Using X-ray diffraction analysis, Katz and coworkers discovered that a previously known inhibitor of trypsin, bis(5-amidino-2-benzimidazolyl)methane (BABIM), inhibits that enzyme by recruiting a single Zn^{2+} (Katz *et al.*, 1998; Katz & Luong, 1999; Janc *et al.*, 2000). The Zn^{2+} coordinates four heteroatoms—two from BABIM and two from enzymic side chains. The value of K_i for BABIM alone is 19 μM , and that for Zn^{2+} alone is 1 mM. Yet, the K_i for BABIM plus Zn^{2+} is 5 nM (Katz *et al.*, 1998).

The ability of metal complexes to inhibit non-metalloenzymes could extend beyond serine proteases (Schirmeister, 1998; Thorp, 1998; Louie & Meade, 1999; Nguyen & Huc, 2001). Herein, we report the first zinc(II)-mediated inhibitor of a ribonuclease. Our ligand is 3'-*N*-hydroxyurea-3'-deoxythymidine 5'-phosphate [pdT-3'-NHC(O)NHOH; **3.1**]. The logic of this choice is as follows. The use of a *deoxynucleoside* creates additional space within the active site of the enzyme–ligand complex. This space could be necessary for Zn^{2+} binding. The use of a thymidine facilitates synthesis from a commercially available starting material (*vide infra*). The 5'-phosphoryl group provides another interaction with a phosphoryl group-binding subsite, as in the binding of a polymeric RNA substrate. Finally, hydroxamic acids are exceptional bidentate chelators of Zn^{2+} (Farkas & Buglyo, 1990).

As a model ribonuclease, we chose ribonuclease Bi (binase; EC 3.1.27.3). Binase is a secretory ribonuclease from *Bacillus intermedius* that catalyzes the cleavage of RNA

without a need for metal ions or cofactors. The structure of crystalline binase is known at a resolution of 1.65 Å (Polyakov *et al.*, 2002). Analysis of this structure, along with that of a complex with a nucleoside 3'-phosphate, (Polyakov *et al.*, 2002) suggests that Glu73 and His102 of binase act as a base and acid, respectively, during catalysis of RNA cleavage. The carboxylate and imidazole groups in the side chains of these residues could also serve as the enzymic ligands for Zn^{2+} (Scheme 3.1).

3.3 Results and Discussion

N-Hydroxyurea **3.1** was synthesized by the route shown in Scheme 3.2, which begins with the commercial reagent 3'-azido-3'-deoxythymidine 5'-monophosphate (AZT monophosphate). The ability of *N*-hydroxyurea **3.1** to inhibit the ribonucleolytic activity of binase was assessed in the absence and presence of Zn^{2+} .

The results of measurements of the binase activity inhibition by *N*-hydroxyurea **3.1** at different concentrations of Zn^{2+} ions are shown in Fig. 3.1. The intercept of the lines on the ordinate is indicative of competitive inhibition.

The data in Fig. 3.1 were used to evaluate the inhibition by *N*-hydroxyurea **3.1** and Zn^{2+} by using eq 3.1:

$$v = \frac{[E]_T [S] k_{\text{cat}}}{[S] + K_M^{\text{obs}}} \quad (3.1)$$

where

$$K_M^{obs} = K_M \left(1 + \frac{[I]}{K_i^I} + \frac{[I \cdot Zn^{2+}]}{K_i} \right) \quad (3.2)$$

In eq 3.1 and 3.2, $[E]_T$, $[S]$, $[I]$, and $[I \cdot Zn^{2+}]$ are the total concentrations of the enzyme, substrate, inhibitor (*N*-hydroxyurea **3.1**), and $I \cdot Zn^{2+}$ complex, respectively; K_M is the Michaelis constant for the hydrolysis of poly(I); K_i^I is the inhibition constant for the inhibitor alone; and K_i is the inhibition constant for the $I \cdot Zn^{2+}$ complex. The relationship between these two inhibition constants and K_d and K_{Zn} (which are the equilibrium dissociation constants of the $I \cdot Zn^{2+}$ and $E \cdot Zn^{2+}$ complexes, respectively) are depicted in Scheme 3.3. In the data analysis, the values of $[I]$ and $[Zn^{2+}]$ were assumed to be equal to the total concentration of inhibitor and Zn^{2+} , respectively, because the concentration of enzyme was much lower than that of inhibitor or Zn^{2+} .

The values of k_{cat} and K_M for the hydrolysis of poly(I) were 162 s^{-1} and $79 \text{ }\mu\text{M}$, which are similar to those reported previously. (Yakovlev *et al.*, 1994) The inhibition constant for *N*-hydroxyurea **3.1** alone (that is, in the absence of Zn^{2+}) was $K_i^I = 1.3 \text{ mM}$. In contrast, no inhibition of enzymatic activity was observed by Zn^{2+} alone in assays performed with $[Zn^{2+}] \leq 5 \text{ mM}$ (data not shown).

The application of eq 3.1 to the data in Fig. 3.1 enabled the calculation of $K_i K_d$ values for different $[I]$ and $[Zn^{2+}]$. As listed in Table 1, these values were approximately constant at $K_i K_d = 3 \times 10^{-7} \text{ M}^2$ if $[I][Zn^{2+}] \leq 10^{-7} \text{ M}^2$. When $[I][Zn^{2+}]$ was increased to $1.7 \times 10^{-6} \text{ M}^2$, the $K_i K_d$ value increased by 10-fold (Table 3.1). Most likely, this increase is

indicative of improper usage of the total concentration of inhibitor and Zn^{2+} rather than the actual concentration. For this reason, no assays were performed with $[\text{Zn}^{2+}] > 5 \text{ mM}$.

The affinity of the $\text{I} \cdot \text{Zn}^{2+}$ complex for the enzyme was discerned from the value of $K_i K_d$. The value of K_d reports on the affinity of I for Zn^{2+} in the assay mixture. The pK_a of a model hydroxamic acid, acetohydroxamic acid ($\text{CH}_3\text{C}(\text{O})\text{NHOH}$), is 9.4, (Wise & Brandt, 1955) indicating that 0.063% of acetohydroxamic acid is deprotonated at pH 6.2. Only the conjugate base of a hydroxamic acid has high affinity for Zn^{2+} , (Farkas & Buglyo, 1990) and the acetohydroxamate- Zn^{2+} complex has an equilibrium dissociation constant near $10^{-5.4} \text{ M}$ (Chang *et al.*, 1987; Farkas *et al.*, 2000a). Thus, the value of $K_d = 10^{-5.4} \text{ M} / (0.063\%) = 6.3 \text{ mM}$ for acetohydroxamic acid at pH 6.2. Using this value of K_d as an approximation for that of the *N*-hydroxyurea **3.1**- Zn^{2+} complex, the value of $K_i = K_i K_d / K_d = 3 \times 10^{-7} \text{ M}^2 / 6.3 \text{ mM} = 47 \text{ }\mu\text{M}$. Thus, the enzyme has approximately 30-fold more affinity for the $\text{I} \cdot \text{Zn}^{2+}$ complex ($K_i = 47 \text{ }\mu\text{M}$) than for I alone ($K_i^I = 1.3 \text{ mM}$).

The affinity of Zn^{2+} for the enzyme was discerned likewise. From Scheme 3, $K_{\text{Zn}} = K_i K_d / K_i^I = 3 \times 10^{-7} \text{ M}^2 / 1.3 \text{ mM} = 0.2 \text{ mM}$. Because no inhibition of enzymatic activity was observed with $[\text{Zn}^{2+}] \leq 5 \text{ mM}$, the enzyme- Zn^{2+} complex had an equilibrium dissociation constant of $>5 \text{ mM}$. Thus, Zn^{2+} has >25 -fold more affinity for the E-I complex than for the enzyme alone. This increase is consistent with the participation of enzymic ligands in the binding of Zn^{2+} to the E-I complex, as is depicted in Scheme 3.1.

3.4 Conclusion

In conclusion, we have demonstrated the efficacy of a new strategy for the inhibition of ribonucleases. This strategy was inspired by the inadvertent recruitment of zinc(II) by a known protease inhibitor (Katz *et al.*, 1998; Katz & Luong, 1999; Janc *et al.*, 2000). In contrast, ribonuclease inhibition relies on the intentional recruitment of Zn^{2+} by an *N*-hydroxyurea moiety attached covalently to a nucleotide. The *N*-hydroxyurea moiety can present Zn^{2+} to the active-site residues of the ribonuclease, and thereby enhance binding beyond that for the inhibitor or Zn^{2+} alone. We anticipate that this strategy can be optimized further and used for the inhibition of a variety of ribonucleases, as well as other types of enzymes.

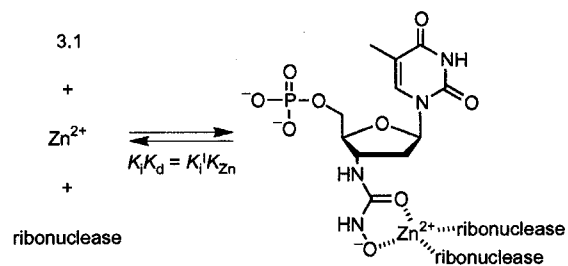
3.5 Materials and Methods

3'-Amino-3'-deoxythymidine 5'-monophosphate. 3'-azido-3'-deoxythymidine 5'-monophosphate (50 mg, 135 μmol), triphenylphosphine (50 mg, 192 μmol), and tetrabutylammonium fluoride (0.10 g, 0.36 mmol) was stirred in pyridine (20 ml) overnight at 20 °C. Aqueous NH_3 (5% v/v; 30 ml) was added, and the resulting solution was stirred for 2 h. The mixture was co-evaporated with ethanol and dried under vacuum. The mixture was used without purification directly in the next step.

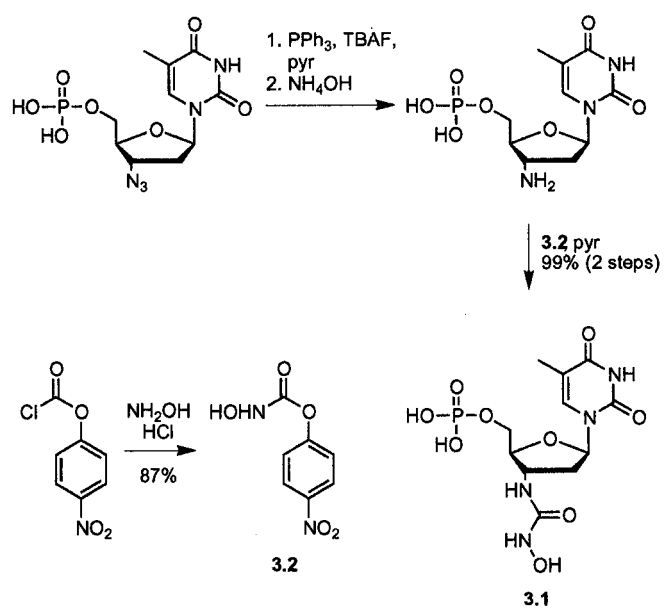
4-Nitrophenyl *N*-hydroxycarbamate (3.2). 4-Nitrophenyl *N*-hydroxycarbamate was synthesized by the route reported for the synthesis of phenyl *N*-hydroxycarbamate. ^1H NMR (300 MHz, D_2O) δ 9.40 (br s, 1H), 6.48 (d, $J = 9$ Hz, 2H), 5.30 (d, $J = 9$ Hz, 2H) (Stewart & Brooks, 1992).

3'-N-Hydroxyurea-3'-deoxythymidine 5'-monophosphate (3.1). 4-Nitrophenyl *N*-hydroxycarbamate (0.10 g, 0.50 mmol) and tetrabutylammonium fluoride (0.20 g, 0.72 mmol) was added to the crude 3'-amino-3'-deoxythymidine 5'-monophosphate and stirred overnight in pyridine (20 ml) at 20 °C. The reaction was quenched with H₂O (20 ml). The mixture was co-evaporated with ethanol and dried under vacuum. The residue was taken up in H₂O (3 ml) and purified by reversed-phase HPLC using an H₂O/acetonitrile gradient and lyophilized to give 54 mg (99% overall) of fluffy white solid. ¹H NMR (300 MHz, D₂O) δ 1.82 (s, 3H), 2.28 (m, 2H), 4.03 (m, 2H), 4.08 (m, 1H), 4.36 (m, 1H), 6.19 (t, 1.3 H, NH), 7.78 (s, 1H). MS (ESI) *m/z* calcd for C₁₁H₁₆N₄O₉P (M – H) 379.07, found 379.00.

Enzyme kinetics. Assays of ribonucleolytic activity were performed by using UV spectroscopy to measure the cleavage of poly(inosinic acid) [poly(I)] at 25 °C in 0.10 M sodium citrate buffer, pH 6.2, containing NaCl (0.10 M). Concentrations of *N*-hydroxyurea **3.1** were determined by its absorbance at 267 nm using the extinction coefficient for pdT, which is $\epsilon = 9.6 \text{ mM}^{-1} \text{ cm}^{-1}$ (Dawson *et al.*, 1989).



Scheme 3.1 Basis for the zinc(II)-mediated inhibition of a ribonuclease by *N*-hydroxyurea **3.1**.



Scheme 3.2 Route for the synthesis of *N*-hydroxyurea **3.1**.

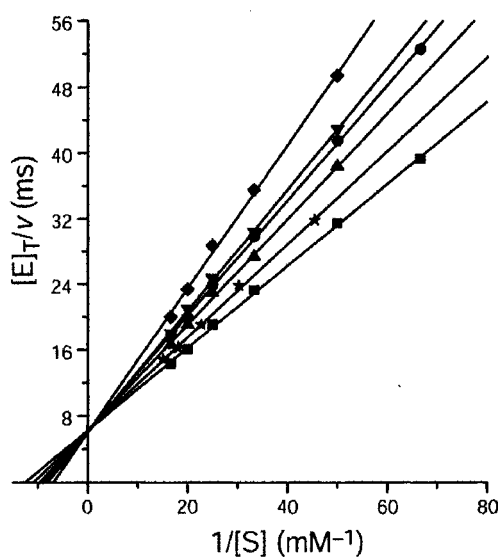
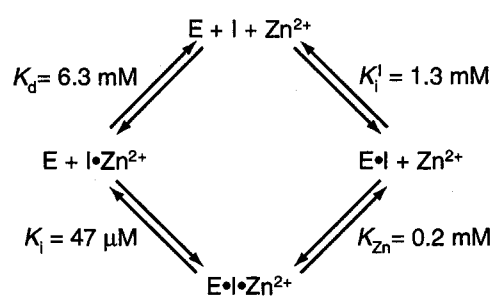


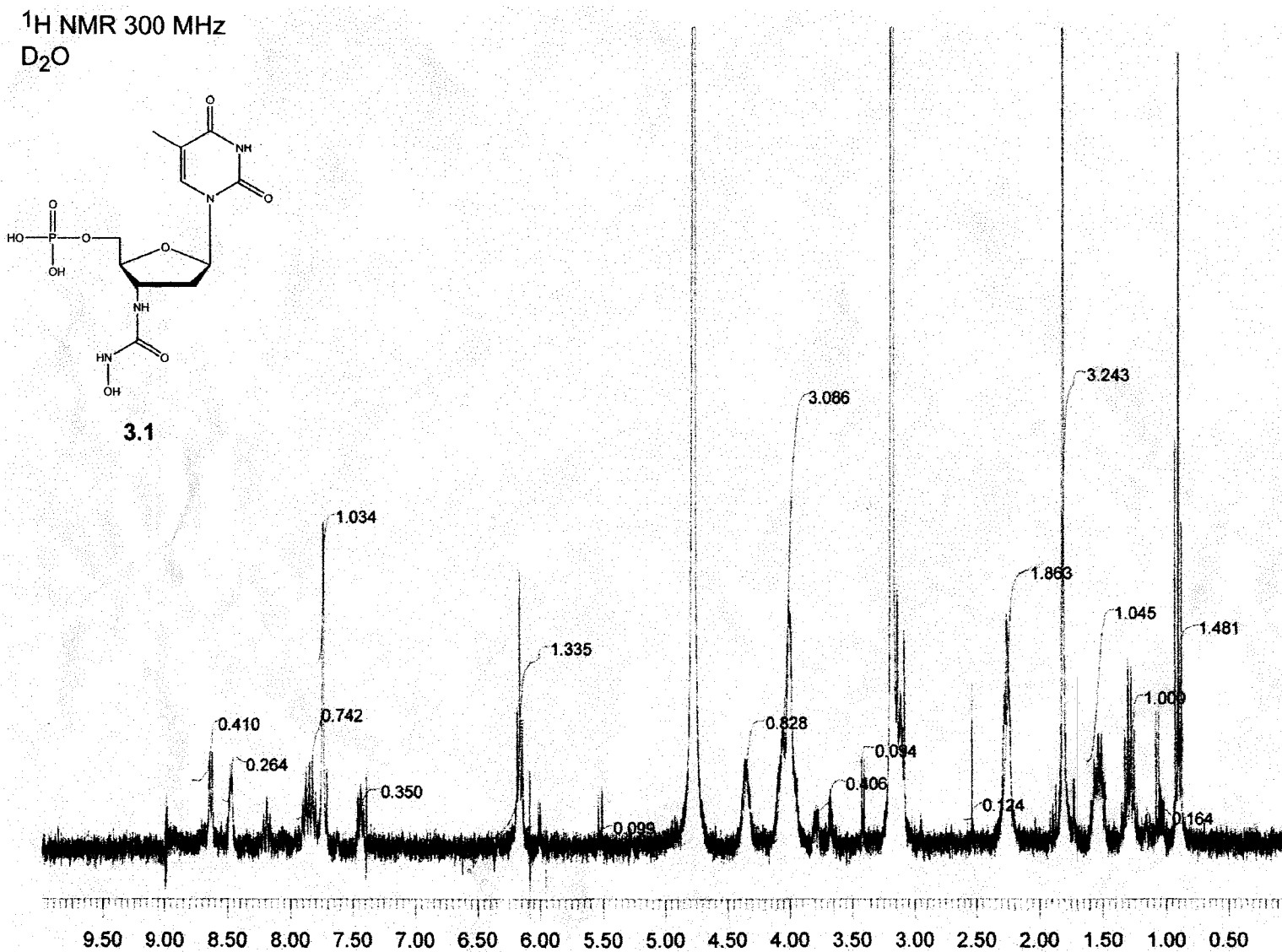
Figure 3.1 Lineweaver-Burk plot for the inhibition of binase by *N*-hydroxyurea 3.1 in the absence and presence of Zn^{2+} . Assays were performed at 25 °C in 0.10 M sodium citrate buffer, pH 6.2, containing NaCl (0.10 M), binase (4.4×10^{-10} M), poly(I), *N*-hydroxyurea 1, and Zn^{2+} . ■, $[\text{I}] = 0$, $[\text{Zn}^{2+}] = 0$ (data with $[\text{Zn}^{2+}] \leq 5$ mM were identical); ★, $[\text{I}] = 0.93 \times 10^{-4}$ M, $[\text{Zn}^{2+}] = 0.25$ mM; ▲, $[\text{I}] = 3.5 \times 10^{-4}$ M, $[\text{Zn}^{2+}] = 0$; ●, $[\text{I}] = 1.0 \times 10^{-4}$ M, $[\text{Zn}^{2+}] = 1.0$ mM; ▼, $[\text{I}] = 3.5 \times 10^{-4}$ M, $[\text{Zn}^{2+}] = 0.25$ mM; ◆, $[\text{I}] = 3.5 \times 10^{-4}$ M, $[\text{Zn}^{2+}] = 5$ mM.

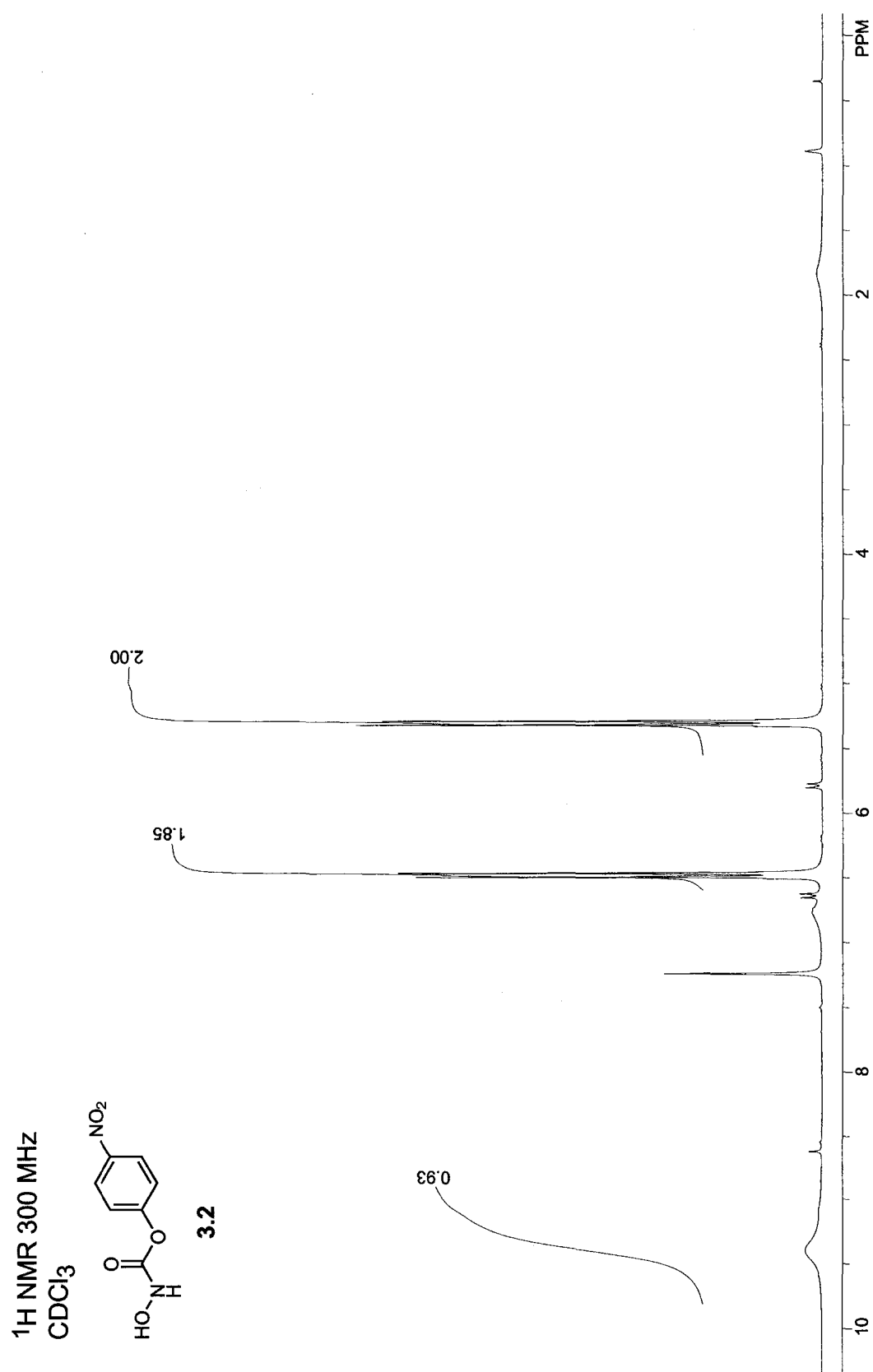


Scheme 3.3 Scheme for zinc(II)-mediated inhibition of enzymatic activity. Values are for inhibition of ribonuclease Bi by *N*-hydroxyurea **3.1**.

$[I] (10^{-4} \text{ M})$	$[Zn] (10^{-3} \text{ M})$	$K_M^{\text{obs}} (10^{-4} \text{ M})$	$K_i [I \cdot Zn^{2+}] (M)^2$	$K_i K_d (10^{-7} M^2)$
0.93	0.25	0.91	12.4	2.9
1.0	1.0	1.12	2.9	2.9
3.5	0.25	1.21	3.8	3.3
3.5	5.0	1.43	1.85	32

Table 3.1 Parameters for inhibition of ribonuclease Bi catalysis by *N*-hydroxyurea **3.1** and Zn^{2+} . Data are for those assays depicted in Figure 3.1 performed in the presence of Zn^{2+} .





Chapter Four

Zinc(II)-Mediated Inhibition of Ribonuclease Sa by an *N*-Hydroxyurea Nucleotide and its Basis

This chapter was accepted for publication as:

Alexander A. Makarov, Gennady I. Yakovlev, Vladimir A. Mitkevich, Joshua J. Higgin and Ronald T. Raines. Zinc(II)-mediated inhibition of a ribonuclease by an *N*-hydroxyurea nucleotide, *Biochemical and Biophysical Research Communications*. (In Press).

4.1 Abstract

Ribonuclease Sa (RNase Sa) is a secretory ribonuclease from *Streptomyces aureofaciens*. Herein, *N*-hydroxyurea-3'-deoxythymidine 5'-phosphate is shown to be a competitive inhibitor of catalysis by RNase Sa. Inhibition is enhanced by nearly 10-fold in the presence of Zn^{2+} , which could coordinate to the *N*-hydroxyurea group along with enzymic residues. The carboxylate of Glu54 is the putative base that abstracts a proton from the 2' hydroxyl group during catalysis of RNA cleavage by RNase Sa. Replacing Glu54 with a glutamine residue has no effect on the affinity of *N*-hydroxyurea **4.1** for the enzyme, but eliminates the zinc(II)-dependence of that affinity. These data indicate that an *N*-hydroxyurea nucleotide can recruit Zn^{2+} to inhibit the enzymatic activity of RNase Sa, and suggest that the carboxylate of Glu54 is a ligand for that Zn^{2+} . These results extend the generality of zinc(II) complexes with an *N*-hydroxyurea nucleotide as inhibitors of ribonucleases.

4.2 Introduction

RNA is the least stable of the biopolymers that effect information transfer in biology (Thompson *et al.*, 1995; Wolfenden & Snider, 2001). Still, the lifetime of RNA *in vivo* is most often determined by the rate of its enzymatic degradation (Ross, 1996). Hence, ribonucleases play myriad roles that garner ever-increasing attention (D'Alessio & Riordan, 1997; Leland & Raines, 2001; Ardelt *et al.*, 2003; Makarov & Ilinskaya, 2003). Likewise, the identification of small molecules that control ribonucleolytic activity is a worthwhile goal (Russo *et al.*, 2001).

Recently, we described a new strategy for the inhibition of ribonucleases (Higgin *et al.*, 2003). Our strategy uses an *N*-hydroxyurea nucleotide to deliver zinc(II) to the enzymic active site. There, the Zn^{2+} ion can be chelated by the two oxygens of the *N*-hydroxyurea group, leaving two Zn^{2+} sites open for chelation by active-site residues (Figure 4.1).

We first tested our strategy with ribonuclease Bi (binase), which is a secretory ribonuclease from *Bacillus intermedius*. We found that 3'-*N*-hydroxyurea-3'-deoxythymidine 5'-phosphate (4.1) is indeed a competitive inhibitor of catalysis by binase (Higgin *et al.*, 2003). Moreover, inhibition is enhanced in the presence of Zn^{2+} , which is consistent with our design. Here, we show that our strategy can be applied to a second ribonuclease, ribonuclease Sa (RNase Sa; Figure. 4.2), which is a secretory ribonuclease from *Streptomyces aureofaciens*. In addition, we use site-directed mutagenesis to identify a residue in the active site of RNase Sa that likely chelates to the

Zn^{2+} ion. The results demonstrate the generality of a zinc(II) complex with an *N*-hydroxyurea nucleotides as inhibitors of ribonucleases.

4.3 Results and discussion

The Zn^{2+} -mediated inhibition of a ribonuclease by *N*-hydroxyurea **4.1** could occur according Figure 4.1, as we described previously for binase (Higgin *et al.*, 2003). Because Zn^{2+} prefers tetrahedral coordination, two enzymic functional groups likely serve as the Zn^{2+} ligands in the ternary complex. By analogy to RNase T₁, which is a homolog of RNase Sa, Glu54 is the base and His85 is the acid during catalysis of RNA cleavage (Takahashi, 1970; Steyaert *et al.*, 1990; De Vos *et al.*, 1998). Specifically, Glu54 abstracts a proton from the 2' hydroxyl group, and His85 protonates the 5'' alkoxide (Figure. 4.2B) (Yakovlev *et al.*, 2003). (A triester-like mechanism has also been proposed for RNase T₁ (Loverix *et al.*, 2000).) The structure of crystalline RNase Sa has been determined by x-ray diffraction analysis (Sevcik *et al.*, 1993). Inspection of this structure suggests that the carboxylate of Glu54 and the imidazole of His85 could be the Zn^{2+} ligands (Figure 4.2A). If Glu54 and His85 chelate to Zn^{2+} as in Figure 4.1, then replacing either would have little effect on the affinity of RNase Sa for *N*-hydroxyurea **4.1** alone but would lead to a marked decrease in the affinity of the enzyme for the *N*-hydroxyurea **4.1**· Zn^{2+} complex.

Previously, we showed that replacing His85 of RNase Sa with another residue leads to the complete loss of measurable ribonucleolytic activity (Yakovlev *et al.*, 2003), making the analysis of inhibition of His85 variants problematic. In contrast, the

conservative E54Q variant loses only *ca.* 700-fold in ribonucleolytic activity (Yakovlev *et al.*, 2003), which still allows for the measurement of inhibition constants. Although the side-chain amide of a glutamine residue can be a ligand for Zn^{2+} , its interaction with Zn^{2+} would be markedly weaker than that of the side-chain carboxylate of a glutamic acid residue. Accordingly, we analyzed the inhibition of RNase Sa and its E54Q variant by *N*-hydroxyurea **4.1** in the absence and presence of Zn^{2+} .

N-Hydroxyurea **4.1** is a competitive inhibitor of catalysis by both wild-type RNase Sa and its E54Q variant. Kinetic parameters for the cleavage of poly(I) by the two enzymes and its inhibition by *N*-hydroxyurea **4.1** were derived from the data shown in Figures 4.3 and 4.4, and are listed in Table 4.1. These parameters indicate that *N*-hydroxyurea **4.1** has a nearly equal affinity for RNase Sa and its E54Q variant. Thus, Glu54 appears to have no role in the binding of *N*-hydroxyurea **4.1** to RNase Sa. In the absence of *N*-hydroxyurea **4.1**, no inhibition of the ribonucleolytic activity of RNase Sa or its E54Q variant by Zn^{2+} was observed, up to a Zn^{2+} concentration of 5 mM. Eq 4.1 and 4.2, which correspond to Figure 4.6 (Higgin *et al.*, 2003), were used to calculate inhibition constants for *N*-hydroxyurea **4.1** in the presence of Zn^{2+} :

$$v = \frac{[E_0][S]k_{\text{cat}}}{[S] + K_M^{\text{obs}}} \quad (4.1)$$

$$K_M^{\text{obs}} = K_M \left(1 + \frac{[I]}{K_i} + \frac{[I \cdot \text{Zn}^{2+}]}{K_i} \right) \quad (4.2)$$

In eq 4.1 and 4.2, K_M is the Michaelis constant for the cleavage of poly(I); K_i^1 is the inhibition constant for *N*-hydroxyurea **4.1** alone (I); and K_i is the inhibition constant for the *N*-hydroxyurea **4.1**· Zn^{2+} complex ($I \cdot Zn^{2+}$). To calculate inhibition constants by eq 4.1, the $[I_0]$ and $[Zn_0^{2+}]$ values were used instead of $[I]$ and $[Zn^{2+}]$, because the enzyme concentration $[E_0]$ was far below the $[I_0]$ and $[Zn_0^{2+}]$ values. A value of $K_d = 6.3$ mM was used to calculate the concentration of the $I \cdot Zn^{2+}$ complex (Higgin *et al.*, 2003).

The affinity of wild-type RNase Sa for *N*-hydroxyurea **4.1** increases in the presence of Zn^{2+} . Parameters that characterize the inhibition of RNase Sa by the $I \cdot Zn^{2+}$ complex are listed in Table 4.2. The value of K_i for RNase Sa is about 0.12 mM for the concentration product $[I][Zn^{2+}] \leq 1 \times 10^{-7}$ M. When the product $[I][Zn^{2+}]$ exceeds this value, the calculated value of K_i grows. (We had observed a similar dependence of the calculated K_i on the $[I][Zn^{2+}]$ product with binase inhibition by *N*-hydroxyurea **4.1** in the presence of Zn^{2+} (Higgin *et al.*, 2003).) Most likely, this effect stems from the improper use of $[I_0]$ and $[Zn_0^{2+}]$ instead of $[I]$ and $[Zn^{2+}]$ in calculations at high $[I][Zn^{2+}]$ values, where a complex between $[I]$ and $[Zn^{2+}]$ could be based on the interaction of the anionic phosphoryl group of the inhibitor and a cationic zinc ion. We therefore believe that the most precise K_i value is obtained at low concentrations of *N*-hydroxyurea **4.1** and Zn^{2+} , and that $K_i = 0.12$ mM for wild-type RNase Sa.

The affinity of E54Q RNase Sa for *N*-hydroxyurea **4.1** does not increase in the presence of Zn^{2+} . The value of K_i for the E54Q variant is approximately 10-fold greater than that for the wild-type enzyme. Moreover, the K_i value for the E54Q variant nearly coincides with the K_i^1 value (Tables 4.1 and 4.3). These data are indicative of a marked

decrease in the affinity of the $I \cdot Zn^{2+}$ complex upon replacing Glu54 with a glutamine residue, which supports inhibition as depicted in Figure 4.1 with one of the ligands being the carboxylate of Glu54.

4.4 Conclusion

RNase Sa and binase are members of the RNase T₁ family of enzymes (EC 3.1.27.3) (Irie, 1997). Yet, the amino acid sequences of RNase Sa and binase are only 24% identical (Hartley, 1997). RNase Sa is an acidic ribonuclease with an isoelectric point of $pI = 3.5$ and highly negative net charge at pH 6.2 (where the inhibition constants were measured herein). In contrast, binase is a basic ribonuclease with an isoelectric point of $pI = 9.6$ and a highly positive net charge at pH 6.2. Yet, the constants for the inhibition of RNase Sa (as well as RNase T₁, unpublished data¹) by *N*-hydroxyurea 4.1 and its complex with Zn^{2+} ion are close to those for the inhibition of binase (Higgin *et al.*, 2003), with the K_i^I values for RNase Sa and binase being 0.95 mM and 1.3 mM, respectively, and the K_i values being 0.12 mM and 0.047 mM, respectively. The active sites of RNase Sa and binase are remarkably similar (Sevcik *et al.*, 1990). This similarity is likely to be responsible for the observed similarity of the inhibition constants. The structural similarity of the active sites of microbial ribonucleases enable us to put forth nucleotide derivatives with an *N*-hydroxyurea moiety in the 3' position as universal inhibitors of these enzymes, whose efficiency increases in the presence of zinc(II).

¹ Inhibition of RNase T₁ with *N*-hydroxyurea 4.1 and Zn^{2+} ($K_i = 0.056$ mM) exhibited a 16-fold increase in inhibition over inhibitor alone ($K_i = 0.89$ mM), and a 7-fold increase over Zn^{2+} alone ($K_i = 0.41$ mM), as shown in Figure 4.5.

4.5 Materials and methods

Chemicals. *N*-Hydroxyurea **4.1** was synthesized as described previously (Higgin *et al.*, 2003). Poly(inosinic acid) [poly(I)] was obtained from Sigma Chemical (St. Louis, MO). All other reagents were of commercial grade or better and were used without further purification.

Enzymes. Wild-type RNase Sa and its E54Q variant were prepared by C.N. Pace and coworkers (Texas A&M University). Briefly, wild-type RNase Sa was prepared as described previously (Shaw *et al.*, 2001). Synthetic oligonucleotides for the construction of E54Q RNase Sa were obtained from Integrated DNA Technologies (Coralville, IA). A cDNA encoding the E54Q variant was constructed with the QuickChange site-directed mutagenesis kit from Stratagene (La Jolla, CA). The mutated gene was sequenced at the Gene Technologies Laboratory at Texas A&M University to confirm the introduction of the desired (but no other) mutation. E54Q RNase Sa was produced and purified as described previously (Shaw *et al.*, 2001). The purity of the E54Q variant was confirmed by SDS-PAGE.

Enzyme kinetics. Steady-state kinetic analyses of catalysis of poly(I) cleavage by wild-type RNase Sa and its E54Q variant were performed at 25°C in 0.10 M sodium citrate buffer, pH 6.2, containing NaCl (0.10 M). Concentrations of RNase Sa and its variant were determined by ultraviolet spectroscopy using the extinction coefficient $\epsilon_{280} = 12,300 \text{ M}^{-1}\text{cm}^{-1}$ (Hebert *et al.*, 1997). The poly(I) concentration was measured likewise using $\epsilon_{248} = 10,000 \text{ M}^{-1}\text{cm}^{-1}$ at pH 7.8 (Chamberlin & Patterson, 1965). Initial reaction rates were determined by recording changes in absorption at 248 nm, using the difference

extinction coefficient $\Delta\epsilon_{248} = 1330 \text{ M}^{-1}\text{cm}^{-1}$ at pH 6.2 (Yakovlev *et al.*, 1992). Assays of inhibitor with RNase T1 were assessed at 25 °C in 2.0 ml of 100 mM MES buffer, pH 6.0, containing NaCl (100 mM), 6-FAM~dArUdAdA~6-TAMRA (60 nM), and RNase T1 (25 nM) as described previously (Kelemen *et al.*, 1999; Park *et al.*, 2001).

Fluorescence (F) was measured using 490 and 515 nm as the excitation and emission wavelengths, respectively. The value of $\Delta F/\Delta t$ was measured for 3 min after the addition of RNase T1. An aliquot of *N*-hydroxyurea **4.1** and/or ZnCl_2 dissolved in the assay buffer was added next, and $\Delta F/\Delta t$ was measured in the presence of the inhibitor and/or metal for an additional 3 min. The concentration of inhibitor **4.1**, ZnCl_2 or both in the assay was doubled repeatedly in 3-min intervals. Excess RNase T1 was then added to the mixture to ensure that <10% substrate had been cleaved prior to completion of the inhibition assay. Apparent changes in ribonucleolytic activity due to dilution were corrected by comparing values to an assay in which aliquots of buffer were added to the assay. Values of K_i were determined by non-linear least squares regression analysis of data fitted to eq 4.3 (Kelemen *et al.*, 1999; Smith *et al.*, 2003).

$$\Delta F / \Delta t = (\Delta F / \Delta t)_0 (K_i / (K_i + [I])) \quad (4.3)$$

In eq 4.3, $(\Delta F/\Delta t)_0$ was the ribonucleolytic activity prior to inhibitor addition.

RNase Sa	k_{cat} (s ⁻¹)	K_{M} (mM)	$k_{\text{cat}}/K_{\text{M}}$ (10 ⁶ M ⁻¹ s ⁻¹)	K_{i}^{I} (mM)
wild-type	189	0.151	1.25	0.95
E54Q	0.7	0.32	0.002	1.15

^a Parameters were obtained from the data in Fig. 4.3.

Table 4.1

Parameters for catalysis of poly(I) cleavage by RNase Sa and its E54Q variant, and for its inhibition by *N*-hydroxyurea 4.1 at pH 6.2 and 25°C ^a

$[\text{Zn}^{2+}]$ (mM)	$[\text{I}]$ (10^{-4} M)	$[\text{I}][\text{Zn}^{2+}]$ (10^{-7} M ²)	$[\text{I-Zn}^{2+}]$ (10^{-5} M)	K_M^{obs} (10^{-4} M)	K_i (10^{-4} M)
0.5	1.0	0.5	0.79	1.76	1.16
0.5	3.0	1.5	2.38	2.25	1.17
1.0	1.0	1.0	1.59	1.83	1.28
1.0	2.0	2.0	3.18	2.17	1.22
1.0	3.0	3.0	4.76	2.46	1.31
1.0	4.0	4.0	6.35	2.70	1.46
2.5	1.0	2.5	3.97	2.01	1.48
2.5	3.0	7.5	11.91	2.60	2.24
5.0	1.0	5.0	7.94	2.14	2.01
5.0	3.0	15	23.81	2.62	3.55

^a Parameters were obtained from the data in Fig. 4.4A.

Table 4.2

Parameters for inhibition of wild-type RNase Sa catalysis by *N*-hydroxyurea
4.1 and Zn^{2+} ^a

$[\text{Zn}^{2+}]$ (mM)	$[\text{I}]$ (10^{-4} M)	$[\text{I}][\text{Zn}^{2+}]$ (10^{-7} M ²)	$[\text{I}\cdot\text{Zn}^{2+}]$ (10^{-5} M)	$K_{\text{M}}^{\text{obs}}$ (10^{-4} M)	K_{i} (10^{-4} M)
1	1	1	1.59	3.50	7.7
1	2	2	3.18	3.75	12.2
1	3	3	4.76	3.98	19.2
1	4	4	6.35	4.28	14.3
5	1	5	7.94	3.46	12.5
5	3	15	23.81	4.05	11.2

^a Parameters were obtained from the data in Fig. 4.4B.

Table 4.3

Parameters for inhibition of E54Q RNase Sa catalysis by *N*-hydroxyurea
4.1 and Zn^{2+} ^a

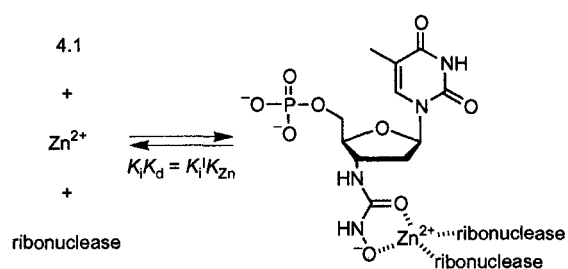
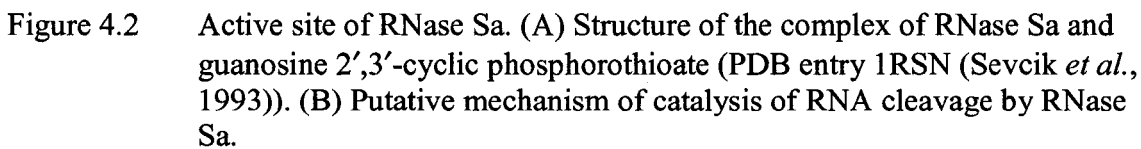


Figure 4.1 Strategy for the Zn^{2+} -mediated inhibition of a ribonuclease by an *N*-hydroxyurea nucleotide.



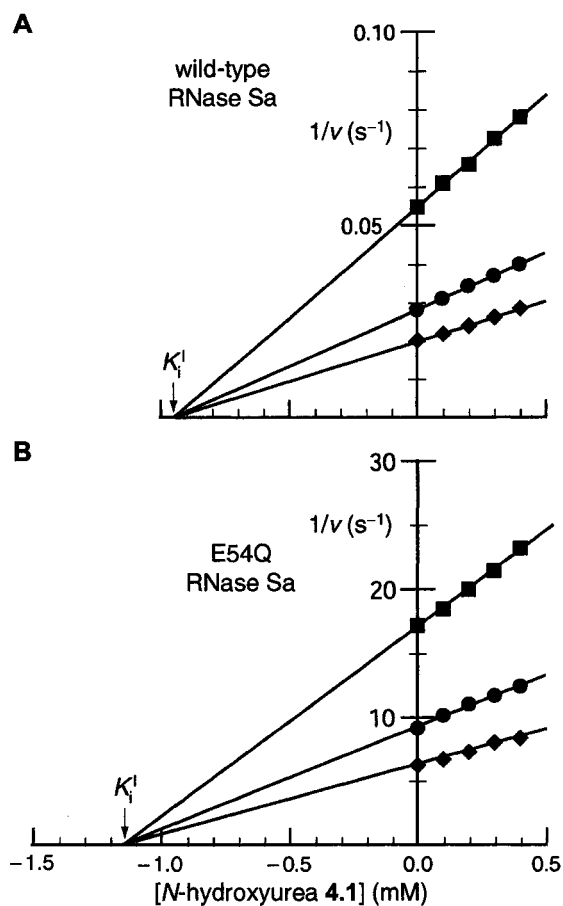


Figure 4.3 Dixon plot for the inhibition of wild-type RNase Sa and its E54Q variant by *N*-hydroxyurea **4.1** in the absence of Zn^{2+} . (A) Wild-type RNase Sa. Assays were performed at 25 °C in 0.10 M sodium citrate buffer, pH 6.2, containing NaCl (0.10 M), wild-type RNase Sa (0.825 nM), poly(I) (■, 17 μM ; ●, 34 μM ; ◆, 50 μM), and *N*-hydroxyurea **4.1** (0.00, 0.10, 0.20, 0.30, or 0.40 mM). (B) E54Q RNase Sa. Assays were performed at 25 °C in 0.10 M sodium citrate buffer, pH 6.2, containing NaCl (0.10 M), E54Q RNase Sa (0.50 μM), poly(I) (■, 25 μM ; ●, 50 μM ; ◆, 75 μM), and *N*-hydroxyurea **4.1** (0.00–0.40 mM).

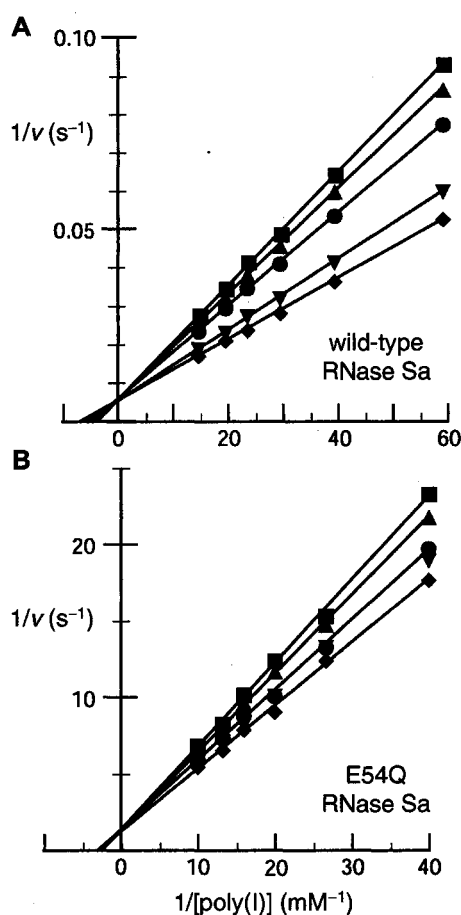


Figure 4.4 Lineweaver-Burk plot for the inhibition of wild-type RNase Sa and its E54Q variant by *N*-hydroxyurea **4.1** in the absence and presence of Zn^{2+} . (A) Wild-type RNase Sa. Assays were performed at 25 °C in 0.10 M sodium citrate buffer, pH 6.2, containing NaCl (0.10 M), RNase Sa (0.825 nM), poly(I) (16.9–67.6 μM), *N*-hydroxyurea **4.1** (I), and Zn^{2+} . (B) E54Q RNase Sa. Assays were performed at 25 °C in 0.10 M sodium citrate buffer, pH 6.2, containing NaCl (0.10 M), E54Q RNase Sa (0.50 μM), poly(I) (25–100 μM), *N*-hydroxyurea **4.1** (I), and Zn^{2+} . ■, [I] = 0.40 mM, $[\text{Zn}^{2+}]$ = 1.0 mM; ▲, [I] = 0.30 mM, $[\text{Zn}^{2+}]$ = 5.0 mM; ●, [I] = 0.10 mM, $[\text{Zn}^{2+}]$ = 5.0 mM; ▼, [I] = 0.10 mM, $[\text{Zn}^{2+}]$ = 1.0 mM; ◆, [I] = 0 mM, $[\text{Zn}^{2+}]$ = 0 mM.

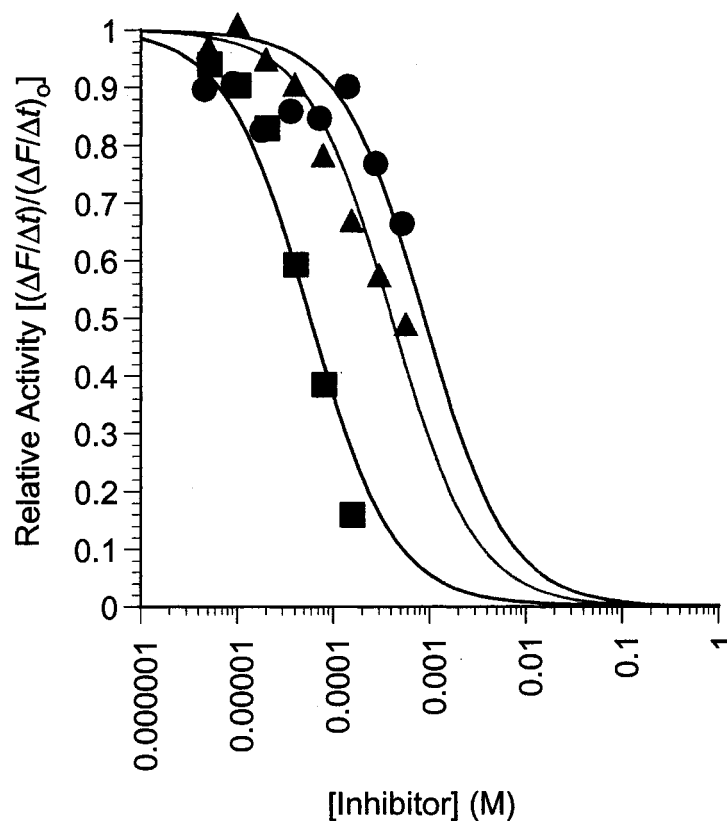


Figure 4.5 Dependence of the relative ribonucleolytic activity of RNase T1 $[(\Delta F/\Delta t)/(\Delta F/\Delta t)_0]$ on the concentration of **4.1** (●), ZnCl_2 (▲), or **4.1** and ZnCl_2 (■). ●, ▲, and ■ represent data collected in independent reactions. Reactions were carried out at 25 °C in 100 mM MES–NaOH buffer, pH 6.0, containing NaCl (100 mM), 6-FAM~dArUdAdA~6-TAMRA (60 nM), and RNase T1 (25 nM). Data were analyzed using eq 4.3.

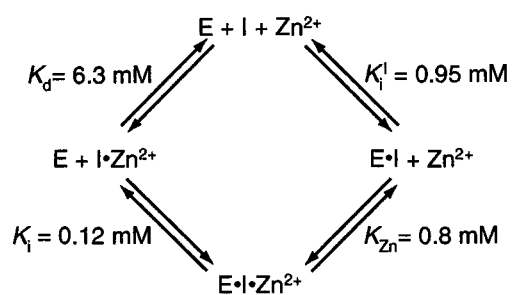


Figure 4.6 Scheme for the Zn^{2+} -mediated inhibition of wild-type RNase Sa by *N*-hydroxyurea **4.1**.

Appendix I

**Site-Specific Conjugation of Folic Acid to Ribonuclease A
Increases its Specific Toxicity for Cancer Cells: Synthesis of
 N^{α} -Pteroyl- N^{δ} -Bromoacetyl Ornithine**

A.1 Abstract

G88R RNase A that has attenuated affinity for the endogenous ribonuclease inhibitor protein (RI) and is toxic to mammalian cells. Ribonuclease toxicity could be limited by the amount of enzyme that enters the cytoplasm. Conjugation to folate is known to enhance the uptake of proteins by cancer cells that over-produce the folate receptor. Here, random conjugation of folate to lysine residues of wild-type RNase A is shown to decrease its catalytic activity by >99.5%, presumably because of the alteration of the key active-site residue: Lys-41. In contrast, random conjugation of folate to K41R/G88R RNase A does not affect catalytic activity and increases cytotoxicity by 10-fold. To effect the site-specific coupling of folate, a folate analog with an electrophilic bromoacetamido group ("BAm-folate") was prepared by chemical synthesis. Conjugation of BAm-folate to G88C RNase A (enabling both RI evasion and cell targeting) or A19C/G88R RNase A enhances toxicity by *ca.* 20-fold for cancer cells that over-produce the folate receptor. Folate conjugation does not enhance the toxicity of RNase A variants for cancer cells that do not over-produce the folate receptor. These data reveal a propitious means for targeting proteins to specific cancer cells. This Appendix describes the chemical synthesis of BAm-folate.

A.2 Introduction

Ribonucleases are among the most toxic enzymes. Cells secrete ribonucleases into the extracellular medium, yet contain an extremely high-affinity proteinaceous inhibitor ($K_d \approx 10^{-15}$ M) to prevent RNA degradation by secretory ribonucleases that inadvertently enter the cytosol (Lee *et al.*, 1989; Beintema & Kleineidam, 1998). Onconase™ (ONC), a secretory ribonuclease from the Northern leopard frog, was discovered based on its ability to kill cancer cells *in vitro* (Ardelt *et al.*, 1991). ONC is not inhibited by the endogenous human ribonuclease inhibitor protein (RI) and can induce apoptosis by digesting cellular RNA (Wu *et al.*, 1993). Other homologs of onconase, including bovine pancreatic ribonuclease (RNase A; EC 3.1.27.5), have an intrinsic ability to cross cell membranes and kill cancer cells, as long as they are able to evade RI (Leland *et al.*, 1998). A single amino acid substitution in RNase A is sufficient to weaken RI affinity and to render it toxic to cancer cells (Leland *et al.*, 1998).

The toxicity of ribonucleases is limited by the amount of enzyme that can cross the cell membrane and reach the cytoplasm. Microinjection experiments show that RNase A is $\sim 10^6$ -fold more toxic when injected than when added to the extracellular medium (Saxena *et al.*, 1991). This intrinsic limitation could be overcome with strategies that enhance binding and uptake of ribonucleases by cells.

Receptors for the B-vitamin folic acid are over-produced on the surface of some cancer cells, such as those derived from ovarian, endometrial, and brain carcinomas (Garin-Chesa *et al.*, 1993; Ross *et al.*, 1994). These receptors can be targeted with protein

toxins conjugated to folate (Leamon & Low, 1991). Protein~folate conjugates enter cells via folate receptor-mediated endocytosis, and exhibit both increased toxicity and specificity compared to corresponding non-targeted toxin (Reddy & Low, 1998). We reasoned that the conjugation of folate to toxic ribonucleases could enable more protein to enter the cytoplasm of cells that over-produce the folate receptor, resulting in increased toxicity and specificity to these cells.

Methods for coupling folate to proteins have relied on nonspecific reactions that lead to a heterogeneous mixture of conjugates (Reddy & Low, 1998). Furthermore, random folate conjugation can affect adversely the structure or activity of a protein toxin (Atkinson *et al.*, 2001). The ability to couple folate to a specific position in a protein would alleviate these problems. Herein, we describe the chemical synthesis of a new folate analog that allows for the attachment of folate at a designated position in a protein of interest. We have attached this folate analog to cytotoxic variants of RNase A. We find that specifically coupled RNase A~folate conjugates are 20-fold more toxic than unmodified control enzymes. This Appendix describes the chemical synthesis of the folate analog.

A.3 Materials and Methods

Synthesis of BAM-folate for Ribonuclease Conjugation

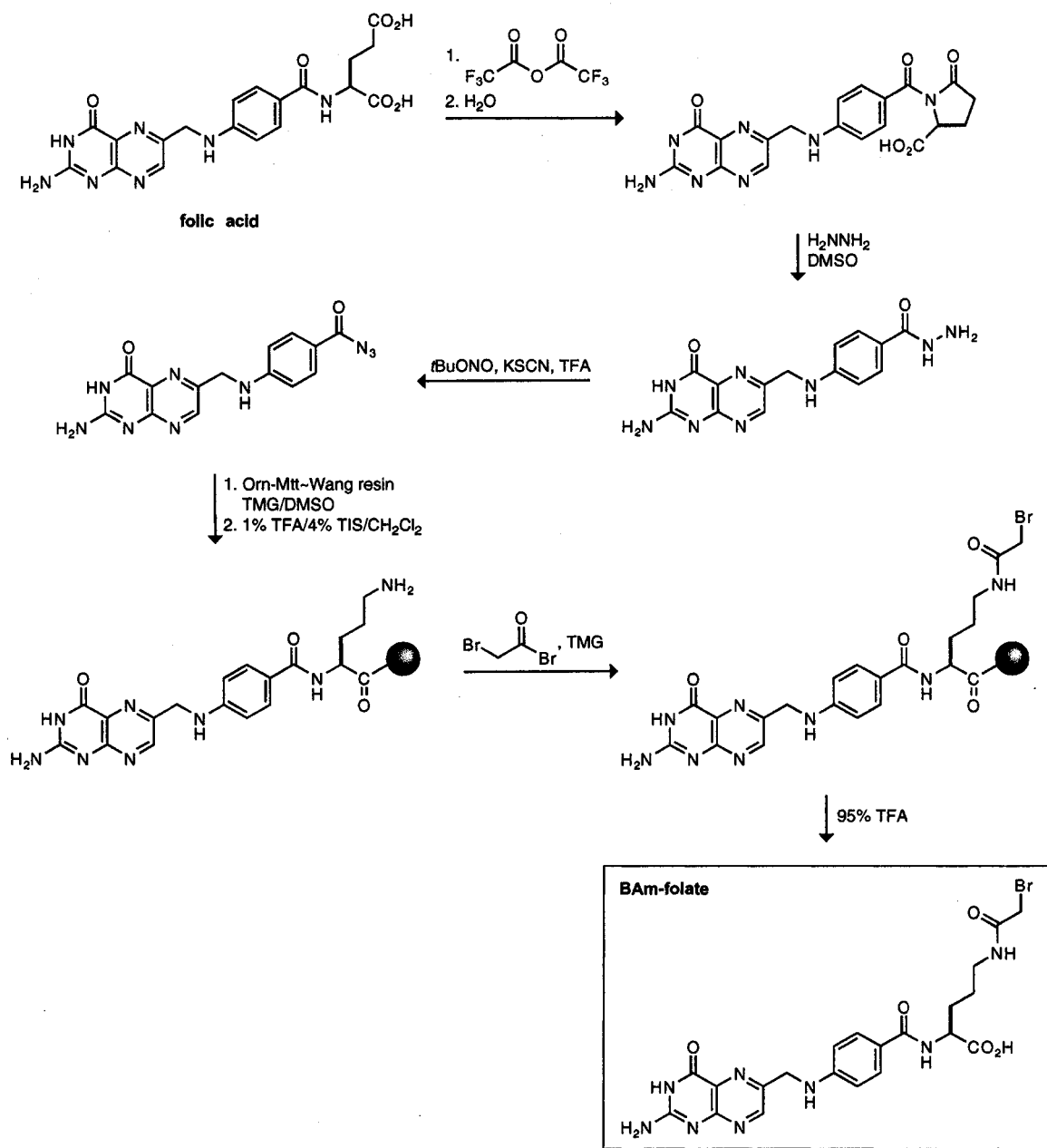
Synthesis of Pterotic Azide. Pterotic azide was synthesized according to Luo *et al.* (Luo *et al.*, 1997) as summarized below. Folic acid dihydrate (10.0 g, 20.9 mmol) was dissolved in THF (100 ml) and the resulting solution was stirred for 10 min and then

cooled to 0 °C. Trifluoroacetic anhydride (16 ml, 113 mmol) was added over 30 min. The reaction mixture was allowed to warm to 25 °C, and stirred overnight. The reaction mixture was concentrated by rotary evaporation to a thick dark viscous liquid, which was dripped into benzene (150 ml) to precipitate. The solid was removed by filtration, washed with ether, and allowed to dry under vacuum. THF (32 ml) was added to the solid along with ice (6.4g), and the resulting slurry stirred for 4 h. The mixture was then poured into ether to precipitate. The precipitate was removed by filtration, washed with ether, and dried under vacuum. The dried solid was then dissolved in DMSO (165 ml) and the resulting solution was stirred at 25 °C in a water bath. Hydrazine (4.9 ml, 156 mmol) was added slowly, and the reaction mixture was stirred for 8 h. MeOH (300 ml) was added to precipitate the hydrazide, which was filtered and washed with MeOH (3x 50 ml), washed with ether (3x 50 ml), and dried under vacuum. The hydrazide was dissolved in ice cold TFA at -10 °C with KSCN (63 mg, 0.648 mmol). tBuONO (1.72 ml, 14.8 mmol) was added slowly, and the reaction mixture stirred for 4 h at -10 °C. The reaction mixture was then allowed to warm to 25 °C and NaN₃ (432 mg, 6.6 mmol) was added and the reaction mixture was stirred for 10 min before isopropanol (150 ml) was slowly added to precipitate the product. The precipitate was collected by centrifugation. The product was washed in a similar manner with water (3x 50 ml), acetonitrile (50 ml), and ether (2x 50 ml). The pterotic azide product was dried under vacuum. Yield 2.84 g; 8.4 mmol. (40 %)

N^α-Pteroyl-N^δ-bromoacetyl ornithine (BAm-folate). BAm-folate was synthesized on a solid support. Wang resin (600 mg, 100-200 mesh, 1.2 mmol/g) and Fmoc-ornithine-N^δ-methyltrityl (880 mg, 1.3 mmol) dissolved in of DMF (10 ml) were

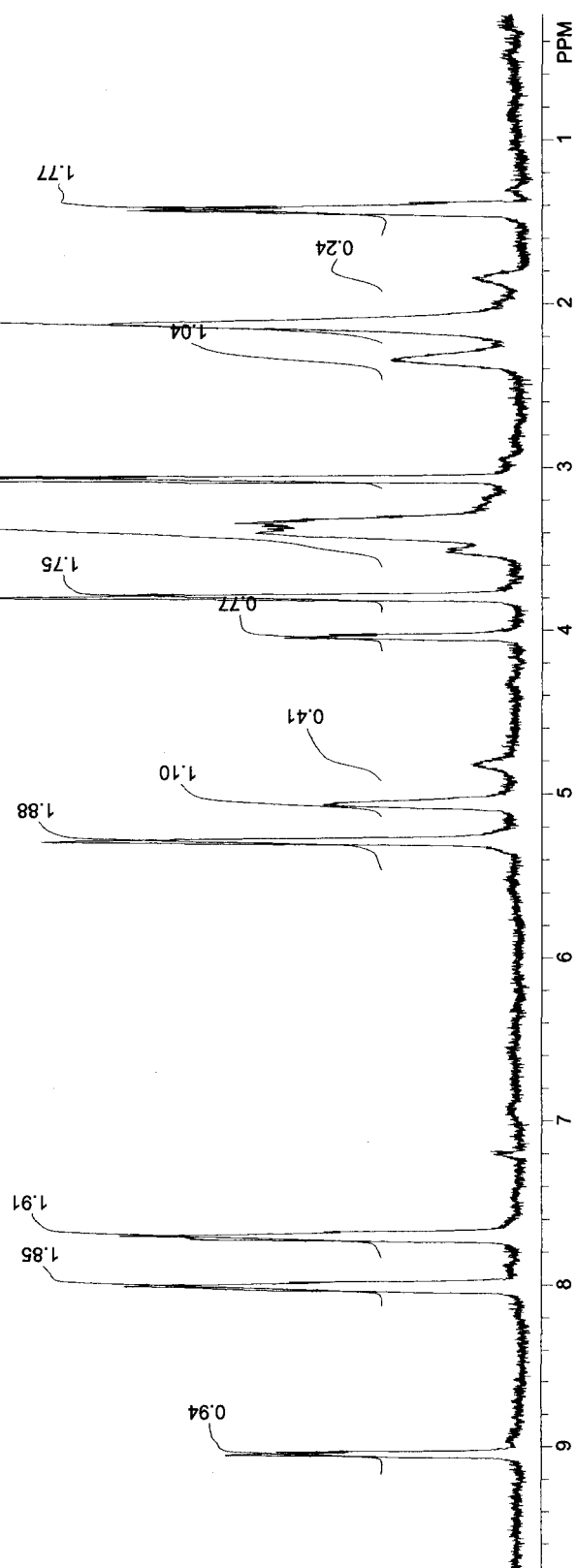
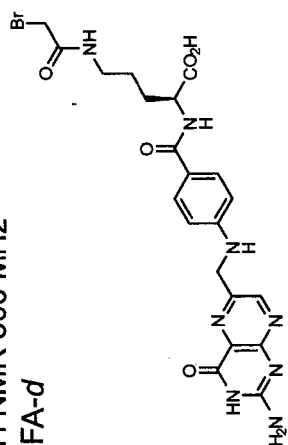
added to a 25-ml solid-phase synthesis vessel. Pyridine (193 μ l, 2.4 mmol) and 2,6-dichlorobenzoyl chloride (209 μ l, 1.5 mmol) were added to the resin, and the reaction mixture was put on an orbital shaker overnight. The resin was washed with DMF (3x 20 ml) and CH_2Cl_2 (3x 20 ml) and dried under vacuum. The resin was swelled in CH_2Cl_2 (8 ml) and benzoyl chloride (290 μ l, 1.8 mmol) was added along with pyridine (290 μ l, 3.6 mmol) to cap the resin. The reaction mixture was allowed to shake overnight. The Fmoc group was removed with piperidine (20% v/v) in DMF (20 ml), and the resin was washed with DMF (3x 20 ml) followed by CH_2Cl_2 (3x 20 ml) and dried under vacuum. The resin was swelled in 50:50 DMSO (12 ml) and DMF (12 ml) were added to the resin along with and pteroyl azide (790 mg, 2.3 mmol) and tetramethylguanidine (TMG; 400 μ l, 3.2 mmol). The mixture was allowed to shake overnight. The resin was washed with DMSO/DMF (50:50 20 ml) followed by CH_2Cl_2 (20 ml), and then dried under vacuum. The methyl trityl group was removed with TFA (1% v/v) in CH_2Cl_2 (40 ml) until no more yellow color was apparent. The resin was washed with CH_2Cl_2 (40 ml), and then dried under vacuum. The resin was added to of CH_2Cl_2 (5 ml) containing bromoacetyl bromide (200 μ l) and TMG (200 μ l), and allowed to shake overnight. The resin was washed with CH_2Cl_2 (40 ml), and then dried under vacuum. The bamfolate product was cleaved from the resin with TFA (neat, 10 ml) and dripped into ice-cold ether. The precipitate was collected by centrifugation. The product was then washed with ether (3x 30 ml). The residue was taken up in H_2O and lyophilized. The fluffy solid was purified by reverse-phase HPLC (20-35% v/v acetonitrile in water) on a Varian C18 column (250 x 21 mm), and the solvent was removed by high-vacuum rotary evaporation and lyophilization.

Yield: 30 mg, 0.05 mmol (7 %) ESI MS m/z (M^+) 547, 549 (characteristic Br doublet); ^1H NMR (TFA- d , 300 MHz) δ 9.0 (s, 1H, Ar), 8.0 (m, 2H, Ar), 7.7 (m, 2H, Ar), 6.6 (m, 2H,), 5.3 (s, 2H, NH), 5.1 (s, 1H, OH), 4.1 (m, 1H, CH), 3.8 (m, 2H, CH_2), 3.4 (m, 4H), 3.1 (m, 3H, NH_3), 2.4 (m, 1H), 2.1 (m, 4H, CH_2CH_2), 1.4 (m, 2H, CH_2).



Scheme A.1 Synthetic scheme for BAM-folate synthesis. Ornithine is linked to the Wang resin via a p-benzyloxybenzyl alcohol linker.

¹H NMR 300 MHz
TFA-d



References

- Abell, A. D., Morris, K. B. & Litten, J. C. (1990). Synthesis and deprotection of [1-(ethoxycarbonyl)-4-[(diphenylmethoxy)carbonyl]-1-methyl-2-oxobutyl]triphenylphosphonium chloride: A key intermediate in the Wittig reaction between a cyclic anhydride and a stabilized ylide. *J. Org. Chem.* **55**(18), 5217-5221.
- Anttinen, H., Ryhanen, L., Puistola, U., Arranto, A. & Oikarinen, A. (1984). Decrease in liver collagen accumulation in carbon tetrachloride-injured and normal growing rats upon administration of zinc. *Gastroenterology* **86**(3), 532-539.
- Appleton, D., Duguid, A. B., Lee, S. K., Ha, Y. J., Ha, H. J. & Leeper, F. J. (1998). Synthesis of analogues of 5-aminolaevulinic acid and inhibition of 5-aminolaevulinic acid dehydratase. *J. Chem. Soc. [Perkin. 1]*.(1), 89-101.
- Ardelt, B., Ardelt, W. & Darzynkiewicz, Z. (2003). Cytotoxic ribonucleases and RNA interference (RNAi). *Cell Cycle* **2**, 22-24.
- Ardelt, W., Mikulski, S. M. & Shogen, K. (1991). Amino acid sequence of an anti-tumor protein from *Rana pipiens* oocytes and early embryos. *J. Biol. Chem.* **266**, 245-251.
- Atkinson, S. F., Bettinger, T., Seymour, L. W., Behr, J. P. & Ward, C. M. (2001). Conjugation of folate via gelonin carbohydrate residues retains ribosomal-inactivating properties of the toxin and permits targeting to folate receptor positive cells. *J Biol Chem* **276**(30), 27930-5.
- Baader, E., Tschank, G., Baringhaus, K. H., Burghard, H. & Gunzler, V. (1994). Inhibition of prolyl 4-hydroxylase by oxalyl amino acid derivatives *in vitro*, in isolated microsomes and in embryonic chicken tissues. *Biochem. J.* **300**, 525-530.
- Babine, R. E. & Bender, S. L. (1997). Molecular recognition of protein-ligand complexes: Applications to drug design. *Chem. Rev.* **97**(5), 1359-1472.
- Barnes, M. J. (1975). Function of ascorbic acid in collagen metabolism. *Ann. N. Y. Acad. Sci.* **258**, 264-277.
- Beintema, J. J. & Kleineidam, R. G. (1998). The ribonuclease A superfamily: General discussion. *Cell Mol Life Sci* **54**(8), 825-32.
- Bella, J., Eaton, M., Brodsky, B. & Berman, H. M. (1994). Crystal and molecular structure of a collagen-like peptide at 1.9 Å resolution. *Science* **266**(5182), 75-81.

- Berg, R. A. & Prockop, D. J. (1973a). Affinity column purification of procollagen proline hydroxylase from chick embryos and further characterization of the enzyme. *J. Biol. Chem.* **248**(4), 1175-1182.
- Berg, R. A. & Prockop, D. J. (1973b). Thermal transition of a nonhydroxylated form of collagen. Evidence for a role for hydroxyproline in stabilizing the triple helix of collagen. *Biochem. Biophys. Res. Commun.* **52**(1), 115-120.
- Bickel, M., Baader, E., Brocks, D. G., Engelbart, K., Guenzler, V., Schmidts, H. L. & Vogel, G. H. (1991). Beneficial effects of inhibitors of prolyl 4-hydroxylase in carbon tetrachloride-induced fibrosis of the liver in rats. *J. Hepatol.* **13**(Suppl. 3), S26-S34.
- Bickel, M., Baringhaus, K. H., Gerl, M., Gunzler, V., Kanta, J., Schmidts, L., Stapf, M., Tschank, G., Weidmann, K. & Werner, U. (1998). Selective inhibition of hepatic collagen accumulation in experimental liver fibrosis in rats by a new prolyl 4-hydroxylase inhibitor. *Hepatology* **28**(2), 404-411.
- Boeker, K., Schwarting, G., Kaule, G., Guenzler, V. & Schmidt, E. (1991). Fibrosis of the liver in rats induced by bile duct ligation. Effects of inhibition of prolyl 4-hydroxylase. *J. Hepatol.* **13**(Suppl. 3), S35-S40.
- Bretscher, L. E., Jenkins, C. L., Taylor, K. M., DeRider, M. L. & Raines, R. T. (2001). Conformational stability of collagen relies on a stereoelectronic effect. *J. Am. Chem. Soc.* **123**(4), 777-778.
- Bruick, R. K. (2003). Oxygen sensing in the hypoxic response pathway: Regulation of the hypoxia-inducible transcription factor. *Genes Dev.* **17**(21), 2614-2623.
- Bruick, R. K. & McKnight, S. L. (2001). A conserved family of prolyl-4-hydroxylases that modify hif. *Science* **294**(5545), 1337-1340.
- Bundgaard, H., Ed. (1985). *Design of prodrugs*. New York: Elsevier.
- Carrigan, C. N., Bartlett, R. D., Esslinger, C. S., Cybulski, K. A., Tongcharoensirikul, P., Bridges, R. J. & Thompson, C. M. (2002). Synthesis and *in vitro* pharmacology of substituted quinoline-2,4-dicarboxylic acids as inhibitors of vesicular glutamate transport. *J. Med. Chem.* **45**(11), 2260-2276.
- Chamberlin, M. J. & Patterson, D. L. (1965). Physical and chemical characterization of the ordered complexes formed between polyinosonic acid, polycytidylic acid and their deoxyribo-analogues. *J. Mol. Biol.* **12**, 410-428.

- Chang, C. A., Sekhar, V. C., Garg, B. S., Guziec, F. S., Jr. & Carrera Russo, T. (1987). Equilibria and kinetics of some metal complexes of peptide hydroxamic acids. *Inorg. Chim. Acta* **135**(1), 11-18.
- Chaston, T. B. & Richardson, D. R. (2003). Iron chelators for the treatment of iron overload disease: Relationship between structure, redox activity, and toxicity. *Am. J. Hematol.* **73**(3), 200-210.
- Chung, S. J. & Kim, D. H. (2001). *N*-(hydroxyaminocarbonyl)phenylalanine: A novel class of inhibitor for carboxypeptidase A. *Bioorg. Med. Chem.* **9**(1), 185-189.
- Clifton, I. J., Hsueh, L.-C., Baldwin, J. E., Harlos, K. & Schofield, C. J. (2001). Structure of proline 3-hydroxylase. Evolution of the family of 2-oxoglutarate dependent oxygenases. *Eur. J. Biochem.* **268**(24), 6625-6636.
- Connolly, P. J., Wetter, S. K., Beers, K. N., Hamel, S. C., Chen, R. H. K., Wachter, M. P., Ansell, J., Singer, M. M., Steber, M., Ritchie, D. M. & Argentieri, D. C. (1999). *N*-hydroxyurea and hydroxamic acid inhibitors of cyclooxygenase and 5-lipoxygenase. *Bioorg. Med. Chem. Lett.* **9**(7), 979-984.
- Costas, M., Mehn, M. P., Jensen, M. P. & Que, L., Jr. (2004). Dioxygen activation at mononuclear nonheme iron active sites: Enzymes, models, and intermediates. *Chem. Rev.* **104**(2), 939-986.
- Crews, C. M. & Splittgerber, U. (1999). Chemical genetics: Exploring and controlling cellular processes with chemical probes. *Trends Biochem. Sci.* **24**(8), 317-320.
- Cunliffe, C. J., Franklin, T. J., Hales, N. J. & Hill, G. B. (1992). Novel inhibitors of prolyl 4-hydroxylase. 3. Inhibition by the substrate analogue *N*-oxaloglycine and its derivatives. *J. Med. Chem.* **35**(14), 2652-2658.
- D'Alessio, G. & Riordan, J. F., Eds. (1997). *Ribonucleases: Structures and functions*. New York: Academic Press.
- Dawson, R. M. C., Elliott, W. H. & Elliott, D. C., Eds. (1989). *Data for biochemical research*. 3rd edit. New York: Clarendon Press.
- De Vos, S., Doumen, J., Langhorst, U. & Steyaert, J. (1998). Dissecting histidine interactions of ribonuclease T₁ with asparagine and glutamine replacements: Analysis of double mutant cycles at one position. *J. Mol. Biol.* **275**, 651-661.
- De Waal, A. & De Jong, L. (1988). Processive action of the two peptide binding sites of prolyl 4-hydroxylase in the hydroxylation of procollagen. *Biochemistry* **27**(1), 150-155.

Farkas, E. & Buglyo, P. (1990). Complex formation between transition metals and DL-aspartic acid- β -hydroxamic acid (*N*-hydroxyasparagine). *J. Chem. Soc. Dalton Trans.*(5), 1549-1551.

Farkas, E., Enyedy, E. A. & Csóka, H. (2000a). Some factors affecting metal ion-monohydroxamate interactions in aqueous solution. *J. Inorg. Biochem.* **79**(1-4), 205-211.

Farkas, E., Enyedy, E. A., Micera, G. & Garribba, E. (2000b). Coordination modes of hydroxamic acid in copper(II), nickel(II), and zinc(II) mixed-ligand complexes in aqueous solution. *Polyhedron* **19**, 1727-1736.

Folkman, J. (1995). Angiogenesis in cancer, vascular, rheumatoid and other disease. *Nat. Med.* **1**(1), 27-31.

Franklin, T. J. (1995). Current approaches to the therapy of fibrotic diseases. *Biochem. Pharmacol.* **49**(3), 267-273.

Franklin, T. J., Hales, N. J., Johnstone, D., Morris, W. B., Cunliffe, C. J., Millest, A. J. & Hill, G. B. (1991). Approaches to the design of anti-fibrotic drugs. *Biochem. Soc. Trans.* **19**(4), 812-815.

Franklin, T. J., Morris, W. P., Edwards, P. N., Large, M. S. & Stephenson, R. (2001). Inhibition of prolyl 4-hydroxylase *in vitro* and *in vivo* by members of a novel series of phenanthrolinones. *Biochem. J.* **353**, 333-338.

Friedman, L., Higgin, J. J., Moulder, G., Barstead, R., Raines, R. T. & Kimble, J. (2000). Prolyl 4-hydroxylase is required for viability and morphogenesis in *Caenorhabditis elegans*. *Proc. Natl. Acad. Sci. U. S. A.* **97**(9), 4736-4741.

Friedman, S. L. (2003). Liver fibrosis -- from bench to bedside. *J. Hepatol.* **38 Suppl 1**, S38-53.

Garin-Chesa, P., Campbell, I., Saigo, P. E., Lewis, J. L., Jr., Old, L. J. & Rettig, W. J. (1993). Trophoblast and ovarian cancer antigen LK26. Sensitivity and specificity in immunopathology and molecular identification as a folate-binding protein. *Am. J. Pathol.* **142**, 557.

Greco, M. N., Hageman, W. E., Powell, E. T., Tighe, J. J. & Persico, F. J. (1992). Benzothiazole hydroxy ureas as inhibitors of 5-lipoxygenase: Use of the hydroxyurea moiety as a replacement for hydroxamic acid. *J. Med. Chem.* **35**(17), 3180-3183.

Groves, J. T. & McClusky, G. A. (1976). Aliphatic hydroxylation via oxygen rebound. Oxygen transfer catalyzed by iron. *J. Am. Chem. Soc.* **98**(3), 859-861.

Gryder, R. M., Lamon, M. & Adams, E. (1975). Sequence position of 3-hydroxyproline in basement membrane collagen. Isolation of glycyl-3-hydroxyproyl-4-hydroxyproline from swine kidney. *J. Biol. Chem.* **250**(7), 2470-2474.

Guenzler, V., Majamaa, K., Hanauske-Abel, H. M. & Kivirikko, K. I. (1986). Catalytically active ferrous ions are not released from prolyl 4-hydroxylase under turnover conditions. *Biochim. Biophys. Acta* **873**(1), 38-44.

Gunzler, V., Brocks, D., Henke, S., Myllyla, R., Geiger, R. & Kivirikko, K. I. (1988a). Syncatalytic inactivation of prolyl 4-hydroxylase by synthetic peptides containing the unphysiologic amino acid 5-oxaproline. *J. Biol. Chem.* **263**(36), 19498-504.

Gunzler, V., Hanauske-Abel, H. M., Myllyla, R., Kaska, D. D., Hanauske, A. & Kivirikko, K. I. (1988b). Syncatalytic inactivation of prolyl 4-hydroxylase by anthracyclines. *Biochem. J.* **251**(2), 365-372.

Gunzler, V., Hanauske-Abel, H. M., Myllyla, R., Mohr, J. & Kivirikko, K. I. (1987). Time-dependent inactivation of chick-embryo prolyl 4-hydroxylase by coumalic acid. Evidence for a syncatalytic mechanism. *Biochem. J.* **242**(1), 163-169.

Gunzler, V. & Weidmann, K. (1998). Prolyl 4-hydroxylase inhibitors. In *Prolyl hydroxylase, protein disulfide isomerase, and other structurally related proteins* (Guzman, N. A., ed.), pp. 65-95. Marcel Dekker, New York.

Guzman, N. A. (1998). Prolyl 4-hydroxylase: An overview. In *Prolyl hydroxylase, protein disulfide isomerase, and other structurally related proteins* (Guzman, N. A., ed.), pp. 1-63. Marcel Dekker, New York.

Hales, N. J. & Beattie, J. F. (1993). Novel inhibitors of prolyl 4-hydroxylase. 5. The intriguing structure-activity relationships seen with 2,2'-bipyridine and its 5,5'-dicarboxylic acid derivatives. *J. Med. Chem.* **36**(24), 3853-3858.

Hanauske-Abel, H. M. (1991). Prolyl 4-hydroxylase, a target enzyme for drug development. Design of suppressive agents and the *in vitro* effects of inhibitors and proinhibitors. *J. Hepatol.* **13**(Suppl. 3), S8-S16.

Hanauske-Abel, H. M. & Guenzler, V. (1982). A stereochemical concept for the catalytic mechanism of prolylhydroxylase. Applicability to classification and design of inhibitors. *J. Theor. Biol.* **94**(2), 421-455.

Harper, J. W. & Vallee, B. L. (1988). Mutagenesis of aspartic acid-116 enhances the ribonucleolytic activity and angiogenic potency of angiogenin. *Proc. Natl. Acad. Sci. U. S. A.* **85**(19), 7139-7143.

- Hartley, R. W. (1997). Barnase and barstar. In *Ribonucleases: Structures and functions* (D'Alessio, G. & Riordan, J. F., eds.), pp. 51-100. Academic Press, New York.
- Hebert, E. J., Grimsley, G. R., Hartley, R. W., Horn, G., Schell, D., Garcia, S., Both, V., Sevcik, J. & Pace, C. N. (1997). Purification of ribonucleases Sa, Sa2, and Sa3 after expression in *Escherichia coli*. *Protein Express. Purif.* **11**, 162-168.
- Hewitson, K. S., McNeill, L. A., Elkins, J. M. & Schofield, C. J. (2003). The role of iron and 2-oxoglutarate oxygenases in signaling. *Biochem. Soc. Trans.* **31**(3), 510-515.
- Hieta, R., Kukkola, L., Permi, P., Pirila, P., Kivirikko Kari, I., Kilpelainen, I. & Myllyharju, J. (2003). The peptide-substrate-binding domain of human collagen prolyl 4-hydroxylases. Backbone assignments, secondary structure, and binding of proline-rich peptides. *J. Biol. Chem.* **278**(37), 34966-34974.
- Higgin, J. J., Yakovlev, G. I., Mitkevich, V. A., Makarov, A. A. & Raines, R. T. (2003). Zinc(II)-mediated inhibition of a ribonuclease by an *N*-hydroxyurea nucleotide. *Bioorg. Med. Chem. Lett.* **13**(3), 409-412.
- Hodges, J. A. & Raines, R. T. (2003). Stereoelectronic effects on collagen stability: The dichotomy of 4-fluoroproline diastereomers. *J. Am. Chem. Soc.* **125**(31), 9262-9263.
- Holmgren, S. K., Taylor, K. M., Bretscher, L. E. & Raines, R. T. (1998). Code for collagen's stability deciphered. *Nature* **392**(6677), 666-667.
- Hope, I. A., Ed. (1999). *C. Elegans: A practical approach*. The practical approach series; 213. Oxford; New York: Oxford University Press.
- Irie, M. (1997). Rnase T1/rnase T2 family rnases. In *Ribonucleases: Structures and functions* (D'Alessio, G. & Riordan, J. F., eds.), pp. 101-130. Academic Press, New York.
- Ito, H., Akiyama, H., Iguchi, H., Iyama, K.-I., Miyamoto, M., Ohsawa, K. & Nakamura, T. (2001). Molecular cloning and biological activity of a novel lysyl oxidase-related gene expressed in cartilage. *J. Biol. Chem.* **276**(26), 24023-24029.
- Ivan, M., Haberberger, T., Gervasi, D. C., Michelson, K. S., Gunzler, V., Kondo, K., Yang, H., Sorokina, I., Conaway, R. C., Conaway, J. W. & Kaelin, W. G., Jr. (2002). Biochemical purification and pharmacological inhibition of a mammalian prolyl hydroxylase acting on hypoxia-inducible factor. *Proc. Natl. Acad. Sci. U. S. A.* **99**(21), 13459-13464.
- Ivan, M., Kondo, K., Yang, H., Kim, W., Valiando, J., Ohh, M., Salic, A., Asara, J. M., Lane, W. S. & Kaelin, W. G., Jr. (2001). HIF α targeted for VHL-mediated destruction by proline hydroxylation: Implications for O₂ sensing. *Science* **292**(5516), 464-468.

- Iwahashi, K., Nakamura, K., Mitsui, Y., Ohgi, K. & Irie, M. (1981). Further evidence for the existence of the p0 site in the active site of ribonuclease. The binding of thymidine 3',5'-diphosphate to ribonuclease. *J. Biochem. (Tokyo)*. **90**(6), 1685-1690.
- Jaakkola, P., Mole, D. R., Tian, Y.-M., Wilson, M. I., Gielbert, J., Gaskell, S. J., von Kriegsheim, A., Hebestreit, H. F., Mukherji, M., Schofield, C. J., Maxwell, P. H., Pugh, C. W. & Ratcliffe, P. J. (2001). Targeting of HIF- α to the von Hippel-Lindau ubiquitylation complex by O₂-regulated prolyl hydroxylation. *Science* **292**(5516), 468-472.
- Janc, J. W., Clark, J. M., Warne, R. L., Elrod, K. C., Katz, B. A. & Moore, W. R. (2000). A novel approach to serine protease inhibition: Kinetic characterization of inhibitors whose potencies and selectivities are dramatically enhanced by zinc(II). *Biochemistry* **39**(16), 4792-4800.
- Jenkins, C. L., Bretscher, L. E., Guzei, I. A. & Raines, R. T. (2003). Effect of 3-hydroxyproline residues on collagen stability. *J. Am. Chem. Soc.* **125**(21), 6422-6427.
- Jenkins, C. L. & Raines, R. T. (2002). Insights on the conformational stability of collagen. *Nat. Prod. Rep.* **19**(1), 49-59.
- Karvonen, K., Ala-Kokko, L., Pihlajaniemi, T., Helaakoski, T., Henke, S., Gunzler, V., Kivirikko, K. I. & Savolainen, E. R. (1990). Specific inactivation of prolyl 4-hydroxylase and inhibition of collagen synthesis by oxaproline-containing peptides in cultured human skin fibroblasts. *J. Biol. Chem.* **265**(15), 8415-8419.
- Katz, B. A., Clark, J. M., Finer-Moore, J. S., Jenkins, T. E., Johnson, C. R., Ross, M. J., Luong, C., Moore, W. R. & Stroud, R. M. (1998). Design of potent selective zinc-mediated serine protease inhibitors. *Nature* **391**(6667), 608-612.
- Katz, B. A. & Luong, C. (1999). Recruiting Zn²⁺ to mediate potent, specific inhibition of serine proteases. *J. Mol. Biol.* **292**(3), 669-684.
- Kaule, G. & Guenzler, V. (1990). Assay for 2-oxoglutarate decarboxylating enzymes based on the determination of [1-14C]succinate: Application to prolyl 4-hydroxylase. *Anal. Biochem.* **184**(2), 291-297.
- Kelemen, B. R., Klink, T. A., Behlke, M. A., Eubanks, S. R., Leland, P. A. & Raines, R. T. (1999). Hypersensitive substrate for ribonucleases. *Nucleic Acids Res.* **27**, 3696-3701.
- Kellner, H. M., Volz, M., Baader, E., Kuerzel, G. U. & Eckert, H. G. (1991). Pharmacokinetics and metabolism of HOE 077: Preclinical studies. *J. Hepatol.* **13**(Suppl. 3), S48-S62.

- Kersteen, E. A. & Raines, R. T. (2003). Catalysis of protein folding by protein disulfide isomerase and small-molecule mimics. *Antiox. Redox Signaling* **5**(4), 413-424.
- Kim, I., Xia, A., Mogford, J. E., Witschi, C., Nafissi, M. & Mustoe, T. A. (2000). Collagen prolyl 4-hydroxylase inhibitor reduces scar elevation in a rabbit ear model of hypertrophic scarring. *Surg. Forum* **51**, 589-591.
- Kitz, R. & Wilson, I. B. (1962). Esters of methanesulfonic acid as irreversible inhibitors of acetylcholinesterase. *J. Biol. Chem.* **237**, 3245-3249.
- Kivirikko, K. I., Myllyla, R. & Pihlajaniemi, T. (1992). Hydroxylation of proline and lysine residues in collagens and other animal and plant proteins. *Post-Transl. Modif. Proteins*, 1-51.
- Kivirikko, K. I. & Myllyla, R. (1982). Posttranslational enzymes in the biosynthesis of collagen: Intracellular enzymes. *Methods Enzymol.* **82**, 245-304.
- Kivirikko, K. I. & Pihlajaniemi, T. (1998). Collagen hydroxylases and the protein disulfide isomerase subunit of prolyl 4-hydroxylases. *Adv. Enzymol. Relat. Areas Mol. Biol.* **72**, 325-398.
- Kramer, R. Z., Bella, J., Mayville, P., Brodsky, B. & Berman, H. M. (1999). Sequence dependent conformational variations of collagen triple-helical structure. *Nat. Struct. Biol.* **6**(5), 454-457.
- Leamon, C. P. & Low, P. S. (1991). Delivery of macromolecules into living cells: A method that exploits folate receptor endocytosis. *Proc. Natl. Acad. Sci. U.S.A.* **88**, 5572-5576.
- Lee, F. S., Shapiro, R. & Vallee, B. L. (1989). Tight-binding inhibition of angiogenin and ribonuclease A by placental ribonuclease inhibitor. *Biochemistry* **28**, 225-230.
- Leland, P. A. & Raines, R. T. (2001). Cancer chemotherapy—Ribonucleases to the rescue. *Chem. Biol.* **8**, 405-413.
- Leland, P. A., Schultz, L. W., Kim, B.-M. & Raines, R. T. (1998). Ribonuclease A variants with potent cytotoxic activity. *Proc. Natl. Acad. Sci. U.S.A.* **95**, 10407-10412.
- Leonidas, D. D., Shapiro, R., Irons, L. I., Russo, N. & Acharya, K. R. (1997). Crystal structures of ribonuclease A complexes with 5'-diphosphoadenosine 3'-phosphate and 5'-diphosphoadenosine 2'-phosphate at 1.7 Å resolution. *Biochemistry* **36**(18), 5578-5588.

- Leon-Lai, C. H., Gresser, M. J. & Tracey, A. S. (1996). Influence of vanadium(V) complexes on the catalytic activity of ribonuclease A. The role of vanadate complexes as transition state analogs to reactions at phosphate. *Can. J. Chem.* **74**(1), 38-48.
- Levy, D. E., Lapierre, F., Liang, W., Ye, W., Lange, C. W., Li, X., Grobelny, D., Casabonne, M., Tyrrell, D., Holme, K., Nadzan, A. & Galardy, R. E. (1998). Matrix metalloproteinase inhibitors: A structure activity study. *J. Med. Chem.* **41**(2), 199-223.
- Lindquist, R. N., Lynn, J. L., Jr. & Lienhard, G. E. (1973). Possible transition-state analogs for ribonuclease. Complexes of uridine with oxovanadium(IV) ion and vanadium(V) ion. *J. Am. Chem. Soc.* **95**(24), 8762.
- Linstead, R. P., Weedon, B. C. L. & Wladislaw, B. (1955). Anodic synthesis. XIII. Chain extension of fatty acids by electrolysis with benzyl half esters. *Journal of the Chemical Society, Abstracts*, 1097-1100.
- Louie, A. Y. & Meade, T. J. (1999). Metal complexes as enzyme inhibitors. *Chem. Rev.* **99**(9), 2711-2734.
- Loverix, S., Winqvist, A., Strömberg, R. & Steyaert, J. (2000). Mechanism of RNase T1: Concerted triester-like phosphoryl transfer via a catalytic three-centered hydrogen bond. *Chem. Biol.* **7**, 651-658.
- Luo, J., Smith, M. D., Lantrip, D. A., Wang, S. & Fuchs, P. L. (1997). Efficient syntheses of pyrofolic acid and pteroyl azide, reagents for the production of carboxyl-differentiated derivatives of folic acid. *J. Am. Chem. Soc.* **119**(42), 10004-10013.
- Majamaa, K., Guenzler, V., Hanauske-Abel, H. M., Myllyla, R. & Kivirikko, K. I. (1986). Partial identity of the 2-oxoglutarate and ascorbate binding sites of prolyl 4-hydroxylase. *J. Biol. Chem.* **261**(17), 7819-7823.
- Majamaa, K., Hanauske-Abel, H. M., Gunzler, V. & Kivirikko, K. I. (1984). The 2-oxoglutarate binding site of prolyl 4-hydroxylase. Identification of distinct subsites and evidence for 2-oxoglutarate decarboxylation in a ligand reaction at the enzyme-bound ferrous ion. *Eur. J. Biochem.* **138**(2), 239-245.
- Makarov, A. A. & Ilinskaya, O. N. (2003). Cytotoxic ribonucleases: Molecular weapons and their targets. *FEBS Lett.* **540**, 15-20.
- Maki, J. M. & Kivirikko, K. I. (2001). Cloning and characterization of a fourth human lysyl oxidase isoenzyme. *Biochem. J.* **355**(2), 381-387.
- McCall, K. A., Huang, C.-C. & Fierke, C. A. (2000). Function and mechanism of zinc metalloenzymes. *J. Nutr.* **130**(5S), 1437S-1446S.

- Miller, T. A., Witter, D. J. & Belvedere, S. (2003). Histone deacetylase inhibitors. *J. Med. Chem.* **46**(24), 5097-5116.
- Milstein, D. & Stille, J. K. (1979). Mild, selective, general method of ketone synthesis from acid chlorides and organotin compounds catalyzed by palladium. *J. Org. Chem.* **44**(10), 1613-1618.
- Mizuno, K., Hayashi, T., Peyton, D. H. & Bachinger, H. P. (2004). The peptides acetyl-(Gly-3(S)Hyp-4(R)Hyp)10-NH₂ and acetyl-(Gly-Pro-3(S)Hyp)10-NH₂ do not form a collagen triple helix. *J. Biol. Chem.* **279**(1), 282-287.
- Mock, W. L. & Cheng, H. (2000). Principles of hydroxamate inhibition of metalloproteases: Carboxypeptidase A. *Biochemistry* **39**(45), 13945-13952.
- Mole, D. R., Schlemminger, I., McNeill, L. A., Hewitson, K. S., Pugh, C. W., Ratcliffe, P. J. & Schofield, C. J. (2003). 2-oxoglutarate analogue inhibitors of HIF prolyl hydroxylase. *Bioorg. Med. Chem. Lett.* **13**(16), 2677-2680.
- Moon, H.-S. & Begley, T. P. (2000). Inhibition of prolyl 4-hydroxylase by oxaproline tetrapeptides *in vitro* and mass analysis for the enzymatic reaction products. *Biotechnol. Bioprocess Eng.* **5**(1), 61-64.
- Myllyharju, J. (2003). Prolyl 4-hydroxylases, the key enzymes of collagen biosynthesis. *Matrix Biol.* **22**(1), 15-24.
- Myllyharju, J. & Kivirikko, K. I. (1997). Characterization of the iron- and 2-oxoglutarate-binding sites of human prolyl 4-hydroxylase. *EMBO J.* **16**(6), 1173-1180.
- Myllyharju, J. & Kivirikko, K. I. (1999). Identification of a novel proline-rich peptide-binding domain in prolyl 4-hydroxylase. *EMBO J.* **18**(2), 306-312.
- Myllyharju, J. & Kivirikko, K. I. (2001). Collagens and collagen-related diseases. *Ann. Med.* **33**(1), 7-21.
- Myllyharju, J. & Kivirikko, K. I. (2004). Collagens, modifying enzymes and their mutations in humans, flies and worms. *Trends Genet.* **20**(1), 33-43.
- Myllyharju, J., Kukkola, L., Winter, A. D. & Page, A. P. (2002). The exoskeleton collagens in *Caenorhabditis elegans* are modified by prolyl 4-hydroxylases with unique combinations of subunits. *J. Biol. Chem.* **277**(32), 29187-29196.
- Myllyla, R., Kuutti-Savolainen, E. R. & Kivirikko, K. I. (1978). The role of ascorbate in the prolyl hydroxylase reaction. *Biochem. Biophys. Res. Commun.* **83**(2), 441-448.

- Nguyen, R. & Huc, I. (2001). Using an enzyme's active site to template inhibitors. *Angew. Chem. Int. Ed.* **40**(9), 1774-1776.
- Outten, C. E. & O'Halloran, T. V. (2001). Femtomolar sensitivity of metalloregulatory proteins controlling zinc homeostasis. *Science* **292**(5526), 2488-2492.
- Pace, C. N., Heinemann, U., Hahn, U. & Saenger, W. (1991). Ribonuclease T1: Structure, function and stability. *Angew. Chem. Int. Ed.* **30**(4), 343-360.
- Park, C., Kelemen, B. R., Klink, T. A., Sweeney, R. Y., Behlke, M. A., Eubanks, S. R. & Raines, R. T. (2001). Fast, facile, hypersensitive assays for ribonucleolytic activity. *Methods Enzymol.* **341**, 81-94.
- Passoja, K., Rautavuoma, K., Ala-Kokko, L., Kosonen, T. & Kivirikko, K. I. (1998). Cloning and characterization of a third human lysyl hydroxylase isoform. *Proc. Natl. Acad. Sci. U. S. A.* **95**(18), 10482-10486.
- Pekkala, M., Hieta, R., Kursula, P., Kivirikko, K. I., Wierenga, R. K. & Myllyharju, J. (2003). Crystallization of the proline-rich-peptide binding domain of human type I collagen prolyl 4-hydroxylase. *Acta Crystallogr. D. Biol. Crystallogr.* **D59**(5), 940-942.
- Peterson, R. T., Shaw, S. Y., Peterson, T. A., Milan, D. J., Zhong, T. P., Schreiber, S. L., MacRae, C. A. & Fishman, M. C. (2004). Chemical suppression of a genetic mutation in a zebrafish model of aortic coarctation. *Nat. Biotechnol.* **22**(5), 595-599.
- Polyakov, K. M., Lebedev, A. A., Okorokov, A. L., Panov, K. I., Schulga, A. A., Pavlovsky, A. G., Karpeisky, M. Y. & Dodson, G. G. (2002). The structure of substrate-free microbial ribonuclease binase and of its complexes with 3'GMP and sulfate ions. *Acta Crystallogr. D. Biol. Crystallogr.* **D58**(5), 744-750.
- Prockop, D. J. & Kivirikko, K. I. (1969). Effect of polymer size on the inhibition of procollagen proline hydroxylase by polyproline II. *J. Biol. Chem.* **244**(18), 4838-4842.
- Prockop, D. J. & Kivirikko, K. I. (1995). Collagens: Molecular biology, diseases, and potentials for therapy. *Annu. Rev. Biochem.* **64**, 403-434.
- Raines, R. T. (1998). Ribonuclease A. *Chem. Rev.* **98**(3), 1045-1065.
- Reddy, J. A. & Low, P. S. (1998). Folate-mediated targeting of therapeutic and imaging agents to cancers. *Crit. Rev. Ther. Drug Carrier Syst.* **15**, 587-627.

- Riordan, J. F. (1997). Structure and function of angiogenin. In *Ribonucleases: Structures and functions* (D'Alessio, G. & Riordan, J. F., eds.), pp. 445-489. Academic Press, New York.
- Rosenbloom, J., Harsch, M. & Jimenez, S. (1973). Hydroxyproline content determines the denaturation temperature of chick tendon collagen. *Arch. Biochem. Biophys.* **158**(2), 478-484.
- Ross, J. (1996). Control of messenger RNA stability in higher eukaryotes. *Trends Genet.* **12**(5), 171-175.
- Ross, J. F., Chaudhuri, P. K. & Ratnam, M. (1994). Differential regulation of folate receptor isoforms in normal and malignant-tissues *in-vivo* and in established cell-lines - physiological and clinical implications. *Cancer* **73**(9), 2432-2443.
- Russo, A., Acharya, K. R. & Shapiro, R. (2001). Small molecule inhibitors of RNase A and related enzymes. *Methods Enzymol.* **341**, 629-648.
- Russo, N. & Shapiro, R. (1999). Potent inhibition of mammalian ribonucleases by 3', 5'-pyrophosphate-linked nucleotides. *J. Biol. Chem.* **274**(21), 14902-14908.
- Russo, N., Shapiro, R. & Vallee, B. L. (1997). 5'-diphosphoadenosine 3'-phosphate is a potent inhibitor of bovine pancreatic ribonuclease A. *Biochem. Biophys. Res. Commun.* **231**(3), 671-674.
- Ryle, M. J., Koehntop, K. D., Liu, A., Que, L., Jr. & Hausinger, R. P. (2003). Interconversion of two oxidized forms of taurine/ α -ketoglutarate dioxygenase, a non-heme iron hydroxylase: Evidence for bicarbonate binding. *Proc. Natl. Acad. Sci. U. S. A.* **100**(7), 3790-3795.
- Sakaida, I., Kubota, M., Kayano, K., Takenaka, K., Mori, K. & Okita, K. (1994). Prevention of fibrosis reduces enzyme-altered lesions in the rat liver. *Carcinogenesis* **15**(10), 2201-2206.
- Sasaki, T., Holeyfield, K. C. & Uitto, J. (1987). Doxorubicin-induced inhibition of prolyl hydroxylation during collagen biosynthesis in human skin fibroblast cultures. Relevance to impaired wound healing. *J. Clin. Invest.* **80**(6), 1735-1741.
- Sawada, F. & Irie, M. (1969). Interaction of uridine 2'(3'),5'-diphosphate with ribonuclease A and carboxymethyl ribonuclease A. *J. Biochem. (Tokyo)*. **66**(3), 415-418.
- Saxena, S. K., Rybak, S. M., Winkler, G., Meade, H. M., McGray, P., Youle, R. J. & Ackerman, E. J. (1991). Comparison of RNases and toxins upon injection into *Xenopus* oocytes. *J. Biol. Chem.* **266**(31), 21208-21214.

Schaus, S. E., Brandes, B. D., Larrow, J. F., Tokunaga, M., Hansen, K. B., Gould, A. E., Furrow, M. E. & Jacobsen, E. N. (2002). Highly selective hydrolytic kinetic resolution of terminal epoxides catalyzed by chiral (salen)CoIII complexes. Practical synthesis of enantioenriched terminal epoxides and 1,2-diols. *J. Am. Chem. Soc.* **124**(7), 1307-1315.

Schirmeister, T. (1998). Metal ions as co-inhibitors of serine proteases: A new approach in the search for specific high-affinity ligands. *Angew. Chem. Int. Ed.* **37**(13/14), 1830-1832.

Schlemminger, I., Mole, D. R., McNeill, L. A., Dhanda, A., Hewitson, K. S., Tian, Y.-M., Ratcliffe, P. J., Pugh, C. W. & Schofield, C. J. (2003). Analogues of dealanylalohopcin are inhibitors of human hif prolyl hydroxylases. *Bioorg. Med. Chem. Lett.* **13**(8), 1451-1454.

Sevcik, J., Lamzin, V. S., Dauter, Z. & Wilson, K. S. (1993). Complex of ribonuclease Sa with a cyclic nucleotide and a proposed model for the reaction intermediate. *Eur. J. Biochem.* **216**, 301-305.

Sevcik, J., Sanishvili, R. G., Pavlovsky, A. G. & Polyakov, K. M. (1990). Comparison of active sites of some microbial ribonucleases: Structural basis for guanylic specificity. *Trends Biochem. Sci.* **15**(4), 158-162.

Shapiro, R. (2001). Cytoplasmic ribonuclease inhibitor. *Methods Enzymol.* **341**, 611-628.

Shapiro, R. & Vallee, B. L. (1989). Site-directed mutagenesis of histidine-13 and histidine-114 of human angiogenin. Alanine derivatives inhibit angiogenin-induced angiogenesis. *Biochemistry* **28**(18), 7401-7408.

Shaw, K. L., Grimsley, G. R., Yakovlev, G. I., Makarov, A. A. & Pace, C. N. (2001). The effect of net charge on the solubility, activity, and stability of ribonuclease Sa. *Protein Sci.* **10**(6), 1206-1215.

Sigel, A. & Sigel, H., Eds. (1998). *Iron transport and storage in microorganisms, plants, and animals*. Vol. 35. Metal ions in biological systems. New York: Marcel Dekker.

Silverman, R. B., Ed. (1992). *The organic chemistry of drug design and drug action*. San Diego: Academic Press.

Smith, B. D., Soellner, M. B. & Raines, R. T. (2003). Potent inhibition of ribonuclease A by oligo(vinylsulfonic acid). *J. Biol. Chem.* **278**(23), 20934-20938.

Stephani, R. A. & Meister, A. (1971). Structure of the dimeric α -keto acid analog of asparagine. *J. Biol. Chem.* **246**(23), 7115-7118.

Stewart, A. O. & Brooks, D. W. (1992). *N,O*-bis(phenoxycarbonyl)hydroxylamine: A new reagent for the direct synthesis of substituted *N*-hydroxyureas. *J. Org. Chem.* **57**(18), 5020-5023.

Steyaert, J., Hallenga, K., Wyns, L. & Stanssens, P. (1990). Histidine-40 of ribonuclease T₁ acts as base catalyst when the true catalytic base, glutamic acid-58, is replaced by alanine. *Biochemistry* **29**, 9064-9072.

Stowell, J. K., Widlanski, T. S., Kutateladze, T. G. & Raines, R. T. (1995). Mechanism-based inactivation of ribonuclease A. *J. Org. Chem.* **60**(21), 6930-6936.

Takahashi, K. (1970). The structure and function of ribonuclease T₁. IX. Photooxidation of ribonuclease T₁ in the presence of rose bengal. *J. Biochem. (Tokyo)*. **67**, 833-839.

Tandon, M., Wu, M., Begley, T. P., Myllyharju, J., Pirskanen, A. & Kivirikko, K. (1998). Substrate specificity of human prolyl-4-hydroxylase. *Bioorg. Med. Chem. Lett.* **8**(10), 1139-1144.

The *C. elegans* Sequencing Consortium, (1998). Genome sequence of the nematode *C. elegans*: A platform for investigating biology. *Science* **282**(5396), 2012-2018.

Thompson, J. E., Kutateladze, T. G., Schuster, M. C., Venegas, F. D., Messmore, J. M. & Raines, R. T. (1995). Limits to catalysis by ribonuclease A. *Bioorg. Chem.* **23**, 471-481.

Thorp, H. H. (1998). Bioinorganic chemistry and drug design: Here comes zinc again. *Chem. Biol.* **5**(6), R125-R127.

Tschank, G., Brocks, D. G., Engelbart, K., Mohr, J., Baader, E., Gunzler, V. & Hanauske-Abel, H. M. (1991). Inhibition of prolyl hydroxylation and procollagen processing in chick-embryo calvaria by a derivative of pyridine-2,4-dicarboxylate. Characterization of the diethyl ester as a proinhibitor. *Biochem. J.* **275**, 469-476.

Tschank, G., Hanauske-Abel, H. M. & Peterkofsky, B. (1988). The effectiveness of inhibitors of soluble prolyl hydroxylase against the enzyme in the cisternae of isolated bone microsomes. *Arch. Biochem. Biophys.* **261**(2), 312-323.

Tschank, G., Raghunath, M., Gunzler, V. & Hanauske-Abel, H. M. (1987). Pyridinedicarboxylates, the first mechanism-derived inhibitors for prolyl 4-hydroxylase, selectively suppress cellular hydroxyprolyl biosynthesis. Decrease in interstitial collagen and clq secretion in cell culture. *Biochem. J.* **248**(3), 625-633.

Tuderman, L., Myllyla, R. & Kivirikko, K. I. (1977). Mechanism of the prolyl hydroxylase reaction. 1. Role of co-substrates. *Eur. J. Biochem.* **80**(2), 341-348.

Valegard, K., Terwisscha van Scheltinga, A. C., Dubus, A., Ranghino, G., Oester, L. M., Hajdu, J. & Andersson, I. (2004). The structural basis of cephalosporin formation in a mononuclear ferrous enzyme. *Nat. Struct. Mol. Bio.* **11**(1), 95-101.

Vallee, B. L. (1988). Zinc: Biochemistry, physiology, toxicology and clinical pathology. *Biofactors* **1**(1), 31-36.

Valtavaara, M., Szpirer, C., Szpirer, J. & Myllyla, R. (1998). Primary structure, tissue distribution, and chromosomal localization of a novel isoform of lysyl hydroxylase (lysyl hydroxylase 3). *J. Biol. Chem.* **273**(21), 12881-12886.

Vuori, K., Pihlajaniemi, T., Marttila, M. & Kivirikko, K. I. (1992). Characterization of the human prolyl 4-hydroxylase tetramer and its multifunctional protein disulfide-isomerase subunit synthesized in a baculovirus expression system. *Proc. Natl. Acad. Sci. U. S. A.* **89**(16), 7467-7470.

Wallace, K. B. (2003). Doxorubicin-induced cardiac mitochondrionopathy. *Pharmacol. Toxicol.* **93**(3), 105-115.

Way, J. C. (2000). Covalent modification as a strategy to block protein-protein interactions with small-molecule drugs. *Curr. Opin. Chem. Biol.* **4**(1), 40-46.

Wise, W. M. & Brandt, W. W. (1955). An investigation of some hydroxamic acids. *J. Am. Chem. Soc.* **77**, 1058-1059.

Wolfenden, R. & Snider, M. J. (2001). The depth of chemical time and the power of enzymes as catalysts. *Acc. Chem. Res.* **34**, 938-945.

Wood, W. B., Ed. (1988). *The nematode Caenorhabditis elegans*. Vol. 17. Cold spring harbor monograph series. Cold Spring Harbor, N.Y.: Cold Spring Harbor Laboratory.

Wright, Stephen W. & Nelson, M. J. (1992). Episulfide inhibitors of lipooxygenase. *Bioorg. Med. Chem. Lett.* **2**(11), 1385-1390.

Wright, G., Higgin, J. J., Raines, R. T., Steenbergen, C. & Murphy, E. (2003). Activation of the prolyl hydroxylase oxygen-sensor results in induction of GLUT1, heme oxygenase-1, and nitric-oxide synthase proteins and confers protection from metabolic inhibition to cardiomyocytes. *J. Biol. Chem.* **278**(22), 20235-20239.

Wu, M. & Begley, T. P. (2000). Beta-scission of the N-O bond in alkyl hydroxamate radicals: A fast radical trap. *Org. Lett.* **2**(10), 1345-1348.

- Wu, M., Moon, H.-S., Begley, T. P., Myllyharju, J. & Kivirikko, K. I. (1999). Mechanism-based inactivation of the human prolyl-4-hydroxylase by 5-oxaproline-containing peptides: Evidence for a prolyl radical intermediate. *J. Am. Chem. Soc.* **121**(3), 587-588.
- Wu, Y., Mikulski, S. M., Ardelt, W., Rybak, S. M. & Youle, R. J. (1993). A cytotoxic ribonuclease. *J. Biol. Chem.* **268**, 10686-10693.
- Yakovlev, G. I., Mitkevich, V. A., Shaw, K. L., Trevino, S., Newsom, S., Pace, C. N. & Makarov, A. A. (2003). Contribution of active site residues to the activity and thermal stability of ribonuclease Sa. *Protein Sci.* **12**(10), 2367-2373.
- Yakovlev, G. I., Moiseyev, G. P., Bezborodova, S. I., Both, V. & Sevcik, J. (1992). A comparative study on the catalytic properties of guanyl-specific ribonucleases. *Eur. J. Biochem.* **204**, 187-190.
- Yakovlev, G. I., Moiseyev, G. P., Struminskaya, N. K., Borzykh, O. A., Kipenskaya, L. V., Znamenskaya, L. V., Leschinskaya, I. B., Chernokalskaya, E. B. & Hartley, R. W. (1994). Mutational analysis of the active site of RNase of bacillus intermedius (binase). *FEBS Lett.* **354**(3), 305-306.
- Yamamoto, M., Tsujishita, H., Hori, N., Ohishi, Y., Inoue, S., Ikeda, S. & Okada, Y. (1998). Inhibition of membrane-type 1 matrix metalloproteinase by hydroxamate inhibitors: An examination of the subsite pocket. *J. Med. Chem.* **41**(8), 1209-1217.
- Yoshida, H. (2001). The ribonuclease T1 family. *Methods Enzymol.* **341**, 28-41.
- Zhang, Z., Ren, J., Stammers, D. K., Baldwin, J. E., Harlos, K. & Schofield, C. J. (2000). Structural origins of the selectivity of the trifunctional oxygenase clavaminic acid synthase. *Nat. Struct. Biol.* **7**(2), 127-133.
- Zhao, Y., Dai, X., Blackwell, H. E., Schreiber, S. L. & Chory, J. (2003). SIR1, an upstream component in auxin signaling identified by chemical genetics. *Science* **301**(5636), 1107-1110.